Electrochemical characterization of tetrahedral amorphous carbon and detonation nanodiamond hybrid electrode for detection of dopamine

Elli Leppänen

School of Electrical Engineering

Thesis submitted for examination for the degree of Master of Science in Technology.

Espoo 23.12.2016

Thesis supervisor:

Prof. Tomi Laurila

Thesis advisor:

M.Sc. Sami Sainio

Aalto University
School of Electrical
Engineering

AALTO UNIVERSITY
SCHOOL OF ELECTRICAL ENGINEERING

ABSTRACT OF THE
MASTER'S THESIS

Author: Elli Leppänen

Title: Electrochemical characterization of tetrahedral amorphous carbon and detonation nanodiamond hybrid electrode for detection of dopamine

Date: 23.12.2016 Language: English Number of pages: 10+78

Department of Electrical Engrineering and Automation

Professorship: Biosensing- and bioelectronics

Supervisor: Prof. Tomi Laurila

Advisor: M.Sc. Sami Sainio

This work concentrated on electrochemical characterization, that was done to evaluate tetrahedral amorphous and detonation nanodiamond (ta-C+ND) hybrid electrodes suitability for dopamine (DA) detection. Characteristics investigated in this work were (i) electrode kinetics by using ruthenium, (ii) water window in perchloric acid, (iii) sensitivity towards DA and (iv) selectivity between DA and ascorbic acid (AA).

Electrochemical characterization was carried out for ta-C and ta-C+ND electrodes with cyclic voltammetry (CV). After the characterization, ta-C+ND electrode was annealed in vacuum at 600°C for 1 hour and measured again in DA solutions. Aim was to investigate how annealing affects the electrochemical performance of the hybrid electrode.

ta-C+ND hybrid electrode properties were equally good or better compared to plain ta-C, where sensitivity towards DA was enhanced. ta-C+ND had reversible kinetics, wide water window of 3.01 V and detection limit of 100 nM DA. Selectivity towards DA in presence of AA was not achieved. With annealed ta-C+ND sensitivity and kinetics towards DA improved considerably compared to non annealed ta-C+ND. In addition, annealing increased resistance to passivation of the hybrid electrode. However, properties of the hybrid electrodes changed over time and measurement results were not reproducible in DA and DA+AA solutions.

Literary review also pointed out that electrochemical behaviour of nanodiamonds is not well understood as the characterization of the used nanodiamonds is insufficient. Additionally, electrochemical experiments conducted with nanodiamonds had some inconsistencies. For more profound understanding of the phenomena, extensive characterization of surface chemistry and morphology is needed.

Keywords: Nanodiamond, tetrahedral amorphous carbon, cyclic voltammetry, dopamine, ascorbic acid

AALTO-YLIOPISTO
SÄHKÖTEKNIIKAN KORKEAKOULU

DIPLOMITYÖN
TIIVISTELMÄ

Tekijä: Elli Leppänen

Työn nimi: Tetraedrinen amorfinen hiili ja nanotimantti hybridimateriaalin sähkökemiallinen karakterisointi dopamiinin havaitsemiseen

Päivämäärä: 23.12.2016 Kieli: Englanti Sivumäärä: 10+78

Sähkötekniikan ja automaation laitos

Professuuri: Biosensing and -electronics

Työn valvoja: Prof. Tomi Laurila

Työn ohjaaja: M.Sc. Sami Sainio

Tässä työssä tutkittiin tetraedrinen amorfinen hiili ja nanotimantti hybridimateriaalin (ta-C+ND) sopivuutta dopamiinin havaitsemiseen sähkökemiallisin menetelmin. Seuraavia sähkökemiallisia ominaisuuksia tutkittiin tässä työssä (i) kinetiikka, (ii) vesi-ikkuna, (iii) herkkyys dopamiinin (DA) havaitsemiseen sekä (iv) selektiivisyys dopamiinin ja askorbiinihapon (AA) välillä.

Sähkökemiallinen karakterisointi suoritettiin ta-C ja ta-C+ND antureille syklisellä voltammetrialla. Karakterisoinnin jälkeen ta-C+ND anturi hehkutettiin vakuumiuunissa 600°C asteessa tunnin ajan. Tarkoituksena oli tutkia kuinka hehkutus vaikuttaa hybridianturin sähkökemiallisiin ominaisuuksiin.

ta-C+ND ominaisuudet olivat yhtä hyviä tai parempia ta-C anturiin verrattuna, missä herkkyys dopamiinin havaitsemiselle parani. ta-C+ND anturilla oli reversiibeli kinetiikka, laaja vesi-ikkuna (3.01 V) sekä 100nM havaitsemisraja dopamiinille. Anturi ei kuitenkaan ollut selektiivinen DA+AA liuoksessa. Hehkutuksen jälkeen ta-C+ND anturin herkkyys ja kinetiikka dopamiiniliuoksessa paranivat huomattavasti. Tämän lisäksi anturin resistanssi likaantumiselle kohentui. Lupaavista tuloksista huolimatta, ta-C+ND anturin ominaisuudet muuttuivat ajan kuluessa ja mittaustulokset eivät olleet toistettavia DA ja DA+AA liuoksissa.

Kirjallisuuskatsauksesta huomataan että nanotimanttien sähkökemiallinen käyttäytyminen on huonosti ymmärretty. Sähkökemiallisiin mittauksiin käytetyt nanotimantit ovat heikosti karakterisoitu, jonka lisäksi itse sähkökemiallisissa mittauksissa on epäjohdonmukaisuutta. Syvemmän ymmärryksen saavuttamiseksi, nanotimantien pintakemiaa ja morfologiaa tulisi karakterisoida tarkemmin.

Avainsanat: Nanotimantti, tetraedrinen amorfinen hiili, sykslinen voltammetria, dopamiini, askorbiinihappo

Preface

First, I would like to thank my supervising professor Tomi Laurila for granting me the opportunity to work with this topic. I appreciate prof. Tomi Laurila for the useful guidance and interest that he has showed throughout this work. Then, I would like to thank my advisor Sami Sainio for the valuable guidance during this project and always encouraging me to do more than I expected. I'm also thankful to Sami for his patience, availability and "academic" conversation that we had on and off the topic.

Furthermore, I want to acknowledge all the people who have contributed to this work. I would like to thank Tommi Palomäki for being my electrochemistry support, Noora Isoaho for teaching me all practical things in electrochemical experiments, Niklas Wester for fabrication of the samples and Mikael Broas for teaching me how to use vacuum furnace. Moreover, I want to thank the whole Microsystem technology group for the past 1,5 years. It has been a pleasure to work under your guidance and share countless hours at the office and lunches.

Then I want to thank my family for the endless support and love. There is absolutely no place like home. I'm also thankful to Minna with whom I have shared this academic path with all ups and down. Those endless jokes, conversations and trips abroad have giving me the energy keep on going. Then the foremost, Hilla-Marja to whom I'm grateful for our friendship that has carried me trough so many years. And finally to all my other wonderful friends, thank you for reminding me that there are so much more than work and studies.

Otaniemi, 23.12.2016
Elli

Contents

Symbols and abbreviations

Symbols

a	activity of the specie
γ	activity coefficient
A	electrode surface area (cm^{-2})
c	concentration of specie (mol/l)
c^*	concentration of the bulk solution (mol/l)
C_{dl}	double layer capacitance (F)
D	diffusion coefficient (cm^2 s^{-1})
E	potential (V)
E_0	stantard electrode potential (V)
E_{eq}	equilibrium potential
E_{ox}	oxidation potential (V)
E_{red}	reduction potential (V)
E_η	potential of polarized electrode (V)
ΔE_p	peak potential separation (V)
F	Faraday constant (9.64853 x 10^4 C)
ΔG	Gibbs free energy change (kJ)
i	current (A)
i_{pa}	anodic peak current (A)
i_{pc}	cathodic peak current (A)
J	diffusional flux (mol cm^{-2} s^{-1})
j	current density (A cm^{-2})
k^0	formal reaction rate constant (cm s^{-1})
m_T	mass transport coefficient (cm s^{-1})
n	number of electrons in moles (mol)
Ox	oxidized specie
r	rate of reaction (mol cm^{-2} s^{-1})
R	ideal gas constant (8.31447 J mol^{-1} K^{-1})
Red	reduces specie
R_{ct}	charge transfer resistance (Ω)
R_Ω	solution resistance (Ω)
v	scan rate (V s^{-1})
t	time
T	temperature (K)
W	Warburg impedance
η	overpotential (V)
δ	diffusion layer thickness (cm)
Ψ	kinetic parameter for cyclic voltammetry

Abbreviations

AA	Ascorbic acid
Ag/AgCl	Silver/silver chloride
BDD	Boron-doped diamond
CE	Counter electrode
CNF	Carbon nanofiber
CNT	Carbon nanotube
CV	Cyclic voltammetry
CVD	Chemical vapor deposition
DA	Dopamine
DAC	Dopamineaminochrome
DHA	Dehydroascorbic acid
DHI	5,6-Dihydroxyindole
DOPAC	3,4-Dihydroxyphenylacetic acid
DAQ	Dopamine-o-quinone
DPV	Differential pulse voltammetry
DTA	Differential thermal analysis
EDL	Electric double layer
EP	Explosion products
EPR	Electron paramagnetic resonance
ET	Electron transfer
FeMeOH	Ferrocenemethanol
$Fe(CN)_6^{-3/-4}$	Ferrocyanide
fMRI	functional Magnetic Resonance Imaging
FTIR	Fourier transform infrared spectroscopy
GC	Glassy carbon
H_2SO_4	Sulfuric acid
$HClO_4$	Perchloric acid
HNO_3	Nitric acid
H_2O_2	Hydrogen peroxide
HRTEM	High resolution transmission electron microscopy
IHP	Inner Helmholtz plane
IrCl	Iridium chloride
$K_2Cr_2O_7$	Potassium dichromate
KOH	Potassium hydroxide
KNO_3	Potassium nitrate
LDC	Leucodopaminechrome
L-DOPA	L-3,4-Dihydroxyphenylalanine
LOD	Limit of detection
Na_2O_2	Sodium peroxide
ND	Nanodiamond
NMR	Nuclear magnetic resonance

OHP	Outer Helmholtz plane
OLC	Onion-like carbon
PBS	Phosphate buffer solution
PECVD	Plasma-enhanced chemical vapor deposition
PG	Pyrolytic carbon
RE	Reference electrode
RGA	Residual gas analyzer
$Ru(NH_3)_6^{+2/+3}$	Hexaammineruthenium(III) chloride
ta-C	tetrahedral amorphous carbon
TDP	Thermal programmed desorption
TGA	Thermogravimetric analysis
WE	Working electrode
XANES	X-ray absorption near edge structure
XPS	X-ray photoelectron spectroscopy
XRD	X-ray crystallography

1 Introduction

Carbon materials are a family of structures with unique electronic, optical, mechanical and chemical properties [1, 2]. Due to these interesting characteristics carbon materials are intensively studied and widely used in various applications for example in transistors, composite materials, lubrication, medical applications and energy storage [1–3]. Carbon is also suitable as a sensor material for detecting neurotransmitters such as dopamine (DA) [3]. For this type of application carbon has several beneficial properties as a sensor material such as chemical inertness, biocompatibility and electrocatalytic activity towards organic and biological molecules. [3, 4] In addition, using carbon-based sensors for detecting neurotransmitters it is possible to reduce use of critical materials such as platinum. Carbon structures that have been under extensive research for detecting of neurotransmitters are glassy carbon (GC) [3], carbon nanotubes (CNT) [3], carbon fibers (CF) [5, 6] and graphene [7].

Detonation nanodiamond (ND) is a carbon nanomaterial that was discovered in Russia 1960's [8]. Although ND particles were discovered decades ago, it has not been widely studied for applications in neurotransmitter detection. There is motivation to investigate ND particles as they can be used as sensor material [9]. Furthermore, ND is suitable for building a feasible sensor for *in vivo* measurements. The required sensor size is $\sim$10 μm in diameter with a length of 25-400 μm to minimize the tissue damage in the brain during insertion [6]. With nanodiamonds these dimension can be fulfilled as the particles average size is 5nm [10]. Also for further sensor development ND particles are CMOS compatible since addition of ND coating does not require high fabrication temperatures unlike CVD or PECVD produced carbon nanomaterials, such as carbon nanofibers (CNF) [11].

There is a great variety of neurotransmitters, one very interesting is dopamine. DA is important neurotransmitter affecting several functions in the mammalian central nervous system. Although effects of DA are complex, it is known to have major role in both of cognitive and behavioral functions such as brain plasticity, learning, emotions, memory and reward system [4, 12–14]. Also abnormal dopamine transmission has been related to several neurological disorders such as Parkinson's disease, schizophrenia and ADHD. [5, 15, 16] Additionally, addiction and severe drug abuse has been known to change mesolimbic dopamine system [17]. To gain more profound understanding of dopamine behavior in the nervous system and to provide reliable diagnostics, there is relevance for an accurate measurement of dopamine level *in vivo*.

Real time detection of dopamine can be achieved with electrochemical methods because DA is an electrochemically active compound. Cyclic voltammetry (CV) is frequently used electrochemical method for detecting DA. CV is a technique that can provide real-time measurement of dopamine transmission in subsecond timescale and with good chemical selectivity. [4, 6] Nevertheless, there are several challenges to overcome before dopamine can be detected accurately with CV. Depending on the region of the brain, the concentration of DA is low, varying from 5 nM to

1 μM [6, 18]. Also the brain consist other electroactive substances that interfere detection of dopamine in the extracellular fluid, such as ascorbic acid (AA), uric acid, epinephrine and serotonin. To detect small concentrations of DA in presence of interfering components, high sensitivity and selectivity for dopamine is required. Other major challenge is biofouling of the electrode in physiological environment [19]. To measure DA reliably *in vivo*, the surface of the electrode should be inert to reduce biofouling.

As stated above, several types of carbon materials have been under investigation for electrochemical detection of dopamine. One potential candidate is tetrahedral amorphous carbon (ta-C) with high fraction of sp^3 hybridization. ta-C is less studied as a sensor material, but in recent years it has received more interest in the field of electrochemical sensing [20–22]. Tetrahedral amorphous carbon has excellent mechanical properties, low background current, chemical inertness, wide potential window [23, 24] and great antifouling properties [25]. Nevertheless ta-C itself is not sensitive [22] or selective [26] enough for detection *in vivo* concentration of dopamine. Electrochemical performance of ta-C can be improved by combining it with different carbon allotropes such as carbon nanotubes or carbon nanofibers (CNF). [11, 21, 26] These hybrid carbon materials have shown higher sensitivity and selectivity toward dopamine. Consequently there is a great motivation to explore other hybrid material together with ta-C.

In this work new tetrahedral amorphous carbon and detonation nanodiamond hybrid material is presented. Electrochemical properties of nanodiamonds are not well know, additionally there is only one report where ND structures are used for electrochemical sensing of dopamine [9]. Thus the goals of this work are (i) to offer literacy review of the present knowledge of nanodiamonds structure, (ii) their electrochemical performance and (iii) evaluate the electrochemical properties of ta-C+ND hybrid material using cyclic voltammetry. In the experimental section ta-C+ND hybrid material is electrochemically characterized by studying electrodes sensitivity, selectivity, electron transfer kinetics and water window.

2 Measuring neurotransmitters

Abnormal transmission of neurotransmitters is reletad to several neurological disorders. However, there is lack of knowledge about exact concentrations of these compounds participating in these events. [13] Therefore accurate measuring of neurotransmitters is needed for efficient diagnostics, but also for deeper understanding the role of neurotransmitters themselves.

Present methods for measuring of neurotransmitters are microdialysis and spectroscopic methods such as positron emission tomography (PET) and functional magnetic resonance (fMRI). Advantages with microdialysis is high selectivity, whereas with spectroscopic methods zero tissue damage as these methods are non-invasive. However, one of the major disadvantages with these methods is low temporal resolution varying from seconds to minutes. With this temporal resolution it is impossible to measure singular events in the brain due to the fact that transmission events in extracellular fluid are in sub-second timescale. [6, 13, 27] Therefore method than can measure neurotransmitters selectively in real time with low tissue damage should be used.

With electrochemical methods it is possible to overcome some problems with present analyzing methods. High temporal resolution and minimum tissue damage can be achieved by using cyclic voltammetry together with microelectrodes that can selectivly detect neurotransmitters. [4,6] In this chapter the basis for neurotransmitter detection, especially for DA, and requirements for sensor materials are discussed. This chapter is condensed version of the theory of detection dopamine. This topic is discussed more detailed in previous theses by Palomäki [28] and Wester [29].

2.1 Electrochemical activity of neurotransmitters

Electrochemical detection of neurotransmitter is based on the electrochemical activity of the molecules. This property indicates that these compounds can undergo redox reactions. With electrochemical methods, electrons participating in these reactions are detected.

Neurotransmitters can be divided in three categories according to the ability to detect them with electrochemical methods. The first category are electrochemically active compounds that can be directly detected by the redox reactions of the target molecule. Several neurotransmitters are electrochemically active such as dopamine, norepinephrine, epinephrine, serotonin, adenosine and histamine. Many of these compounds precursors and metabolites are under this category, for example dopamine precursor L-DOPA and metabolite DOPAC. In addition to neurotransmitters, other molecules present in the brain are also electrochemically active such as ascorbic acid, uric acid, nitrite oxide and hydrogen peroxide. [13] In Table 1 a non-exhaustive list shows electrochemically active compounds present in the brain and their oxidation potentials.

The second category includes neurotransmitters that are not inherently electrochemically active. These compounds cannot be detected directly oxidizing the target molecule. However with enzymatic reaction these neurotransmitters can be measured as their consumption or reaction products are electrochemically active. For example glutamate detection requires an enzymatic reaction. [13,30] More detailed information about enzymatic detection of glutamate is discussed in thesis [31].

The third group of neurotransmitters cannot be detected with electrochemical methods. This group includes neuropeptides and some amino acid neurotransmitters. [13]

Table 1: *Oxidation potentials and concentrations of some electrochemically active compounds presented in the brain. Symbol n is the number of samples where the concentrations are measured from.*

Molecule	**Concentration** (in whole brain if not specified differently)	**Charge**	**Oxidation potential** (vs Ag/AgCl)	**Reference**
Dopamine	5-700 nM, 845 ± 66 ng/g, n= 5 [(a)]	+	+ 0.2 V	[6,13,32]
Norepinephrine	54-336 pmol/g, n= 1 [(b)]	+	+ 0.2 V	[33,34]
Epinephrine	1.2 - 9.2 ng/g, n= 3, substantia nigra [(b)]	+	+ 0.2 V	[13,35]
Serotonin	0.1-2.5 nmol/g, n= 21-25 [(b)]	+	+ 0.35 V	[13,36]
L-DOPA	4 ± 4 ng/g, n= 5 [(a)]	0	+ 0.4 V	[13,32]
DOPAC	4-5784 pmol/g, n= 1 [(b)]	0	+ 0.2 V	[13,33]
Ascorbic acid	309±47 μg/g, n=3, substantia nigra [(b)]	-	+ 0.2 V	[13,37]
Uric acid	102 nmol/g, n= 1 [(b)]	-	+ 0.3 V	[13,38]

(a) Molecules concentration was measured from postmortem rat
(b) Molecules concentration was measured form postmortem human

2.2 Electrochemical detection of dopamine

2.2.1 Oxidation of dopamine

Dopamine is electrochemically active compound as mentioned in the previous chapter. Therefore DA can be directly detected through its oxidation reaction where DA is transformed into dopamine-o-quinone (DAQ) by the loss of two electrons [39]. However, dopamine oxidation is not this straightforward phenomena. DAQ is highly reactive and it can spontaneously continue oxidation reaction [40]. Also it is possible that under alkaline solution DA polymerizes into polydopamine film [41, 42]. These reactions are problematic, because dopamine oxidation products can chemically foul the sensors surface. Adsorption of the oxidation products on the surface passivate the electrodes and therefore reduces measured redox currents [43]. Chemical fouling mechanism of DA oxidation products is not that well known phenomena and therefore it is difficult to say what exactly happens on this event. However, it is found that chemical fouling depends on concentration of dopamine and scanning speed used in

the given electrochemical method. The phenomena is reduced when DA concentration is small [41, 42] and high scanning speed is used [43, 44]. On the other hand, it is also proposed that layer of DA is needed for faster electron transfer [45].

On the oxidation pathway of dopamine, DA oxidizes first into DAQ as mentioned above. After this reaction, DAQ can spontaneously form leucodopaminechrome (LDC) through intramolecular cyclization via 1,4-Michael-type addition. In addition LDC itself oxidizes into dopaminechrome (DAC). [46] The reaction mechanisms of DA oxidation is expected to be one of the following EC [47], ECC [48], ECE [49] where E stands for electrochemical reaction and C for chemical reactions. DA can continue oxidizing further and form a polydopamine structure [40, 41, 44]. General model for polydopamine formation is eumelanin model, where suggested reaction for DA polymerization is ECECEE [50, 51]. The reaction chain is presented in Figure 1. Under alkaline solutions DA reacts into DAC as described above. DAC continues reaction through isomerization to form 5,6-dihydroxyindole (DHI) substance, which easily oxidizes into 5,6-indolequinone. Last two products in the reaction chain can undergo branching reactions at positions 2, 3, 4 and 7 (see Figure 1), which leads to formation of isomers and dimers. Problem with eumelanin model is that there aren't enough experimental evidence to support it [52].

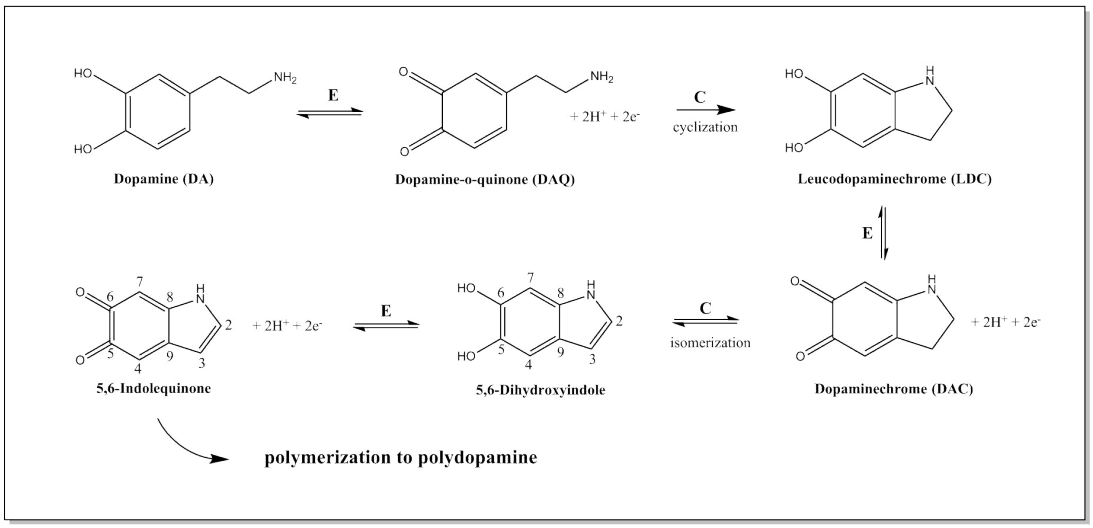

Figure 1: *Formation of polydopamine by eumelanin model. Reaction pahtway is suggested to be ECECEE [50, 51]*

In addition for eumelanin model, there are other suggested polymerization mechanisms for polydopamine. According to Dreyer et al. [53] polydopamine is formed from LDC and its derivatives such as DAC. Then again Lee et al. [54] suggested that DHI undergoes two different reaction pathways, oxidative polymerization and physical self-assembly, where DHI reacts with dopamine that is not oxidized. Resulting polydopamine is constructed from both reaction pathways products. Vecchielli et al. [55] emphasizes that resulting polydopamine structure depends on the preparation conditions, such as the starting concentration of DA and the used buffer solutions.

Depending on the initial conditions, there are three competing pathways for DA polymerization mechanism.

2.2.2 Interfering components

There are several problems to overcome before DA can be measured reliably *in vivo*. One of the major challenges are the interfering compounds present in the same brain area of interest, that oxidizes at similar potentials as dopamine [13]. Major interfering compound is ascorbic acid. It is problematic especially, because its oxidation potential is often seen at the same position as DA. As a result measured signals of DA and AA are overlapping. Additionally AA concentration can be 10^4 to 10^6 higher than DA [56, 57]. Therefore without selective electrode it is difficult to evaluate what is measured concentration of dopamine.

Ascorbic acid does not only act as interferer on DA detection. AA also catalyzes DA oxidation reaction by regenerating dopamine from its oxidation product DAQ. [39, 40, 46, 58] Due to this catalyzed oxidation reaction of dopamine, measured DA signal in presence of AA may correspond to more amplified values than bare DA signal. [39, 58]

This phenomena makes evaluation of DA concentration *in vivo* hard as the exact mechanism of catalyzed reaction of DA is unknown. On the other hand AA acts as antioxidant in physiological environment and prevents formation of polydopamine. Therefore chemical fouling of the electrode surface is expected not to be as significant issue in *in vivo* measurements. [40] It is also suggested that AA could be used as amplifier for detecting small concentration of DA [40, 58].

There are two electrocatalytic mechanism proposed for regeneration of DA in presence of AA. Commonly proposed mechanism is [39, 46]

$$DA \longleftrightarrow DAQ + 2H^+ + 2e^- \tag{1}$$

$$DAQ + AA \rightarrow DA + DHA \tag{2}$$

where DHA is dehydroascorbic acid. After oxidation of DA, DAQ is reduced back to DA in presence of AA. During reduction of DAQ, ascorbic acid oxidizes into DHA. Mechanism is presented in Figure 3.

Another proposed mechanism suggests that DA oxidizes into dopamine semiquone instead of dopamine-o-quinone [58, 59]. Then AA regenerates DA from dopamine semiquinone. Suggested reactions are

$$DA \longleftrightarrow DAsemiquinone + 2H^+ + e^- \tag{3}$$

$$2DAsemiquinone + AA \rightarrow 2DA + DHA \quad (4)$$

This theory is based on result that DA oxidation potential is pH dependent, which indicates that dopamine oxidation is $1e^-/2H^+$ process instead of $-2e^-/2H^+$ process [59].

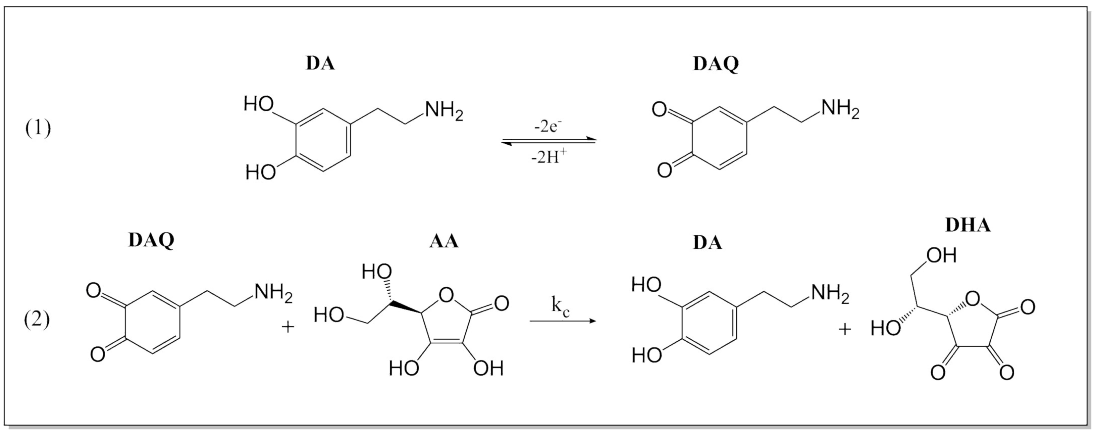

Figure 2: *Catalyzing effect of ascorbic acid. Dopamine is regenerated from its oxidation product dopamine-o-quinone in precence of ascorbic acid, where the catalytic rate (k_c) of reaction (2) is sufficiently fast that it can produce DA for the (1) reaction. [39]*

2.3 Requirements for the sensor material

To measure DA reliably in presence of interfering compounds, the sensor material need to fulfill several quality requirements. Before sensor can be implanted *in vivo*, these characteristics need to be taken under consideration for producing feasible and reliable sensor:

(1) Required *sensitivity* is determined by the lowest concentration levels of target analyte in measurement environment of interest [19]. In case of dopamine concentration can be low as 5 nM in the brain area of interest [6].

(2) *Selectivity* describes the sensors ability to detect target analyte in presence of interfering compounds [19]. For dopamine detection signals of interfering compounds are required to be separated from DA signal. Possible approaches is to shift compounds oxidation potential from dopamine oxidation potential or to prevent oxidation of these compounds on the sensors surface.

(3) *Miniatirazation* of the sensor decreases the tissue damage during implantation. Required size of the measuring head is 10 μM or less. [6] Thus the electrode material should be suitable for fabrication in this scale size. Other advantages for miniaturized sensors are improved signal-to-noise ratio and increased temporal resolution [4].

(4) *Biocompatibility.* Sensor material is safe to implant into physiological medium without foreign body or inflammation reaction. [60]

(5) *Resistance against biofouling.* To successfully measure DA *in vivo*, sensor material is required to be biocompatible in a way that interaction between sensor and the body does not affect sensors performance.

(6) *Stability* characterizes known behavior of the sensor. During measurements baseline of the sensors output stays constant and only changes in the signal are observed due to changes in DA concentration. [61]

(7) *Response time* describes sensors ability to measure concentration changes [61]. With electrochemical measurements it can be related to the DA oxidation reaction kinetics. The kinetics of the reaction must be fast enough to provide real time information of dopamine concentration and its changes.

(8) *Linearity* is the concentration range over which the sensitivity of the sensor is reliable [61]. During concentration changes the output of the sensor should be linearly dependent on the concentration.

It is a challenge to find a material that fulfills first three features. Scientists have found many materials that are either sensitive or selective, but not both at the same time. Also several materials that show promising results are not suitable for miniaturization. Thus more research is needed to find feasible material that does not only fulfill few of the presented characteristics.

Motivation for investigating nanodiamond particles is their promising properties. Nanodiamonds are new and uncharacterized material in field of electrochemical detection. As new solutions are needed for sensor development, ND may provide some possibilities as these particles are biocompatible [62], minituarizatable [10] and electroactive toward neurotransmitters [9]. Also nanodiamond sensors can be futher developed into different carbon structures as they can act as a seed layer for growth of carbon nanotubes [63].

3 Electrochemistry

3.1 Electrochemical reactions

An electrochemical reaction is a process where electron transfer (ET) occurs from one species to another. Reaction takes place at the interface of two phases and therefore is defined as a heterogeneous reaction. Commonly solid-liquid interface is used, but electrochemical reactions can occur also at the liquid-liquid interface. In case of electrode-electrolyte (solid-liquid) interface, electrochemical experiments are done in an electrochemical cell that consists of at least two electrodes, an electrolyte and an external circuit that connects the electrodes together. Two electrodes are required to ensure electroneutrality of the system as two reactions always take place in an electrochemical system. These reactions are oxidation (5) and reduction (6):

$$Red \rightarrow Ox + ne^- \tag{5}$$

$$Ox + ne^- \rightarrow Red. \tag{6}$$

During oxidation Red reacts to Ox by the loss of n electrons. Reduction is the reverse reaction of oxidation as Ox reduces to Red by gaining n amount of electrons. These reactions are also referred as anodic and cathodic reaction. Redox reactions are driven by the change in Gibbs free energy of system ΔG. Magnitude of ΔG describes the probability of how likely the system proceeds towards its equilibrium state. The more negative value ΔG gets, the more likely the redox reactions occur. The cell potential resulting from the reactions between two electrodes is given by

$$\Delta E = \frac{-\Delta G}{nF}, \tag{7}$$

where F is the Faraday constant (C mol^{-1}). [64] In an electrochemical system redox reactions can occur spontaneously when ΔG value is negative and chemical energy is released. These cells are described as galvanic cells. When redox reactions are forced by using external energy, the system is referred to electrolytic cell. Electrochemical measurements are electrolytic because the wanted reactions are forced by using external energy. [65]

Kinetics of the electrochemical reactions defines how quickly the system proceeds towards equilibrium state. During redox reactions a current j passes through the electrode due to electron transfer within the reacting species in the solution. Quantity of current is related to the rate of the reaction and therefore it describes the kinetics of the system. This is known as the Faraday's law

$$j = nFr, \tag{8}$$

where j (A cm^{-2}) is current density and r is the rate of reaction (mol cm^{-2} s^{-1}). [65] The electrode reaction $Ox + ne^- \leftrightarrow Red$ is composed of a series of steps (see Figure

3) where the slowest steps determines the overall rate of reaction. This is also known as the rate-determining step. The major processes that affect the rate of electrode reaction are mass transfer of the species from bulk solution to the electrode surface, adsorption of the species and electron transfer at the electrode, which is dependent upon potential of the system. [64, 66]

It can be established that overall electrode reaction is dependent on cell potential, mass transfer of solution species and electrode properties such as kinetics of ET. These phenomenas are described in more detail in the upcoming sections. More profound theory and derivation of presented equations can be found from works of Bard [66] and Compton [67].

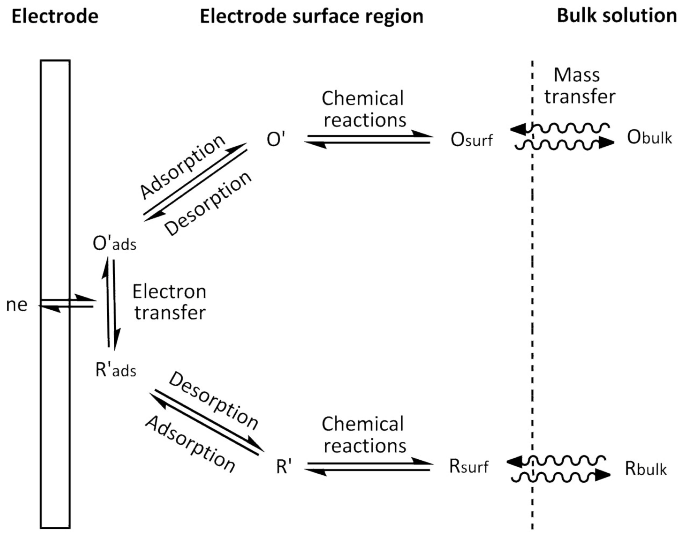

Figure 3: *Different steps of electrode reaction. In some systems chemical reactions may occur before or after electron transfer. Reactions might be for example dimerization or catalytic decomposition.*

3.1.1 Electric double layer

Electrochemical reactions are heterogeneous as they take place at the electrode-electrolyte interface. In the electrode surface region, electrolyte solution structure deviates from the bulk solution due to the electric interaction between electrode and electrolyte. This interface is called the electric double layer (EDL) that consists of several layers.

The inner layer closest to the electrode surface contains both adsorbed solvent molecules and specifically adsorbed anions. The electric locus of the anion sets the thickness of the inner layer. This locus is called inner Helmholtz plane (IHP). Next to the IHP is the outer Helmholtz plane (OHP) that contains more solvent molecules and electrostatically adsorbed solvated cations. In these Helmholtz planes molecules are in stationary state. [64, 66]

Beyond the OHP is the diffuse layer which extends from OHP into the bulk solution. In this layer molecules are distributed due to the effect of thermal motion and weak electrostatic forces. The diffuse layer generally contains anions and cations. The thickness of this layer depends on the total ionic concentration in the solution and it is of the order of 10 to 100 μm. [65] Structure of the EDL is illustrared in Figure 4(a).

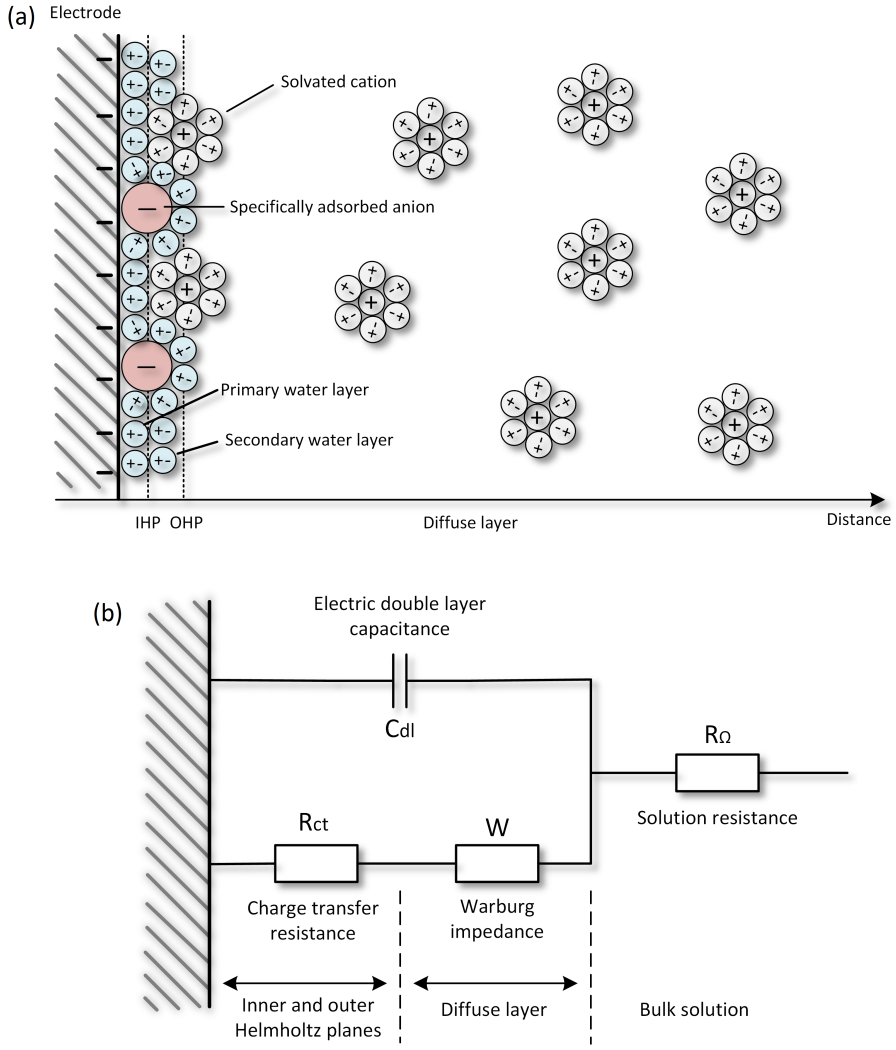

Figure 4: *Schematic diagrams of (a) electric double layer structure and (b) its equivalent circuit. In the circuit, components R_Ω and W are added in addition to EDL structure. R_Ω is the bulk solution resistance and W is the Warburg impedance, which describes the mass transport of the species.*

Electrochemical events at the electrode-electrolyte interface are either Faradaic or non-Faradaic processes. Processes abide by Faraday's law, where quantity of reacted species and measured current are interdependent. In Faradaic processes the quantity of current changes when potential is changed in the system. Whereas in non-Faradaic processes electron transfer does not occur. The surface itself is affected by the

change of the potential, but no current over the interface is measured. Non-Faradaic processes are for example adsorption and desorption. [64]

To understand how potential affects the electric double layer, electrode reactions at the interface can be modeled with a simplified equivalent circuit. In the equivalent circuit, Faradaic processes such as ET is represented by the resistance R_{ct} and non-Faradaic processes such as double-layer capacitance C_{dl}. [64] An equivalent circuit is shown in Figure 4(b), where mass transfer and the effect of bulk solution are also included. The effect of mass transfer and solution resistance are described in more detail in chapters 3.1.4 and 3.2.2.

3.1.2 Electrode potential

The cell potential E over electrodes was defined with equation (7). This potential describes a situation where a infinitely large impedance is set between the electrodes and no current passages through the system. E is defined with several names, for example equilibrium cell voltage, electromotive force or open circuit voltage. In case of defining potential E in standard state, it is referred to as standard electrode potential E^o. In this state the pressure of surrounding gases is 1 atm, temperature 25°C and activity a of the species is 1. However, equation (7) is inconvenient to describe equilibrium state as the system rarely is in standard state. [64] With the Nernst equation, the equilibrium potential E_{eq} is evaluated when temperature and activity of the species deviate from standard state. It is expressed as

$$E_{eq} = E^o + \frac{RT}{nF} ln \frac{a_{ox}}{a_{red}}, \tag{9}$$

where R (J mol^{-1} K^{-1}) is the ideal gas constant and T (K) is temperature [67]. In standard state Nernst equilibrium potential is $E_{eq} = E^o$. However in Nernst equation activity a of the species are rarely know. Therefore using activity coefficient γ is more convenient. With γ activity is defined as $a_i = \gamma_i c$, where c (mol/l) is the concentration of the species i. With γ Nerst equilibrium potential is expressed as

$$E_{eq} = E_f^o + \frac{RT}{nF} ln \frac{c_{ox}}{c_{red}}, \tag{10}$$

where $E_f^o$is the formal potential

$$E_f^o = E^o + \frac{RT}{nF} ln \frac{\gamma_{ox}}{\gamma_{red}}. \tag{11}$$

Formal potential E_f^o is the quantity measured in electrochemical cell. [66]

When external potential is applied over the electrochemical cell, the potential of the electrode deviates from equilibrium. In this state the electrode is polarized. Overpotential of the electrode is defined as

$$\eta = E_\eta - E_{eq}, \tag{12}$$

where E_η is the polarized potential of the electrode. In case of $E_\eta > E_{eq}$ anodic reactions take place, whereas in state $E_\eta < E_{eq}$ catodic reactions take place. Polarization of the electrode is a result of slow electrode reactions. Reaction kinetics are mainly limited by electron transfer and mass transfer. If the speed of the reaction was infinitely fast, electrode would not polarize and the potential of the electrode would be E_{eq}. [64, 66]

3.1.3 Reaction kinetics

Faraday's law defined in equation (8) state that the amount of reacted substance at the electrode is directly proportional to the quantity of electrical charge passed through the electrode. The reaction speed r describing the kinetics of redox reaction at the electrode surface is given by

$$r = k_c c_{ox} - k_a c_{red}, \tag{13}$$

where k (cm s^{-1}) is the electrochemical rate constant and c is the concentration of oxidized and reduced species. Subscripts c and a indicate cathodic and anodic reactions respectivly. At the equilibrium potential E_{eq} there is no net current i flowing trough the cell indicating that the anodic and cathodic reactions occur at the same rate, where $r = 0$ and $c_{ox} = c_{red}$. Thus

$$k^0 = k_c(E = E_{eq}) = k_a(E = E_{eq}), \tag{14}$$

where k^0 is the formal reaction rate constant. [65] k^0 is an important parameter as it describes kinetic facility of a redox couple on the electrode surface [66]. Characterization of electrode kinetics is done by defining k^0. Relation between the formal reaction rate constant and electrode kinetics will be addressed more thoroughly in section 3.2.4.

If the electrode is polarized, a net current i passages through as $k_c \neq k_a$. The relation between overpotential and net current is given by the Butler-Volmer equation

$$i = i_c - i_a = nFAk^0 \left[c_{ox} e^{\alpha F \eta} - c_{red} e^{(1-\alpha)F\eta} \right], \tag{15}$$

where α is charge transfer coefficient. Butler-Volmer formula is the most fundamental equation in electrochemical kinetics. It is used to describe heterogeneous reaction kinetics, when the reaction is limited by the electron transfer. [66]

3.1.4 Mass transfer

The redox reaction can only occur if the substance of interest is transported to the electrode-electrolyte interface from the bulk solution. Mass transport can happen through three different modes:

(1) *Diffusion* - movement of chemical species from higher concentration to lower concentration driven by the concentration gradient.

(2) *Migration* - movement of charged particles in presence of an electric field.

(3) *Convection* - natural or forced flow of solution. Natural flow is caused by density differences in the solution and forced flow is caused for example by mixing the solution externally.

Electrochemical systems are designed so that contributions from migration and convection are negligible. Therefore mass transport is mainly controlled by diffusion. [64, 66]

The electrode-electrolyte interface a diffusion layer is formed with thickness δ. As a result of the redox reactions the concentration of the solution changes only in this layer. Outside of the diffusion layer the concentration of the electroactive species is maintained at the value of bulk concentration c^* (see Figure 5). Diffusional flux J (mol cm^{-2} s^{-1}) of the electroactive species is derived from Fick's first law, where the flux J at point x is presented by

$$J(x) = \frac{i}{nFA} = D\frac{dc}{dx}, \tag{16}$$

where D is the diffusion coefficient (cm^2 s^{-1}) and c is the concentration of the species at point x. At the interface of diffusion layer and bulk solution, the distance from the surface is $x = \delta$. Therefore diffusional flux J is defined as

$$J = D\frac{c^*}{\delta}. \tag{17}$$

Corresponding current at $x = \delta$ is derived from equations (16) and (17)

$$i = \frac{nFADc^*}{\delta} = nFAm_T c^*, \tag{18}$$

where A (cm^2) is the surface area of the electrode and the term

$$m_T = \frac{D}{\delta} \tag{19}$$

is the mass transport coefficient (cm s^{-1}). Based on m_T diffusion of the species to the surface is controlled by the thickness of the diffusion layer. Higher flux and redox current is achieved when the thickness of the layer decreases. [67]

In addition, m_T has same units as the electrochemical rate constant k^0. Thus direct comparison can be done between these two quantities. The relation between the relative speeds of electron transfer and mass transport provides information on the electrode kinetics. This will be discussed further in section 3.2.4.

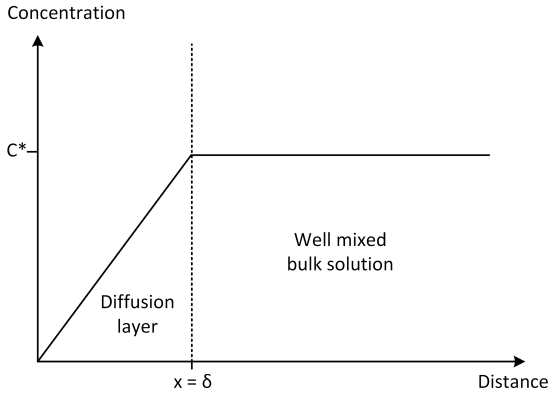

Figure 5: *Diffusion layer model, where concentration of the specie is presented as distance from the electrode surface.*

3.2 Cyclic voltammetry

In this chapter cyclic voltammetry is described in more detailed as this method is used in this work for the characterization of the ta-C+ND samples. The goal is to present basics of CV and explain what information the experimental data provides.

3.2.1 Background

Cyclic voltammetry is a potential sweep method where a linear potential is applied to the electrode as function of time. The waveform of the potential is illustrated in Figure 6(a), where E_1 is the starting potential. From this value potential is linearly increased to potential E_2. At time t_s when E_2 is attained, the potential is linearly decreased back to the starting value E_1. The rate at which the potential changes is called the scan rate v (V s^{-1}). Potential E at the electrode can be written as [67]

$$0 < t < t_s, \quad E = E_1 + vt, \tag{20}$$

$$t > t_s, \quad E = E_1 + 2vt_s - vt. \tag{21}$$

During CV experiment response current is measured as function of potential. The obtained diagram is called a cyclic voltammogram. In Figure 6(b) basic features of the voltammogram are presented. When potential is swept into positive direction from E_1 to E_2, oxidation of the solution species is seen as an anodic current peak. When scanning from E_2 into negative direction, reduction of the oxidized species is shown and cathodic current is measured. [67] If a simple electrolyte environment is considered containing only dopamine, during forward scan DA oxidizes into DAQ and at the reverse scan DAQ reduces back to DA. Potential interval values $[E1, E2]$ V is selected so that oxidation and reduction reactions of interest is shown.

The shape of the current peaks is a result of changing concentration of the reacting species at the electrode surface as function of time. For example when the potential achieves a value in which oxidation reaction starts, concentration gradient is formed at the surface. As the forward scan potential increases, the reaction speed (current) is increased too.

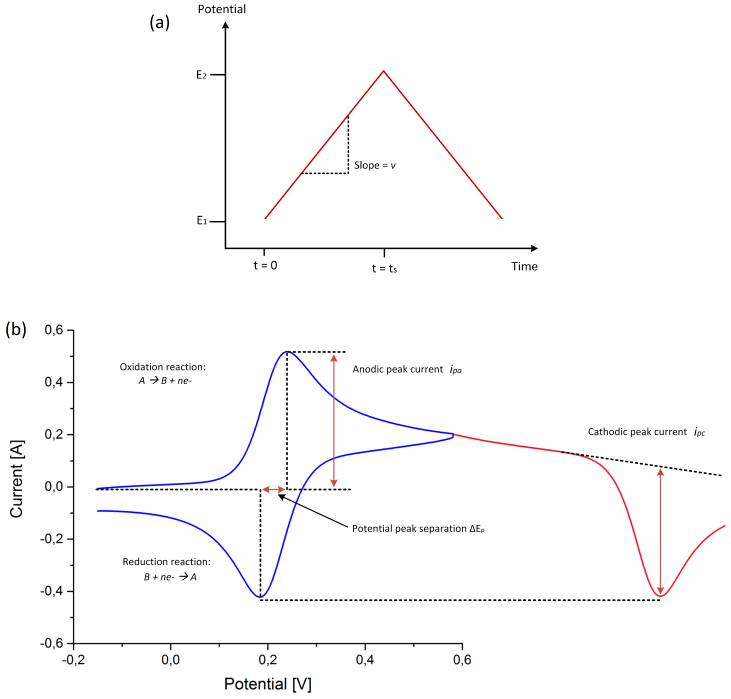

Figure 6: *(a) The potential wave form applied into electrochemical cell and (b) measured current as function of potential in cyclic voltammetry. For the cathodic peak evaluation current is presented as function of time (red line).*

This also affects the concentration gradient. The current and concentration gradient will increase until the gradient at the surface has reached its maximum. At this point peak current value i_{pa} is achieved. After this, the concentration gradient does not change, but current will decrease as the diffusion layer at the electrode increases. [64, 67]

3.2.2 Experimental setup

In electrochemical measurements a three electrode system is used including a working electrode (WE), a reference electrode (RE) and a counter electrode (CE). Working electrode is the electrode of interest. For example in this work WE is the ta-C + ND electrode where the oxidation of DA takes place, so the potential of WE is changed. External potential is applied between working electrode and reference electrode, where RE is a material that does not polarize easily. Therefore RE acts as a reference potential for the electrochemical system. Common reference electrode is silver-silverchloride (Ag/AgCl).

Current passing through the electrochemical cell is measured between working electrode and counter electrode. Because CE does not affect the performance of the WE, any conductive material is suitable for counter electrode. For example platinum and graphite are generally used as CE. However it is required that the surface area of CE is large enough compared to WE so that the area does not limit the amount of reacting species and thus the current.

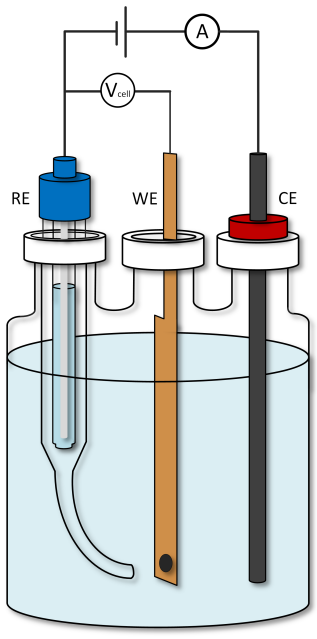

Figure 7: *Electrochemical cell with a three electrode system. External potential is applied between working and reference electrode, whereas the current arising from redox reactions is measured between working and counter electrode.*

The three electrode system is used instead of the two electrode system because in electrochemical measurements it is important to accurately control the applied potential. In a two electrode system RE is also used as a CE. Thus current and potential are measured with the same electrodes. The current passing through may affect the potential stability. Therefore 3 electrode system is more reliable for accurate measuring of the potential. However it is required that reference and working electrode are placed near each other in the cell. The solution between RE and WE acts as a resistance R_Ω that causes an error to the applied potential (see Figure 4). This phenomena is called IR-drop which can be reduced by using conductive electrolyte solution and placing RE close to WE. The RE is placed in the Luggin capillary filled with solution. [64, 65] Configuration of three electrode system with Luggin capillary is illustrated in Figure 7.

3.2.3 Water window and double layer capacitance

The water window defines the potential window limits where no Faradaic currents occur. This window is referred as water window because generally water is the solvent in the solution of the electrochemical cell. Potential limits are set by the electrolysis of water where the evolution of oxygen starts at the anodic limit and hydrogen at the cathodic limit. Water window and electrolysis of water are shown in Figure 8.

Defining working electrode's water window is important as it show's the potential range where WE is stable. This is essential when the purpose of the working electrode is to measure an analyte of interest from the solution. For example if the electrode's water window is [-0.6, 0.2] V it is not suitable for detecting dopamine as its oxidation potential generally is +0.2 V. In this type of case Faradaic response of DA oxidation is covered under oxygen evolution.

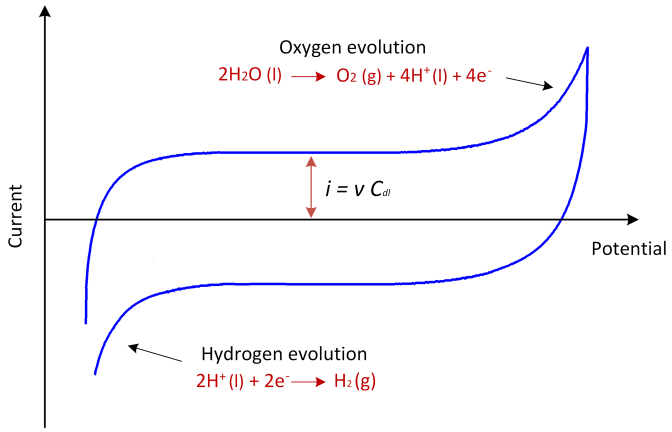

Figure 8: *Voltammogram of water window with oxygen and hydrogen evolution.*

If the working electrode has its own characteristic Faradaic peaks, these can be also seen from the water window measurements if pure solution is used. Generally measurements are done in diluted acids such as sulfuric acid (H_2SO_4) or perchloride acid ($HClO_4$).

Water window is also used for determining double layer capacitance C_{dl}. With cyclic voltammetry when linear potential sweep is applied, the non-Faradaic current of the system is

$$i = vC_{dl}[1 - e^{-t/R_{ct}C_{dl}}] \tag{22}$$

when at time t = 0 current i = 0. [66] Current quickly attains a steady state value vC_{dl} as term $exp(-t/R_{ct}C_{dl})$ approaches zero as function of time. From here it is seen that the steady state current of water window is

$$i = vC_{dl}. \tag{23}$$

With CV i and v are known quantities, thus double layer capacitance C_{dl} can be evaluated.

3.2.4 Measuring electrode kinetics

CV is a useful tool for characterizing the kinetics of the electrode of interest. As stated in previous sections, the formal reaction rate k^0 of electron transfer describes the electrode kinetics. The electron transfer process is usually referred to 'slow' or 'fast' based on the rate costant k^0. From a voltammogram, this seen as the change of anodic and cathodic potential peak separation ΔE_p. In case of 'slow' behavior ΔE_p values are significantly larger than in 'fast' behavior. Estimating k^0 from ΔE_p is discussed more in upcoming page.

Defining the behavior of electrode kinetics is done in relation to mass transport. In case of 'fast' kinetics the system is described as electrochemically reversible, whereas in 'slow' kinetics the system is described as electrochemically irreversible. The relation between k^0 and mass transport coefficient m_T is stated as

- reversible, when $k^0 \gg m_T$,
- quasi-reversible, when $k^0 \sim m_T$ and
- irreversible, when $k^0 \ll m_T$. [67]

In reversible behavior, electron transfer at the electrode of interest is fast enough that all electroactive species brought at the surface are immediately oxidized or reduced. Therefore the electrode reaction is limited by mass transfer. Estimated ΔE_p value for reversible system is $59/n$ mV at 25°C [65]. In case of irreversible behavior, electrode kinetics is limited by the electron transfer process itself. Species are brought to the

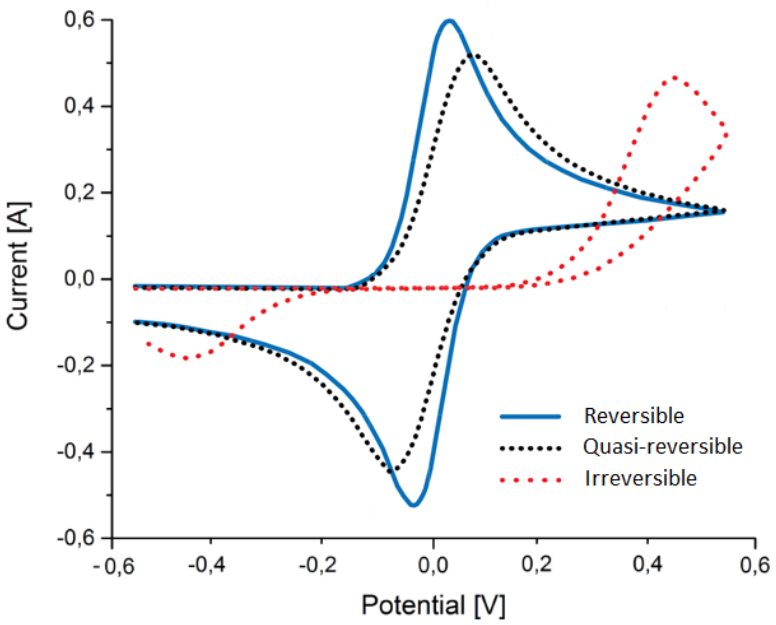

Figure 9: *Effect of the formal reaction rate constant* k^0 *on potential peak separation* ΔE_p *, where* $k^0{}_{reversible} > k^0{}_{quasi-reversible} > k^0{}_{irreversible}$.

electrode surface much faster than they can actually react. The quasi-reversible behavior is between reversible and irreversible kinetics. Effect of electrode kinetics on potential peak separation ΔE_p is illustrated in Figure 9

Based on equation (19), rate of mass transport is defined by the thickness of the diffusion layer. In CV the mass transport coefficient m_T is also dependent on the used scan rate v. Relation between mass transport coefficient m_T and scan rate v is

$$m_T \sim \sqrt{D\frac{Fv}{RT}}. \tag{24}$$

From this relation and equation (19) it can be understood that with slow scan rates mass transport is slower as the diffusion layer thickness δ is larger. When applying higher v, thickness of δ decreases and the mass transport increases. In this case more species are brought to the surface from the bulk solution. As stated before high rate of m_T leads to more irreversible behavior if the rate of electron transfer is not sufficiently high. Therefore it can be stated that high v leads to greater electrochemical irreversibility meaning that even reversible systems turns into irreversible with high enough scan rates. [67]

However in this work scan rates are max 1 V/s, thus reversible systems generally stay reversible. If measured ΔE_p is dependent on the used scan rate, system behavior is defined as quasi-reversible. In other words electrode kinetics is affected by the electron transfer kinetics. Estimating the formal reaction rate constant k^0 from the

voltammogram can be done with the Nicholson method [68]. In this method potential peak separation ΔE_p from experimental data is related to the parameter Ψ, which is defined as

$$\Psi = \frac{k^0 (D_0/D_R)^{\alpha/2}}{\sqrt{\frac{\Pi D_0 v n F}{RT}}} \tag{25}$$

where D_0 is the diffusion coefficient of oxidized specie, D_R is the diffusion coefficient of reduced species and α is generally 0.5 at 25°. Peak separation ΔE_p corresponds to a certain value of Ψ (see table 2). When Ψ is known, the formal reaction rate constant k^0 can be estimated from the equation above assuming that other constants are also known. However, Nicholson method is most suitable for quasi-reversible systems where $\Psi < 1$. As shown in table 2, the error in estimating k^0 decreases with larger peak separation as the variation in the parameter Ψ is smaller.

Electrode kinetics are measured with CV using different scanning rates with outer sphere probes as electroactive species. These probes are usually one solvent layer away from the surface and the electron transfer of these probes are not dependent on the surface chemistry of the electrode. Therefore outer sphere systems can be treated in a more general way than inner sphere system, where chemical interaction between probe and surface are important. As outer sphere probes are not affected by the surface chemistry, they give more information on the actual electron transfer over the electrode regardless of the surface chemistry. Outer sphere probe is for example ruthenium. [66]

Table 2: *Dependency of peak separation ΔE_p on parameter Ψ at temperature 25° C. [68]*

Ψ	n x ΔE_p (mV)
20	61
7	63
6	64
5	65
4	66
3	68
2	72
1	84
0.75	92
0.5	105
0.35	121
0.25	141
0.1	212

3.2.5 Measuring dopamine and ascorbic acid

Cyclic voltammetry is the method used for detecting dopamine at the electrode of interest, but it is also used for characterizing the electrode properties. For dopamine detection, essential characteristics are high sensitivity toward DA and ability to separate DA from interfering components. Sensitivity of the electrode is determined measuring different concentrations of DA in phosphate buffer solution (PBS). Selectivity is determined using PBS that contains both DA and an interfering component, which in this work is ascorbic acid.

As both dopamine and ascorbic acid redox reactions are inner-sphere, there are strong interaction between compound and the electrode surface. In this case reactions involve specific adsorption of the analyte. [45,66] Therefore surface chemistry of the electrode has important role in detecting of DA. With CV surface chemistry of these systems cannot be evaluated, but it gives more information about the interaction between the surface and the analyte. However, with different scanning rates it is possible to estimate the electrode kinetics of the system. As stated in section 3.2.4, increasing the scan rate v it is possible to see if the peaks separation ΔE_p changes. If so, the speed of electron transfer is not sufficiently high and it is affected by the scan rate v. Also evaluating the relation of anodic current peak with scan rate, it can be established if electrode reaction is either adsorption or diffusion controlled. If i_{pa} is directly proportional to v, the reaction is adsorption controlled. If i_{pa} is directly proportional to square root of v [65], then the reaction is diffusion controlled [67].

4 Carbon materials for dopamine detection

Several carbon allotropes have been investigated as a sensor material for detection of dopamine, such as glassy carbon [69], graphene [7, 70, 71], carbon nanofibers [11], carbon nanotubes [26, 72, 73], tetrahedral amorphous carbon [22], boron doped diamond [73, 74] and pyrolytic graphite [75]. Every carbon allotrope has its own characteristic properties. However it is difficult make comparison between different carbon allotropes as materials under same category are fabricated with different parameters. For example CNT electrodes can be fabricated by growing nanotubes directly on the substrate for example with CVD and PECVD [11, 26] or preparing CNT-paste by mixing mineral oil and commercial carbon nanotubes [76]. Thus, it is highly unlikely that the properties of the CNT electrodes are the same. Additionally carbon-based electrodes are mixed with polymers or metallic particles [74], which further changes properties of the material.

Another problem with the found literature is that there is no protocol for DA measurements. Generally cyclic voltammetry is used to measure high concentrations of dopamine to state if the carbon electrode of interest can detect DA. Then the actual evaluation of electrodes sensitivity and selectivity towards DA is carried out with differential pulse voltammetry (DPV). [69–71, 75] In DPV external voltage is applied as series of pulses with increasing amplitude, where current is sampled just before the pulse and end of the pulse to remove capacitive charge (non-Faradaic current) from the measured current [66]. Thus lower concentrations of DA can be detected with DPV. Generally sensitivity is stated as a theoretical value called limit of detection (LOD) [75]. This value is calculated from higher measured DA concentrations. Therefore LOD does not describe the the real performance of the electrode in experimental conditions. Furthermore DPV time resolution is considerably lower [6, 13] when compared to CV, which enhances this methods selectivity as there is more time for the redox reactions to occur. As the DPV time resolution is low, it is not suitable method for *in vivo* where the measured events are in sub-second timescale. Therefore electrode properties determined with DPV do not meet the requirements for *in vivo* measurements.

For the reasons stated above, a non-exhaustive list of selected publications reporting different carbon-based materials used for DA detection is presented in table 3. The aim is to illustrate (i) variety of investigated carbon materials and (ii) how experimental and theoretical values differ from each other. From table 3 it can be seen that carbon nanotubes are selective material with CV. However sensitivity is not investigated as high concentrations of DA is used. Only in one study sensitivity is measured with CV, where the lowest detected DA concentration is 500nM. Furthermore pyrolytic carbon [75] and some graphene [69, 71] electrodes are selective in presence of AA. However in these papers sensitivity is not determined experimentally. From these studies it can be seen that theoretical detection limit for DA is low, but actual concentration used in experiments are remarkably higher.

Table 3: *A non-exhaustive list of different carbon based materials used for dopamine detection in precence of ascorbic acid. Presented concentration for DA is the lowest detected concentration with CV.*

Electrode material	**DA** (μM)	**Detection limit** (μM)	**AA** (μM)	**Selective** [c] (yes/no)	**Reference**
Glassy carbon (GC)	100	-	1000	no	[69]
Nitrogen doped graphene + GC	1000	0.25 [a]	1000	(d)	[70]
Electrochemically reduced graphene oxide (GO) + GC	500	0.5 [a]	5000	yes	[71]
3D graphene nanoflake	100	0.17 [a]	1000	yes	[69]
Boron doped diamond (BDD)	200	-	1600	no	[73]
Hydrogen terminated BDD	50	-	1000	no	[74]
CNF	1000	-	2000	no	[73]
Edge plain pyrolytic graphite (PG)	40	0.09 [a]	40	yes	[75]
Multi-walled nanotube (MWTN) + graphite	20	-	1000	yes	[72]
MWNT	110	-	1780	yes	[73]
ta-C	10	-	1000	no	[11]
ta-C+CNT	0.5	0.0013 [b]	1000	yes	[26]
ta-C+CNF	0.5	-	1000	no	[11]
ta-C+ partially reduced GO	0.01	0.0026 [b]	1000	no	[77]

(a) Measured with DPV
(b) Measured with CV
(c) Selectivity is determined by using CV
(d) DA and AA were not measured simultaneously

5 Detonation nanodiamonds

5.1 Synthesis of nanodiamonds

Nanodiamonds (ND) from detonation origin are produced by detonation of solid explosives with a negative oxygen balance in non-oxidizing atmosphere. The resulting product is called detonation soot, which contains a mixture of nanodiamond particles with diameter of ∼4-5 nm, other carbon allotropes and impurities. To gain high content of nanodiamond particles, post-synthesis steps are needed to separate non-diamond carbon and impurities from the detonation soot. This requires use of strong liquid oxidants. [78,79] The structure and surface chemistry of ND is strongly affected by every production step. Therefore the main steps of detonation synthesis and post-synthesis are described in more detail during the following chapters.

5.1.1 Detonation synthesis

In detonation synthesis, the explosive itself provides both carbon source and energy for the formation of detonation soot. Usually a mixture of 2,4,6-trinitrotoluene and hexagon is used in a ratio from 40/60 to 70/30. [1,78] Synthesis is carried out in a closed detonation chamber (Figure 10) filled with a cooling medium. This medium can be an inert gas or water (ice). When inert gas is used, process is referred as 'dry' synthesis. Respectively when water is used, process is called 'wet' synthesis. [80]

Synthesis of ND particles are divided in four different stages according to the motion of the shock wave after detonation of an explosive charge [81]:

(1) The detonation of the explosive charge. During this stage nanodiamond particles are formed. The temperature and pressure of detonation wave corresponds to the region of thermodynamics of stability of diamond (P $\geq$ 10 GPa, T$\geq$3000 K) [79].

(2) The flight of the explosion products (EPs) into the undisturbed cooling medium. At this stage EPs temperature is quickly decreased via gas-dynamic cooling.

(3) The shock wave is reflected from the chamber walls. Reflection produces circulation and turbulent motion of the EPs with the cooling medium. During this stage temperature increases.

(4) Heated EP-medium mixture is cooled down rapidly by a cold outer shell.

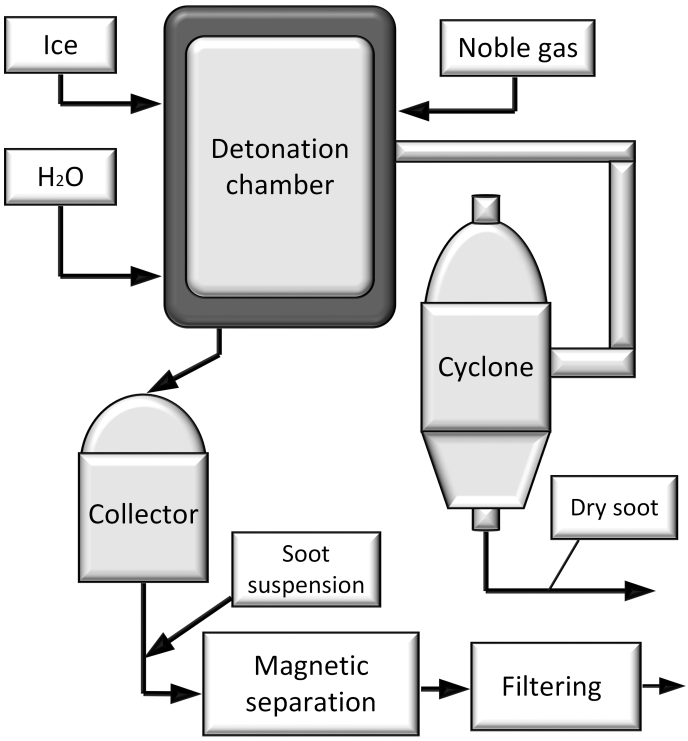

Figure 10: *Schematic diagram of a detonation chamber.*

Average temperature and time dependency of these stages is presented in Figure 11. From this figure, it can be seen how different cooling mediums affect temperature during different stages. During stage (2), highest cooling rate is observed in vacuum due to fast scattering of the EP. However, after the shock wave reflection temperature in vacuum arises close to detonation temperature. For this reason no solid phase carbon is left after synthesis. Therefore vacuum is not used as a cooling medium. [81]

The cooling kinetics of detonation synthesis is important parameter because it determines structure and composition of the particles in the detonation soot. After the first stage of detonation, the pressure and and temperature go trough the diamond region of kinetics instability. In this region diamond starts to transform into graphite. To preserve diamond phase of the particles, high cooling rate (3000-4000 K/min) is required for the detonation synthesis. Formation of sp^2 carbon cannot be prevent completely, but with higher cooling rate there are less time for the graphitization of the sp^3 particles. [78]

In the detonation soot, ND particles are covered with sp^2 carbon shells. It is shown that the shell thickness differ between 'dry' and 'wet' synthesis [82]. During 'dry' synthesis (see Figure 12) EPs goes through the unstable region of diamond slower than in 'wet' synthesis. Therefore the thickness of sp^2 carbon shell is greater in 'dry' synthesis.

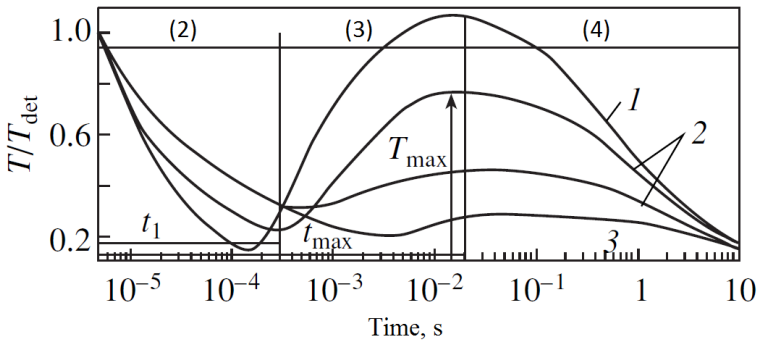

Figure 11: *Average EPs temperature during detonation stages in different cooling mediums: (1) explosion of an explosive charge in vacuum, (2) explosion in a gaseous medium, and (3) explosion of an explosive charge surrounded by a water shell.* T_{det} *= 3270 K is the temperature of detonation (stage 1). [81]*

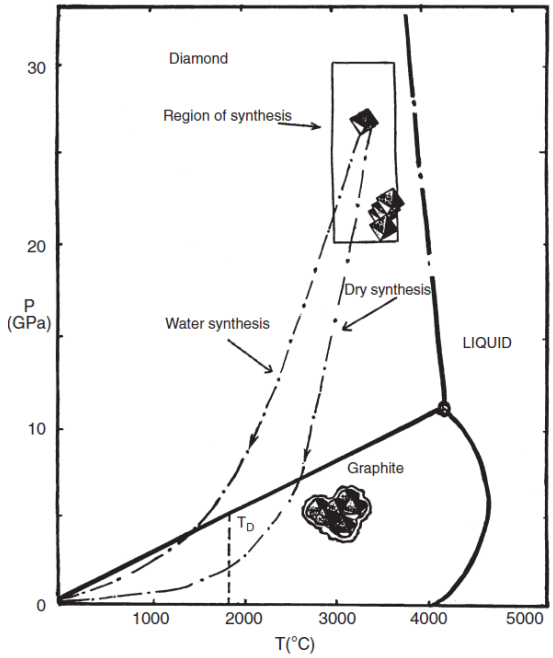

Figure 12: *P-T phase diagram for carbon and the cooling kinetics of explosion products in the case of 'dry' and 'wet' synthesis [78].*

5.1.2 Post-synthesis

With optimal synthesis conditions, detonation soot can contain 75wt% nanodiamond particles [79]. The rest of the detonation soot is sp^2 hybridized carbon and incombustible impurities such as metals and oxides. Metal impurities are originated from the detonation chamber steel walls and the used explosive charge. [83] Due to high content of impurities, purification of detonation soot is required to gain pristine nanodiamond particles.

Post-synthesis treatment of nanodiamonds is the most complicated and expensive process in making pristine ND due to use of strong liquid oxidants. Chemical purification step is based on the fact that sp^2 carbon is oxidized easier than sp^3 carbon [84]. Several types of liquid oxidants are used for removing sp^2 carbon and incombustible impurities from detonation soot, such as HNO_3, a mixture of H_2SO_4 and HNO_3, $K_2Cr_2O_7$ in H_2SO_4, KOH/KNO_3, Na_2O_2, HNO_3/H_2O_2 or $HClO_4$ [78, 79, 83]. The most effective purification method available on industrial scale is based on using aqueous solution of nitric acid. This purification process includes generally 10 steps [78, 80]:

(1) *The preparation of detonation soot* for chemical purification. This includes mechanical removal of larger debris by sieving, magnetic separation and drying to a definite humidity.

(2) *The preparation of aqueous solutions of nitric acid.* Solutions are prepared from fresh concentrated acid and recycled acid from the purification process.

(3) *The preparation of mobile homogenized detonation soot suspension* in aqueous solutions of nitric acid.

(4) *Thermal oxidation of the suspension* in a continuous mode under high pressure (8-10MPa). Oxidation is done in temperature 240°C. During this process sp^2 carbon is gasified, possible organic impurities are decomposed and metal impurities are transformed into water-soluble salts.

(5) *The separation of oxidation products.* ND suspension is separated from nitric acid and gaseous products (destruction products and nitric oxides) by sedimentation. Nitric acid is returned for recycling, destruction products are subjected to re-oxidation by air and nitric oxides are removed to acidic adsorption.

(6) The nitric acid recycle, where nitric oxides are re-oxidized and higher oxides are absorbed to produce absorption acid.

(7) *The ND washing from the acids* in de-ionized water.

(8) *Waste processing.*

(9) *The production of normalized stabilized ND suspensions in distilled water.* The final commercial ND product can be in an aqueous solution or a water-organic medium.

(10) *The production of dry homogeneous ND powder.*

Industrial purification process discribed above is illustrated in Figure 13.

After purification, the final ND product still contains small fraction of non-diamond carbon. Also nanodiamonds surface is functionalized due the oxidative chemical treatments. The resulting ND purity can be high as $\geq$ 98.5 wt% [80]. These

residuals give arise to electrostatic interaction and covalent bonds between ND particles. [84, 85] Therefore agglomeration takes place in ND products, specially in dry homogeneous ND powders. Size of the aggregates varies between submicron and micron particles. [78] Deagglomeration of the ND aggregates can be done with ultrasonic treatment, shock waves or by a milling process [78, 85].

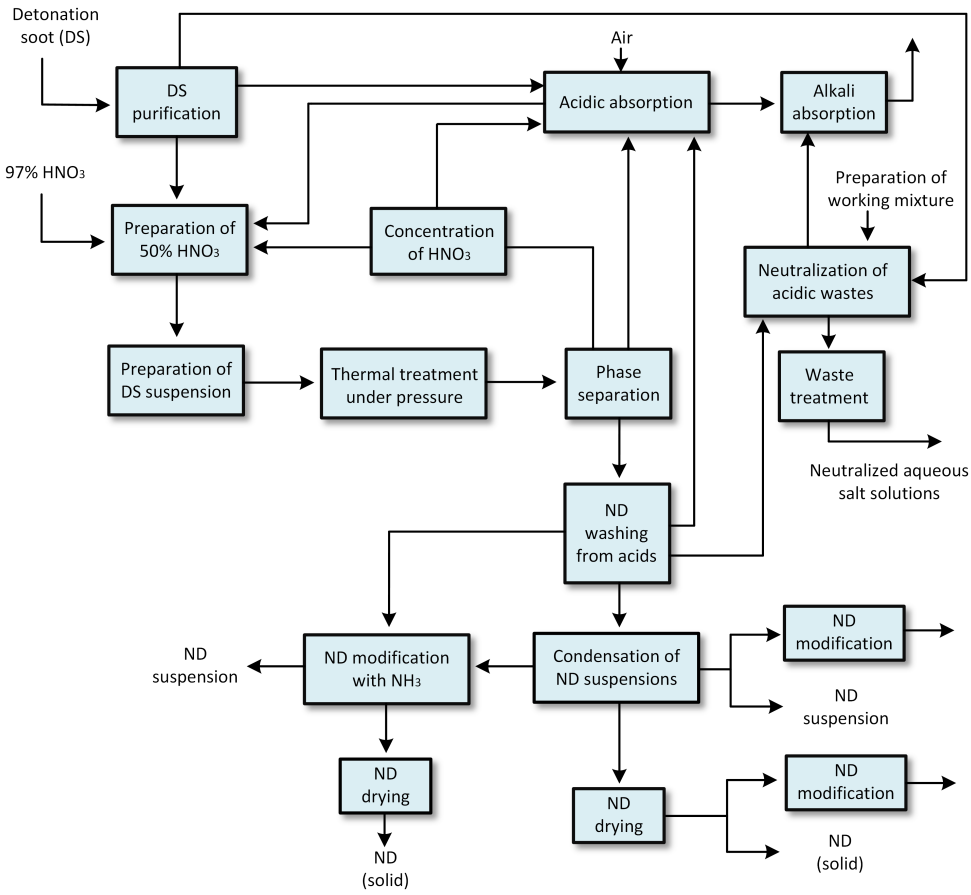

Figure 13: *Block diagram from nitric acid purification process. Modified from [78].*

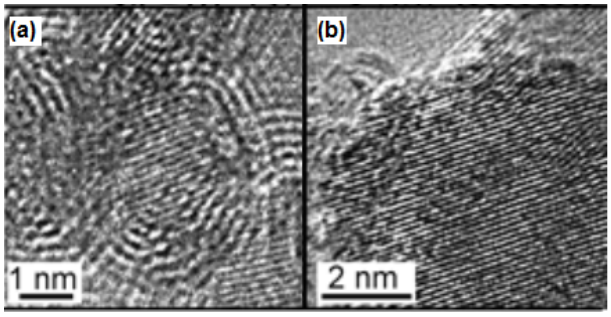

Figure 14: *HRTEM images of (a) raw detonation soot containing non-diamond structures and (b) purified nanodiamond powder [86].*

5.2 Structure of nanodiamonds

Nanodiamond structure and surface chemistry is heavily affected by every synthesis step. So it is important to understand that characteristics of each ND product is a result of its detonation synthesis conditions and purification method. However, every nanodiamond particle contain these three structural elements (Figure 15):

(1) A core of sp^3 crystalline diamond with a diameter of ∼4-6 nm. The core consist 70-90 % of all carbon atoms. [78, 80]

(2) Carbon shell around the core with thickness around 4-10 Å. This outer layer contains 10-30 % of carbon atoms. Two alternative models are suggested for the carbon shell structure:

   i. 'Bucky-diamond' model where the core is covered with fullerene-type shell of sp^2 carbon. [87–91]

   ii. Unstructured amorphous carbon outer layer with mixture of sp^2 and sp^3 hybridised carbon. [78, 92, 93]

   The shell structure and thickness is affected by the cooling kinetics of the detonation synthesis as mention in chapter 5.1.1.

(3) The surface layer is covered by a variety of functional groups [1, 84, 86, 92, 94]. These groups terminate the highly reactive dandling bonds of the ND surface. The mass of hetero-atoms (H, O, N) may be up to 10 – 14 % of the total mass of the particle. Oxygen is the main component of the surface groups (see table 4).

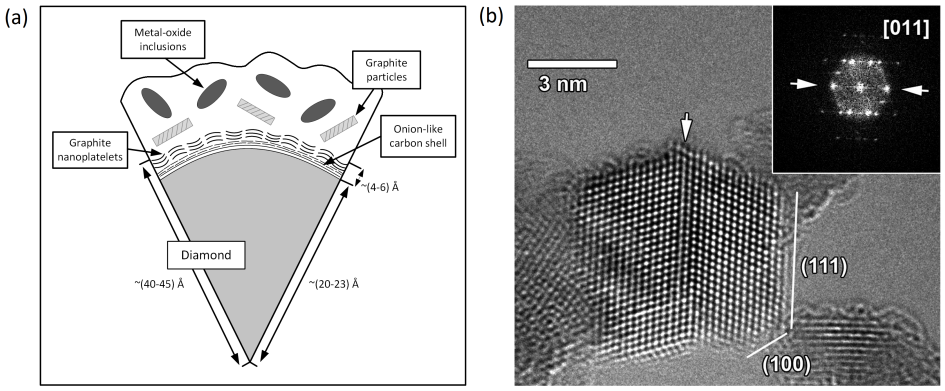

Figure 15: *(a) Suggested structure of non-purified ND particle. The diamond core is surrounded with fullerene-type of shell. [82] (b) HRTEM figure from higly ordered diamond core with low fraction of non-diamond carbon. High purity of the ND particle was gained together with acidic purification and ozone treatment. [95].*

Table 4: *Elemental composition of ND powders based on the combustion microanalysis.*

ND sample	Oxidant	C%	N%	H%	S%	O%	Ignition residue (%)
A [96]	$HClO_4$ + HNO_3	85.87	1.95	0.6	-	∼11	0.37
B [96]	HNO_3 + H_2SO_4	87.58	2.14	0.62	0.16	∼10	0.12
C [97]	Perchloric acid	81.5-82.0	1.35	1.0	-	∼15-16	1.1-1.6

(a) Content of oxygen was estimated by subtractions

Due to the small size of ND particle, it has high surface-to-volume ratio. Therefore nanodiamonds physical and chemical properties are strongly determined by its surface. Surface chemistry of nanodiamond particles are widely investigated in number of papers with characterization methods such as Fourier transform infrared spectroscopy (FTIR) [86, 92, 94, 98, 99], X-ray photoelectron spectroscopy (XPS) [100] and thermal programmed desorption (TDP) [101]. It is found that the surface groups and their concentration depends on the used oxidative agent. Table 4 shows how different oxidants effects on the elemental composition of ND powders. Although there are considerable differences between samples, studies have shown that the main oxygen-containing functional groups after chemical purification are ≥C-OH (hydroxyl), ≥C-O-C≤ (ether or bridge oxygen), >C=O (ketonic),-COOH (carboxyl), -C(O)-O-C≤ (ester or lactone) and –C(O)-O-(O)-C (cyclic acid anhydride) [92, 96, 97, 102]. Also hydrocarbons $–CH_x$ and nitrogen containing groups can be found from ND particles surface [1, 86, 92, 94]. However, the ratios of the surface groups are not evaluated in the found literature.

5.3 Stability of nanodiamond particles

At microscale graphite is carbons stable and diamond metastable form. The energy difference between these two phases is only 0.002eV/atom, but due to the high activation barrier (∼0.4eV/atom) high temperatures and pressures are needed to diamond-graphite phase transformation. [1, 78] Triple point for graphite-diamond-liquid is approximately 12 GPa/500 K [103]. Considering the stability of nanodiamond particles, size of the particle need to be added as part of phase diagram. Shenderova [1] build a 3D phase diagram from Viecellis results [104], where size of the particle is added as a third parameter (Figure 16). Based on Viecellis calculations triple point of ND particles shifts to lower temperatures and higher pressures compared to bulk diamond. According to Shenderova [1], the nanodiamond phase is most stable phase at ambient conditions.

On the experimental section of this thesis, some of the nanodiamond samples are heat treated. Therefore stability of nanodiamonds under chancing temperatures must be taken under evaluation. During annealing particles surface chemistry and structure is changed. Two aspects that are affected by thermal annealing, are discussed below.

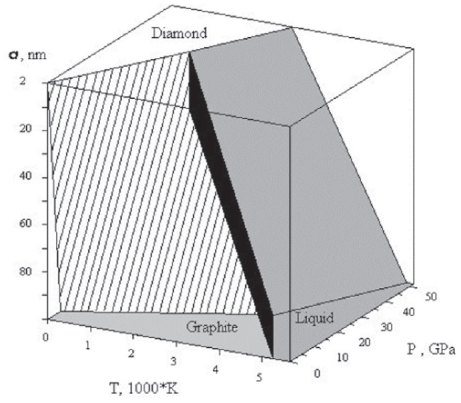

Figure 16: *Schematic 3-D phase diagram for carbon. [1].*

5.3.1 Thermal stability of surface groups

Thermal stability of ND surface groups have been investigated in different atmospheres and temperatures. It is found that the changes to the surface chemistry are dependent on the annealing conditions. Thermal stability of surface groups have been studied with FTIR [86, 99–101, 105, 106], thermogravimetric analysis (TGA) [86, 107], TPD [101], XPS [100] and differential thermal analysis (TGA) [106].

When annealing is done in ambient air at low temperatures (350-450°C), ND surface is oxidized and covered by oxygen-containing groups [86, 99, 100, 106]. According to measured FTIR data, content of C=O, -OH and -COOH groups are increased after oxidation. It is suggested that during oxidation ketones, aldehydes and esters on the surface are converted into carboxylic acids, anhydrides and cyclic ketones [86, 100]. Also decomposition of -CH_x groups was detected along with the increasing annealing temperature up to 600°C [100, 106]. Effect of annealing in low temperature can be seen from FTIR spectra which is show in Figure 17. At higher temperature range of 700-900°C, annealing is proposed to lead to progressive removal of -OH groups [108].

Decomposition of surface groups occurs in vacuum or inert gas at temperature range 300 – 900°C [101, 105, 107]. Butenko et al. [101] propose that at low-temperature region of 227-627°C two prosesses occur in vacuum: (1) The condensation of different oxygen-containing groups releasing water molecules, and (2) the decomposition of acidic groups (carboxyl, anhydride and lactone groups) releasing CO_2 and CO gases. Ether and ketonic groups decompose at higher temperature region of 600-900°C. Finally, decomposition of hydrocarbon groups is observed in temperature range of 700-1150°C. Decomposition of surface groups were measured with TDP and FTIR. Results are presented in Figure 18.

In a inert gas atmosphere, decomposition of the surface groups was studied as a weight loss with thermogravimetric analysis [107]. It was found that ND sample weight decreased 3 % at 550°C and 11.5% at 900°C. Cataldo and Koscheev [107] also suggested that weight loss is related to condensation of ND surface groups and release of water molecules.

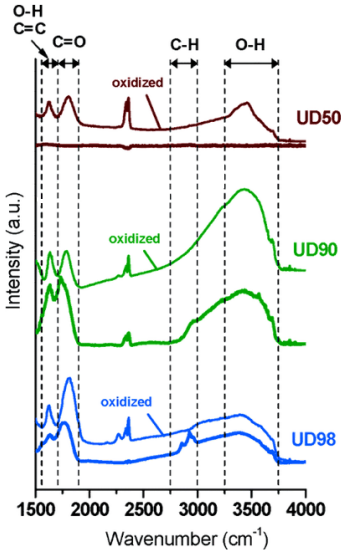

Figure 17: *FTIR spectra before and after oxidation with three different ND samples with sp^3 content of 50, 90 and 98 %. Oxidation was done at 425 °C for 5 h. [86].*

Surface groups of the ND particle do not only determine properties of the material, but also stabilizes and prevents ND surface from graphitization [78]. Based on computational modelling it was shown that after decomposition of surface groups, bare diamond surface undergo more easily graphitization and ND surface is transformed into more stable fullerene-like shell. [89, 90]

The effect of annealing to ND particles surface groups in different atmospheres are summarized in table 5.

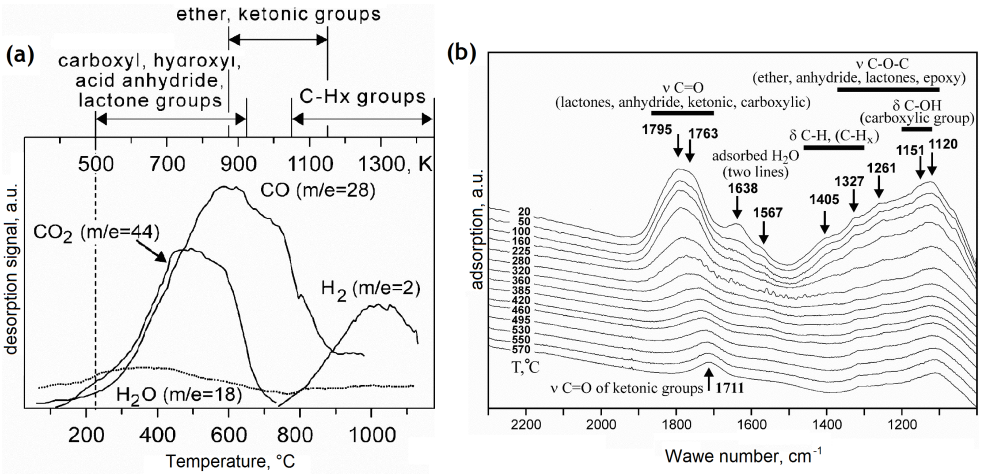

Figure 18: *(a) TDP curves of CO, CO_2, H_2O and H_2 gases originating from decomposation of surface groups during annealing. (b) FTIR spectra of ND surface groups at low annealing temperatures. [101].*

Table 5: The effect of thermal annealing to ND particles surface chemistry.

	Initial sample		Annealed sample			Characterization		
Ref	**Purification**	**Surface chemistry**	**Atmosphere**	**Annealing temperature**	**Surface chemistry**	**Surface chemistry**	**Other information**	**Method**
[86]	-	-OH, -COOH, -CH_3 and -CH_2	Air	Up to 600°C	At 425°C: -CH_x [(a)], -OH[(b)], -COOH, -C(O)-O-(C)-C, cyclic ketone [(c)]	FTIR	At 425°C sp^2 ↓ 19 → 4%, and sp^3 ↑, 81% → 96%	Raman, XANES, TGA, TEM
[100]	Chromic anhydride + H_2SO_4	-OH, C=O, -COOH, -NH_2, -CH, -CH_2, -CH_3	Air	350-450°C	-CH_x [(a)], C=O, -COOH, -C-O-C-, -C(O)-O-C-, -C(O)-O-(O)C- [(b)]	FTIR, XPS	After oxidation sp^2 carbon vanish	XPS
[106]	H_2SO_4 +$HClO_4$	-OH, C=O, -CH_2, -C-O-C/-C-N-C*	Air	Up to 590°C	-CH_2 [(a)], C=O, -C-O-C/ -C-N-C [(b)], -OH [(d)]	FTIR	-	-
[99]	HNO_3 + HCl	-OH, C=O, -C-O-C, -CH_x	Air	400 and 600°C	At 400°C: C=O, -CH_x [(a)], -COOH [(c)] At 600°C: -OH and -COOH [(a)]	FTIR	-	-
[101]	H_2SO_4 + $HClO_2$	-OH, -C=O, -COOH, -C-O-C-, -C(O)-O-C, -C(O)-O-(O)-C, -CH_x	Vacuun	Up to 877°C	At 227-627°C: -COOH, -C(O)-O-(O)-C, -C(O)-O-C [(a)] At 597-877°C: C=O ,-C-O-C [(a)] At 777-1127°C: -CH_x [(a)]	FTIR XPS TDP	-	-
[105]	-	-OH, C=O, -COOH, -C-O-C-, -CH_x	Vacuum	550, 700, 800, 900 and 1100°C	At 550-800°C: -OH, C=O, -COOH, -C-O-C [(a)], -CH_x [(d)]	FTIR	Above 550°C sp^2 ↑	Raman
[107]	-	-OH, -COOH, -NH	N_2	Up to 900°C	Above 500°C: -C(O)-O-(C), -C(O)-O-(O)C [(c)], above 900°C all oxygenated groups are released	FTIR TGA	-	-

(a) Full or partial removal of surface groups from the ND surface
(b) Content of the surface group is increased
(c) The surface group is formed due to conversion of other oxygen-containing surface groups such as C=O, -C(O)-O-C, -C-O-C, -COOH, -OH
(d) No significant change in surface group content

* Same adsorption band in FTIR spectra
↑ Content of carbon increases
↓ Content of carbon decreases

5.3.2 'Low' temperature nanodiamond graphitization

ND is a metastable form of carbon in ambient atmosphere and low temperatures. With increasing temperature ND particles starts to graphitize, where sp^3 carbon is transformed into sp^2 carbon. Transformation starts from outer surface layers propagating deeper with increasing temperature. With high temperatures of 1100-1800°C, onion-like carbon (OLC) structures can be produced by annealing ND particles in vacuum or in inert gas atmosphere [108–111]. In this work, interest is directed into to lower annealing temperatures where early stages of graphitization starts to occur. Results of low temperature graphitization in literary are strongly dependent on experimental conditions and what characterization methods were used [108, 110–112]. General trend is, that the size of the ND particle affects the graphitization process. With small particles graphitization starts at lower temperature than with larger particles [78].

Increase of sp^2 content is first observed at temperatures of 550-600°C [105, 108, 110]. In vacuum, progressive increase of sp^2 carbon was detected with NMR by increasing temperature from 600°C to 800°C (see Figure 19) [108]. Average size of the annealed ND particle was 5 nm. According to Panich et al. [108] at 800 °C diamond core is covered with more than single sp^2 layer. Different result were found by Zou et al. [110]. Based on their work HRTEM and Raman analysis, ND particle with same size starts to transform into amorphous carbon from the particle edges. Diamond phase was completely transformed into amorphous carbon at 750°C. Petit et al. [112] did not observe phase transition from sp^3 to sp^2 until above 900°C by XPS. Below 900°C, the ND surface was suggested to reconstruct to graphitic domain without altering the diamond core [112].

In argon atmosphere Cebic et al. [111] proposed the graphitization onset temperature to be 600°C. Steps for the ND graphitization is illustrated in Figure 20. This investigation was based on Raman spectroscopy. Again there are different result of the onset temperature for phase transformation in argon atmosphere. According to Chen et al. [113], ND phase transformation is detected above 800°C when the size of ND particles decreases.

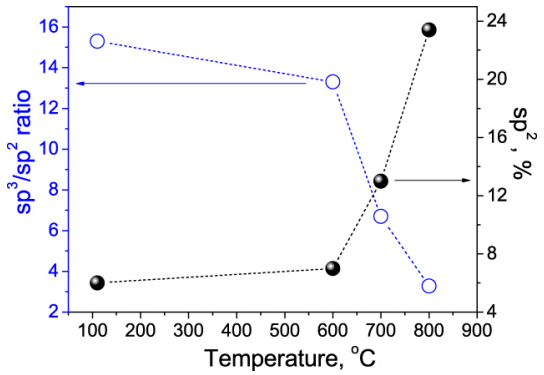

Figure 19: *Sp^3/sp^2 ratio and sp^2 content presented as function of annealing temperature. Results are based on 13^C NMR measurements. [108]*

The variation of the graphitization onset temperature is difficult to explain when the experimental condition and chacterazation methods are different between researchers. However, it is suggested that graphitization process can be affected by the reactive gases that are decomposed from the ND structure during annealing [78]. Oxygen-containing gases may have catalytic effect on diamond graphitization [114, 115].

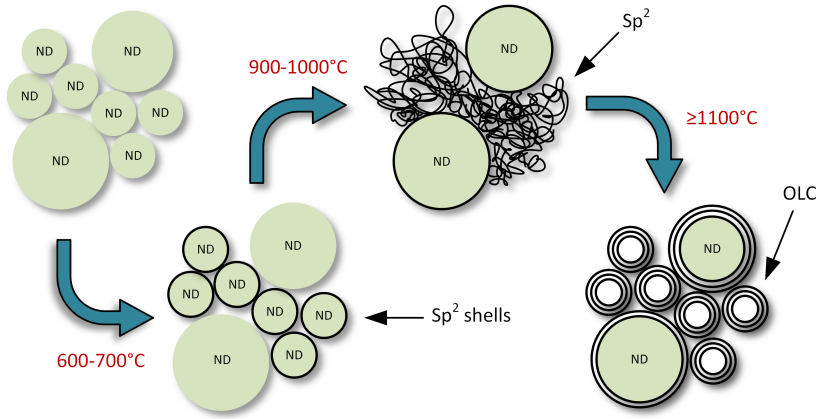

Figure 20: *Schematic of ND graphitisation to onion-like carbon under an inert gas atmosphere.*

Table 6: *Low temperature graphitization of ND particles in different atmospheres.*

	Initial sample		Annealed sample				Characterization
Ref	**Purification**	**Content of sp^3 and sp^2 carbon**	**Atmosphere**	**Annealing temperature**	**Graphitization onset temperature**	**Temperature effect on sp^2 carbon**	**Carbon content**
[108]	Oxidation in air at 425°, boiling in $HCl + HNO_3$	Sp^3 94 wt.%	Vacuum	600, 700, 800 and 1800°C	600°C	At 600-800°C: sp^2 ↑ 23.4%, at 1800°C: OLC is fabricated	NMR EPR
[110]	H_2SO_4 + $HClO_4$	-	Vacuum	From 500 to 1400°C	600°C	At 600°C: a-C formation starts, at 750°C ND transforms completely into a-C, at 800°C OLC formation starts	HRTEM Raman
[112]	-	Only sp^3 is detected	Vacuum	700, 900 and 1100°C	700°C	Above 700°C sp^2 ↑, above 900°C ND core starts to graphitize	XPS
[111]	-	Sp^3/sp^2 ratio ~ 0.75	Argon	Up to 1000°C	600°C	See Fig. 20	Raman TEM TGA XRD
[113]	-	Sp^3 90 wt.%	Argon	300, 600, 800, 1000, and 1150°C	800°C	Above 800°C sp^2 ↑	XRD Raman

↑ Content of carbon increases
↓ Content of carbon decreases

5.4 Electrochemical properties

5.4.1 Origins of nanodiamonds electrochemical activity

Bulk diamond is an insulating material with a band gap of 5.47 eV. Regardless of this insulating character, ND particles have shown remarkable electrochemical activity towards several redox probes [116–118]. It is unanimously proposed that the electrochemical behavior of ND particles arises due to the high content of oxygen-containing surface groups [92,98,105]. When surface-to-volume ration is high, surface properties of the material becomes more dominant than the bulk properties [118]. It could be also assumed that conductive sp^2 shell around ND has important role in electrochemical behaviour of the material. However this is not speculated in any publications found from the literature.

ND particles electrochemical behaviour is studied only in limited amount of papers. In those papers ND particles are deposit as a surface layer on the other electrode materials such as boron-doped diamond (BDD) [92, 117, 118], glassy carbon (GC) [98,105], gold [98] and platinum [116,119]. Some experiments have been performed with several types of redox probes including $Ru(NH_3)_6^{2+/3+}$ [98], FeMeOH [118], $Fe(CN)_6^{3-/4-}$ [92,98,116,117,119] and $IrCl_6^{3-/4-}$ [92,117]. As there are considerable differences between the reported studies, it can be concluded that nanodiamonds are not well characterized material in electrochemical systems. However, in most of the experiments it is shown that ND enhances redox currents.

The role of oxygen functionalities have been studied by modifying the surface chemistry of the ND particles. Holt et al. [98] measured three ND-gold electrodes with different surface functionalization in 1 mM $Ru(NH_3)_6^{2+/3+}$. Type of ND powders drop casted onto gold electrode were referred as 'untreated', 'oxygenated' and 'hydrogenated'. 'Untreated' powder was used as received from the supplier. 'Oxygenated' powder was prepared by oxidizing untreated powder in air at 420°C for 5 h [86], whereas 'hydrogenated' powder was prepared by heating in a H_2/N_2 gas flow at 800°C for 2h. This procedure removed oxygen functionalities from the ND surface. Measurements were done with DPV and results are presented in Figure 21. It is shown that redox currents are enhanced when gold electrode is modified with 'untreated' and 'oxygenated' ND powder. In case of 'oxygenated' powder $Ru(NH_3)_6^{2+/3+}$ redox peaks and additional peaks at -0.5 V are slightly enhanced compared to 'untreated' powder. 'Hydrogenated' gold electrode did not show any remarkable difference compared to bare gold electrode. These results supports the theory that nanodiamonds electrochemical activity is based on oxygen functionalities.

Zang et al. [105] used glassy carbon electrodes coated with ND powders annealed in different temperatures. Annealing of the ND powders was done in vacuum at temperatures 550, 700 and 850°C for 1 h. Due to the annealing surface groups were expected to decompose. CV measurements were done in 0.01 M $Fe(CN)_6^{3-/4-}$ with scan rate of $v = 20$ mV/s (Figure 22(a)). From the measured voltammograms it can be seen that ΔE_p of the electrode increases when annealing is applied to the ND

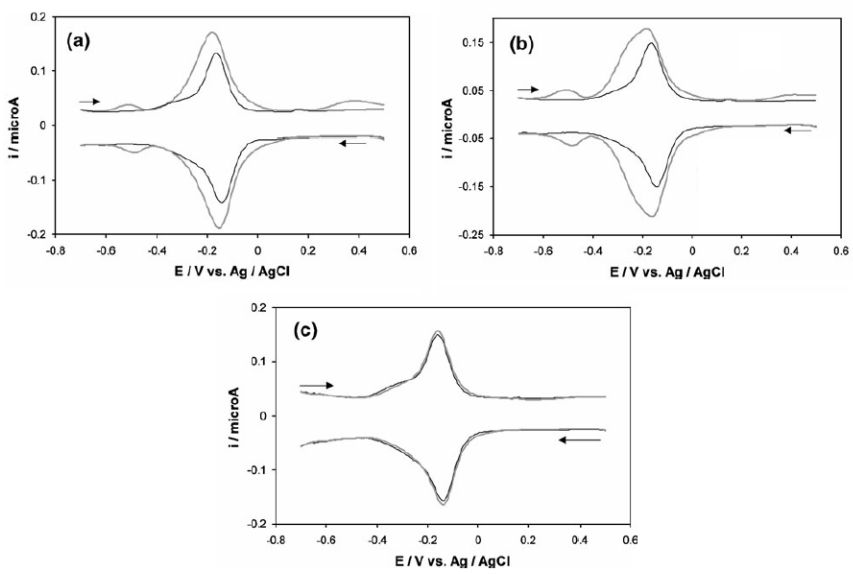

Figure 21: *Differential pulse voltammetry measurements of 1mM $Ru(NH_3)_6^{2+/3+}$ in 0.1 M PBS pH 7 with gold (thin black line) and ND-modified gold electrodes (thick gray line), where (a) is 'untreated' ND powder, (b) 'oxygenated' and (c) 'hydrogenated'. [98]*

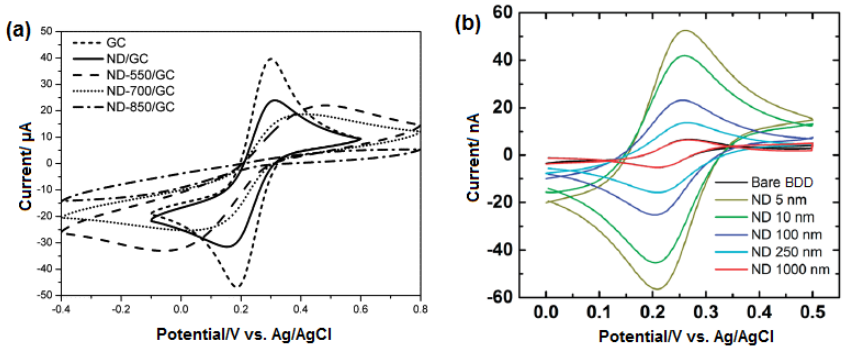

Figure 22: *(a) CV results for annealed ND-GC electrodes in 0.01 M $Fe(CN)_6^{3-/4-}$. Samples were annealed in vacuum at 550-850 °C [105]. (b) CV of 1 µM FcMeOH in 0.1 M KCl pH 5.88 with different ND particle size. Before CV measurements ND particles were oxidized in air to maximize the content of oxygen-containing groups [118].*

powder. This also indicates importance of oxygen-containing functional groups on the ND surface for reversible redox reactions.

Also the role of oxygen-containing groups was studied by changing the size of ND particles [118]. CV measurements were carried out in 1 μM FeMeOH with particle sizes 5, 10, 100, 250 and 1000 nm. Increasing redox peak currents were observed in the order 1000 nm $<$ 250 nm $<$ 100 nm $<$ 10 nm $<$ 5nm as shown in Figure 22(b). These results were also related to the role of surface functionalities due the fact that smaller particles have higher surface-to-volume ratio.

Holt et al. [92, 98] have proposed that electrochemical activity of ND particles is based on a 'molecule-like' redox reactions. It is suggested that specific surface group molecular orbitals are overlapping on the surface of the ND particle. This gives arise to electronic states with energies within the band gap of diamond (Figure 23(a)). In other words, overlapping orbitals results as a delocalized electrons that are not tied into one state. Arisen electronic states allows electrons to be injected or removed from these surface states at specific potentials. Such surface states may originate from localized sp^2 carbon sites or overlapping C=O groups producing delocalized π character due to unsaturated bonding. Schematic diagram of delocalization and formation of surface states is illustrated in Figure 23(c). During electrochemical measurements these surface states may be occupied by reduction at the electrode or by a solution redox species (Figure 23(b)). Based on this theory ND is suggested to act as a catalyst by regenerating solutions redox species. Proposed atalytic mechanisms for redox probes are discussed more detailed in the next chapter.

According to Holt et al. [92] 'molecule-like' redox nature of ND is supported by result that ND itself can undergo both oxidation and reduction reactions [92, 98]. Redox activity of ND is shown in Figure 24(a), where ND modified boron-doped electrode is scanned with DPV in 0.2 M PBS. However, the redox process of ND particles is complex. From the voltammogram it can be seen that oxidation scans differs from each other when scans are done more than once. Also not all oxidation reactions are reversible. Complexity of ND particles is also supported by the fact that the ND surface states are dependent on pH (Figure 24(b)).

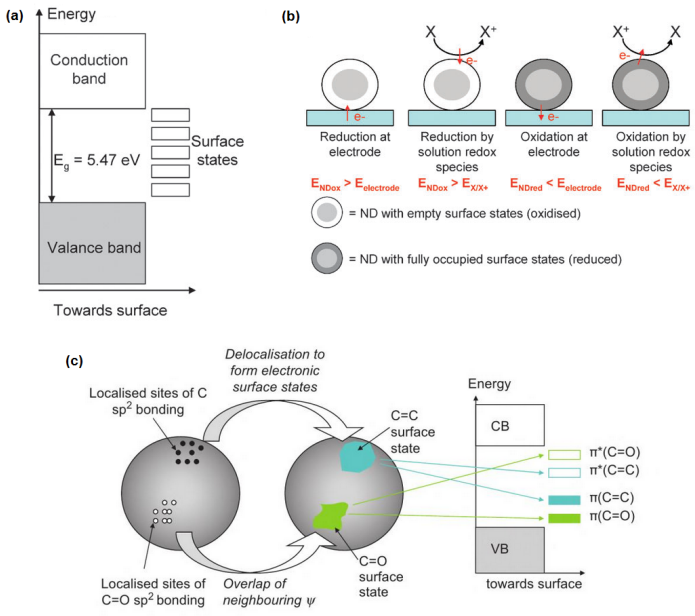

Figure 23: *(a) Diamond band gap with possible surface states arising from surface groups overlapping molecular orbitals. (b) Surface states may be occupied by reduction at the electrode or by a solution redox species. (c) The formation of electronic surface states on the surface of the ND particle. [92]*

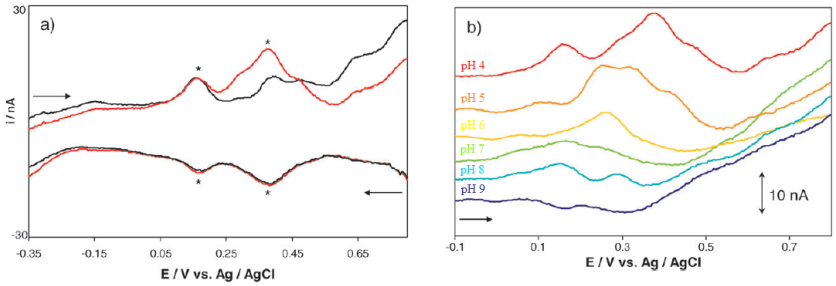

Figure 24: *(a) ND redox activity measured in 0.2 M pH 4 PBS with DPV. Mark * in the voltammograms indicate reversible reactions. (b) ND oxidation reactions dependency of pH. Both measurements were done with ND-modified BDD electrode. [92]*

5.4.2 Interaction with redox probes

It is shown that nanodiamond deposition on top of electrode materials enhances the redox currents [98, 117, 118]. Only proposed explanation for this is Holt's theory [98] where nanodiamonds 'molecular like' nature can regenerate redox species. On this section ND particles feedback mechanism is discussed in more detail for redox analytes $Ru(NH_3)_6^{2+/3+}$, FcMeOH and $Fe(CN)_6^{3-/4-}$. It should be noted that presented explanations below are only theories, where the role of sp^2 is not taken under evaluation. Summary of electrochemical experiments performed with ND coated electrodes is presented in table 7.

5.4.2.1 Ruthenium

ND effect on redox currents in 1 mM $Ru(NH_3)_6^{2+/3+}$ in 0.1 M 7 pH PBS are shown in Figure 21. As described before, 'untreated' and 'oxygenated' ND modified gold electrodes enhances oxidation and reduction currents of ruthenium. To understand the role of ND particles during redox reactions, behavior of ND particles were investigated in 0.1 M pH 7 PBS without any redox species with ND modified GC electrode. [98] Result are shown in Figure 24. It can be seen that ND particles have oxidation peaks at -0.4 V and -0.15 V. Also clear reduction peaks occurs at -0.4 V and -0.2 V. These reactions are not seen with blank GC electrode. Therefore it is concluded that these redox peaks are ND particles characteristics oxidation and reduction reaction in pH 7. Combining these findings with $Ru(NH_3)_6^{2+/3+}$ results Holt have suggested that during reduction following reactions can take a place:

$$Ru(NH_3)_6^{3+} + e^- \rightarrow Ru(NH_3)_6^{2+}, \quad E = -0.15V \tag{26}$$

$$ND_{ox} + ne^- \rightarrow ND^0, \quad E \sim -0.2V \tag{27}$$

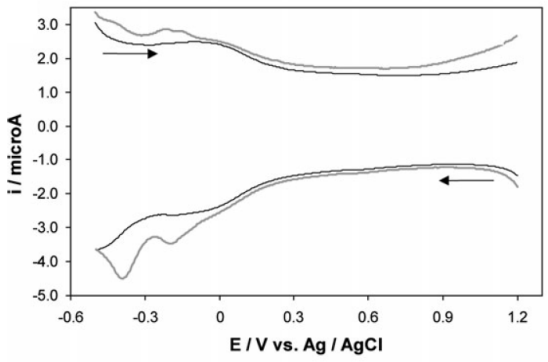

Figure 25: *DPV voltammograms for GC (black line) and ND modified GC (grey line) electroed in 0.1 M pH 7 PBS. [98]*

$$ND^0 + ne^- \rightarrow ND_{red}, \quad E \sim -0.4V \tag{28}$$

where ND_{ox} is ND particle in its highest oxidation state in 'oxygenated' ND/gold electrode (see Figure 21(b)). 'Oxygenated' sample is chosen because it has strongest enhancement in reduction current. [98]

During reduction $Ru(NH_3)_6^{2+}$ is produced as shown in equation (26). Also ND_{ox} undergo reduction by receiving electrons from $Ru(NH_3)_6^{2+}$. During this reaction ND_{ox} is reduced into ND^0 and $Ru(NH_3)_6^{2+}$ is oxidized back to $Ru(NH_3)_6^{3+}$. Through this regeneration of ruthenium there are more $Ru(NH_3)_6^{3+}$ available for reduction reaction. Therefore reduction current is enhanced on the surface of 'oxygenated' ND electrode. Proposed reaction is likely possible due to the fact that ND reduction potential (-0.2 V) is close to the $Ru(NH_3)_6^{3+}/Ru(NH_3)_6^{2+}$ couple redox potential (-0.15 V). The overall reaction is

$$Ru(NH_3)_6^{2+} + ND_{ox} \longleftrightarrow Ru(NH_3)_6^{3+} + ND^0 \tag{29}$$

This catalyzed reaction can continue when ND_{ox} is regenerated by $Ru(NH_3)_6^{3+}$.

Another possible explanation for current enhancement in ruthenium is electrostatic interaction. $Ru(NH_3)_6^{3+}/Ru(NH_3)_6^{2+}$ are positively charged molecule than could adsorb onto negatively charged ND surface. [98] However, it should be noted that surface charge depends on the nature of the surface groups. As disscussed in section 5.2 functionalization depends on the used liquid oxidant used in the purification process.

5.4.2.2 Ferrocenemethanol

Nanodiamond particles redox response in FcMeOH solution was studied with ND-modified BDD electrode [118]. Results with different size of ND particles are presented in Figure 26(b) It is clearly shown that adding ND layer top of the BDD electrode,

ferrocenemethanol oxidation and reduction currents are enhanced. The enhancement is considerably higher than in $Ru(NH_3)_6^{2+/3+}$ solution. According to Varley et al. [118] the current enhancement is affected by two catalytic processes: (1) electron transfer between the solution redox species and redox active groups on the ND surface; (2) electron transfer mediated by $FcMeOH^+$ adsorbed onto the ND surface.

The first process is similar to catalyzed feedback process in $Ru(NH_3)_6^{3+}$. During reduction $FcMeOH^+$ is spontaneously regenerated by oxidation of FcMeOH at the ND surface. The overall reaction is proposed in following way

$$FcMeOH + ND_{ox} \longleftrightarrow FcMeOH^+ + ND_{red} \tag{30}$$

During oxidation the opposite reaction is proposed to take place. Similar redox potentials are required for ND surface functionalities and FcMeOH for this mechanism to be feasible. Varley et al. [118] proposed for this process to be thermodynamically possible, the ND oxygen-containing groups at the surface must undergo redox reactions at a higher potentials than the redox probe. It was also suggested that unsaturated ketone groups on the ND surface participate on the catalytic process between ND particles and redox species. In addition it was shown that this process depends on scanning speed, size of the ND particle, solutions pH and ion strength.

The second process is driven by electrostatic interactions between positive $FcMeOH^+$ and negatively charged ND surface oxygen functionalities. Due to this interaction redox probe can be adsorbed closer to ND surface. Therefore electron tunneling

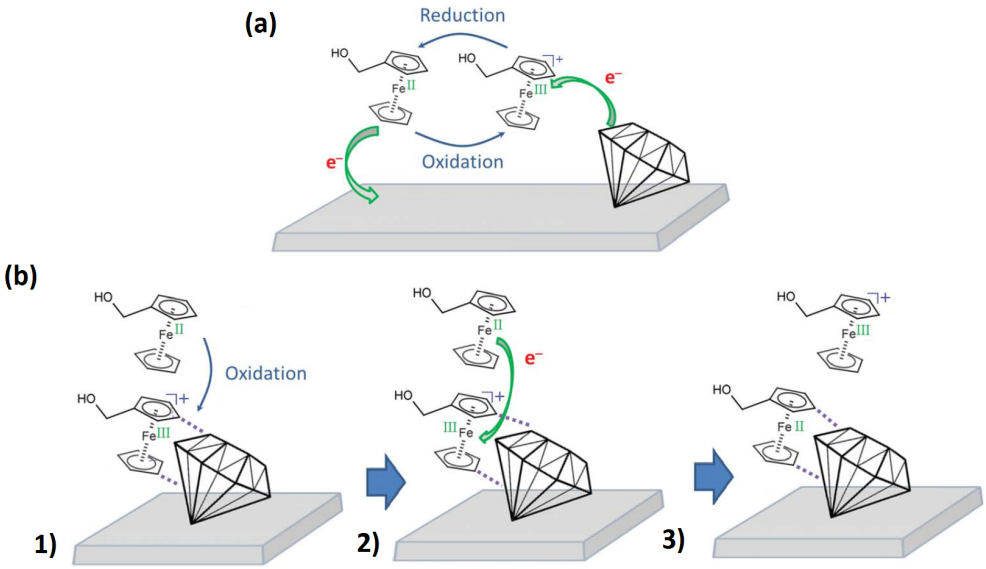

Figure 26: *Two proposed catalytic processes, where a) FcMeOH is regenerated by the redox active surface groups on the ND surface and b) ET is mediated by adsorbed $FcMeOH^+$. Modified from [118].*

can take place between these two. It was suggested that the oxidized $FcMeOH^+$ absorbs onto the ND surface and undergoes electron exchange with FcMeOH solution. As a result FcMeOH is generated at the surface and $FcMeOH^+$ in the solution. Current is enhanced while regenerated FcMeOH oxidizes again at the surface. [118] Both catalytic processes are illustrated in Figure 26.

5.4.2.3 Ferrocyanide

A similar mechanism is suggested for $Fe(CN)_6^{3-/4-}$ regeneration on ND modified BDD-electrode [117]. Below pH 8 enhancement of reduction current is observed. Holt et al. [117] proposes that during reduction Fe(II) oxidizes immediately back to Fe(III) at the ND surface. As continuous regeneration of Fe(II) at the ND and BDD interface leads to enhanced reduction currents. However, reversed affect was observed with ND coated GC electrode [105]. With ND-GC redox currents decreased in $Fe(CN)_6^{3-/4-}$ compared to plain GC electrode.

5.4.3 Dopamine detection with nanodiamond particles

As stated in chapter 5.4.1 electrochemical characterization of nanodiamonds is mainly carried out with outer sphere redox probes. Only one paper is published by Peltola et al. [9] where ND particles are used for detection of dopamine. In this research ta-C was fabricated with nanodiamonds by two different deposition methods: drop-casting and spray coating. In drop-casting method heat treatment was used, where fabricated samples were annealed at 85°C for 10 min. Four types surface functionalized nanodiamonds were used in both deposition methods, where the functionalization were hydrogen, amino, carboxyl and amino+carboxyl.

According to the research [9], deposition method had significant effect on the electrochemical behavior of ta-C+ND electrodes. With spray coated electrodes sensitivity towards DA decreased significantly compared to drop-casted electrodes. Amino and carboxyl terminated ta-C+ND electrodes did not detect dopamine at all, whereas detection limit for hydrogen and amino+carboxyl terminated electrodes were 5 μM. With drop-casted electrodes detection limit was in range 50-500 nM, where the hydrogen terminated ta-C+ND had the lowest value and the carboxyl terminated the highest value. Results are shown in Figure 27.

It is generally proposed that the electrochemical activity of ND particles arises due to the high content of oxygen-containing groups [92, 105, 116]. Therefore low DA detection limit of hydrogen terminated ta-C+ND electrode is in contrast with this assumption. However, it must be underlined that in research [9] used electrode material and redox analyte are different from previous studies. Here inner sphere analyte dopamine was used. Therefore it can be understood that the interaction mechanism between nanodiamonds and redox analyte is different from results presented in previous sections.

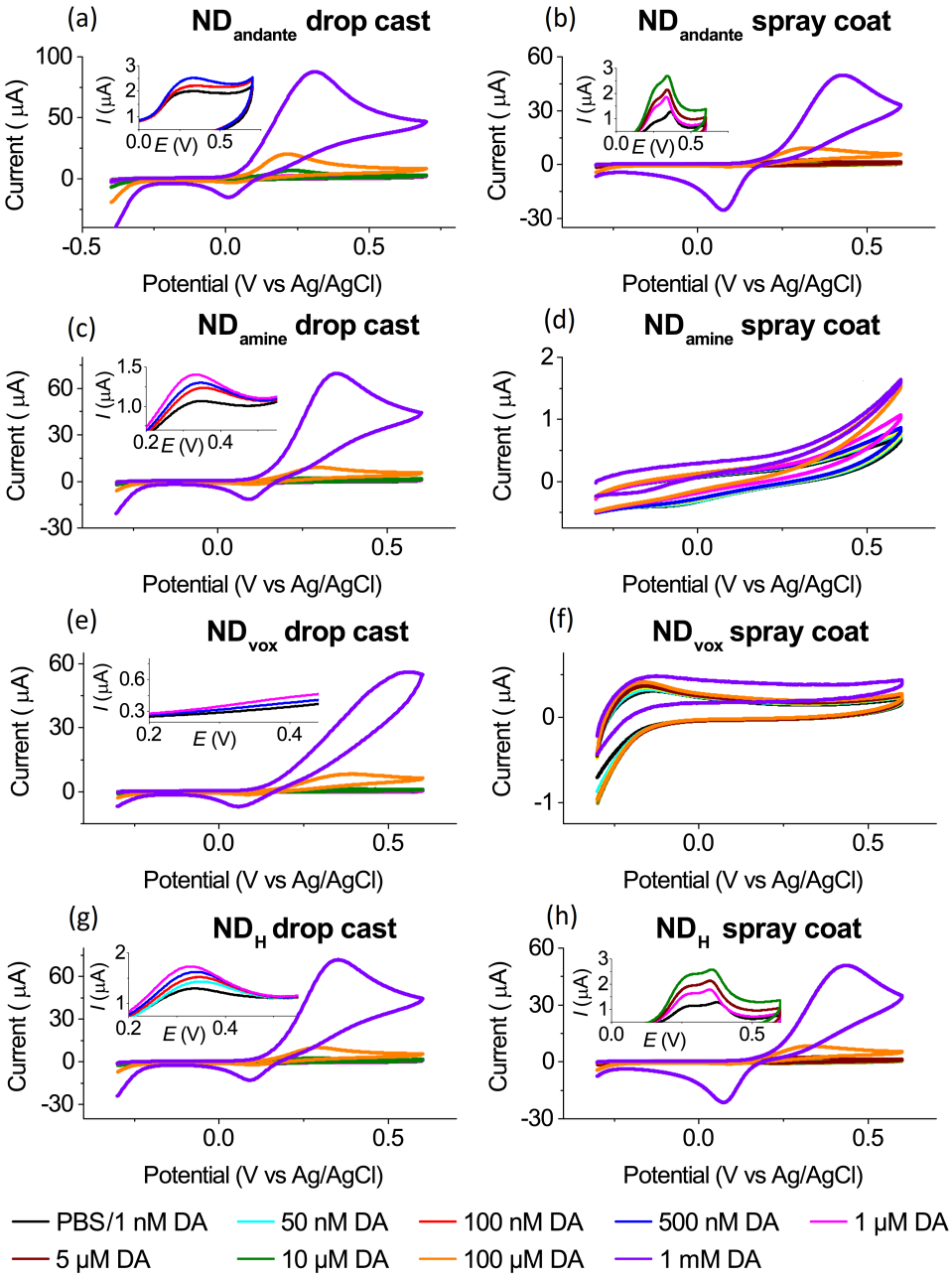

Figure 27: *DA results with drop-casted and spray coated ND-electrodes. Subscripts in ND refers to functionalization of the nanodiamond, where 'H' is hydrogen, 'andante' is amino+carboxyl, 'vox' is carboxyl and 'amino' is amino. [9]*

Table 7: Electrochemical experiments performed with ND coated electrodes.

Ref	Electrode	Modification	Method	Reference	Redox probe	Solvent	Scanning speed (mV/s)	Potential range (V)	ΔE_p (mV)	Redox reaction	ND effect on the electrode
[120]	ND	-	CV	Ag/AgCl	0.01 M $Fe(CN_6)^{3-/4-}$	1 M KCl	10, 20, 50 & 100	[-0.7, 1.2]	$\sim$ 100	Quasi-reversible	-
[116]	Pt wire[(a)]	ND heated in vacuum	CV	SCE	-	0.1 M PBS	100	[-0.5. 1.8]	-		-
	Pt wire[(a)]	ND heated in vacuum	CV	SCE	0.01 M $Fe(CN_6)^{3-/4-}$	0.5 M KCl	10, 20, 50, 100, 200 & 500	[-0.4, 0.9]	72 - 122	Quasi-reversible	-
[119]	Pt wire[(a)]	ND heated in vacuum	CV	SCE	0.01 M $Fe(CN_6)^{3-/4-}$	0.1 M KCl	10, 20, 50, 100 & 200	[-0.2, 0.6]	70 - 284	Quasi-reversible	-
[105]	Pt wire[(a)]	ND heated in vacuum at 550, 700 & 850°C	CV	Ag/AgCl	-	0.1 M KCl	100	[-1.0, 2.5]	-	-	When T $\uparrow$, anodic and catodic reactions $\downarrow$
	ND/GC[(b)]	ND heated in vacuum at 550, 700 & 850°C	CV	Ag/AgCl	0.01 M $Fe(CN_6)^{3-/4-}$	0.1 M KCl	20	[-0.4, 0.8]	ND $\rightarrow$ $\sim$100 550°C $\rightarrow$ $\sim$450 700°C $\rightarrow$ $\sim$350 850°C $\rightarrow$ -	-	-
[117]	ND/BDD[(b)]	Oxidized in air at 425°C	DPV	Ag/AgCl	-	0.2 M PBS, pH 5, 6, 7, 8 and 9	10	[0, 0.7]	-	-	-
	ND/BDD[(b)]	Oxidized in air at 425°C	CV	Ag/AgCl	1 μM $Fe(CN_6)^{3-/4-}$	0.2 M PBS, pH 5, 6, 7, 8 and 9	10	[0, 0.5]	$\sim$ 70	-	At pH 8 and 9 i_{ox} $\uparrow$, at pH 5, 6 and 7 i_{red} $\uparrow$
[98]	ND/Gold[(b)]	-	DPV	Ag/AgCl	1 mM $Ru(NH_3)_6^{3+}$	0.1 M PBS	-	[-0.7, 0.5]	-	-	i_{redox} $\uparrow$
	ND/Gold[(b)]	Oxidized in air at 420°C	DPV	Ag/AgCl	1 mM $Ru(NH_3)_6^{3+}$	0.1 M PBS	-	[-0.7, 0.5]	-	-	i_{redox} $\uparrow$
	ND/Gold[(b)]	Hydrogenated in H_2/N_2 gas flow at 800°C	DPV	Ag/AgCl	1 mM $Ru(NH_3)_6^{3+}$	0.1 M PBS	-	[-0.7, 0.5]	-	-	No effect
[118]	ND/BDD[(b)]	Oxidized in air at 425°C	CV	Ag/AgCl	1 μM FcMeOH	0.1 M KCl, pH 5.88	20	[0, 0.5]	$\sim$ 30	-	i_{redox} $\uparrow$
	ND/BDD[(b)]	Oxidized in air at 425°C	CV	Ag/AgCl	1 μM FcMeOH	0.1 M KCl, pH 5.88	1, 2, 50, 100, 200 and 500	[0, 0.6]	-	Quasi-reversible	-
	ND/BDD[(b)]	Oxidized in air at 425°C	CV	Ag/AgCl	1 μM FcMeOH	0.1 M K_2HPO_4 & KH_2PO_4, pH 5, 6, 7, 8 and 9	5	[0, 0.6]	$\sim$ 30	-	i_{redox} $\uparrow$, strongest at pH 5,weakest at pH 9

(a) Microcavity electroded was prepared by placing a Pt wire inside of a glass tube and filling the microcavity with ND particles

(b) ND particles were dropcasted top of the electrode

$\uparrow$ Quantity is increased

$\downarrow$ Quantity is decreased

6 Experimental

6.1 Fabrication of the electrodes

6.1.1 ta-C

The ta-C samples were fabricated on p-type conductive Si wafer (Ultrasil) with 0.001–0.002 Ωcm resistivity. Before deposition wafer was cleaned by standard RCA cleaning method. First, 20 nm titanium interlayer was deposit on the Si wafer to improve adhesion of ta-C [20]. Deposition of Ti was carried out with magnetron sputter (DC-MS). After this step, 7 nm of ta-C film was deposit on top of the Ti. Carbon deposition was performed by pulse filtered cathodic vacuum arc (p-FCVA).

Deposition of Ti layer was carried out under the following conditions: discharge power fixed at 100 W, total pressure 0.67 Pa and argon gas flow rate 28 sccm. Deposition was done at a distance 220 mm in room temperature, where time for deposition was 350 s. ta-C film deposition was carried out with p-FCVA system (Lawrence Berkeley National Laboratory) equipped with a 45° bent magnetic filter. Filter was used to reduce contamination of the macroparticles. As a carbon source, two graphitic rods (Goodfellow) with purity 99.95 % were used as the cathodes. The 2.6 mF capacitor bank was charged to 400 V. Pulses were triggered at 1 Hz frequency where resulted arc current had amplitude of 0.7 kA and pulse width of 0.6 ms. For 7 nm t-C layer 360 pulses were applied. Deposition was done under vacuum, where total pressure was below 1 x 10-4 Pa. Wafer was placed in a rotating holder to form homogeneous film during deposition.

6.1.2 ta-C+ND

ta-C+ND samples preparation was carried out with a spraying technique. First carboxyl functionalized nanodiamond-water suspension (Carbodeon uDiamond, Carbodeon) with concentration of 5 wt-% was diluted with ethanol to 0.05 wt-%. The deposition was done on top of ta-C samples with a painting gun. Pressured air (3.5 mbar) was used as a carrying gas. Spraying of nanodiamonds on ta-C surface was performed ten times from a distance of ∼10 cm.

6.2 Characterization

6.2.1 HRTEM

Nanodiamonds surface structure was examined by high-resolution transmission electron microscopy (HRTEM). HRTEM was carried out with a double-aberration corrected microscope JEOL JEM-2200FS (JEOL) operating at 200 kV. The HRTEM micrographs were recorded with a Gatan 4k x 4k UltraScan 4000 CCD camera.

6.2.2 Annealing and RGA

Vacuum annealing was performed to investigate the role of ND surface groups. In vacuum surface groups decompose during annealing which is expected to have an effect on the electrochemical properties of the nanodiamonds [93,97]. 600°C degrees was selected as the annealing temperature. In this temperature decomposition of oxygen containing groups is assumed to take a place [97] without graphitizing nanodiamonds surface [100] or changing ta-C properties. For further discussion, see sections 5.3 and 5.4.

For the annealing p-type silicon wafer was diced in half and fabricated with as received ND suspension diluted with ethanol. For both half wafers 10 ml of 0.05wt-% ND suspension was drop casted. Samples were dried at room temperature. Annealing of Si+ND samples was carried out at two different times. After fabrication and 6 weeks later. Annealing was carried out with vacuum furnace Red Devil M (R.D. Webb Company). First ND coated half wafer was placed in a furnace, and the chamber pressure was pumped down to $\sim 2e^{-7}$ mbar. The chamber was heated to 600°C for 1 hour with ramp speed of 10°C/min. After annealing chamber let to cool down over night. Chamber pressure was increased back to 1mbar with N_2 flow (5 sccm).

At annealing step removal of water and oxygen containing gases were recorded using Transpector MPH100M (Inficon) residual gas analyzer (RGA). Spectrum was scanned from 0 to 50 amu with dwell time of 128 ms.

ta-C+ND samples for cyclic voltammetry experiments were annealed with same specs as Si+ND.

6.2.3 Cyclic voltammetry

Cyclic voltammetry was carried out with CHI potentiostat in a three-electrode cell (see Fig. 8). As a reference electrode Ag/AgCl (Radiometer Analytical) electrode was used. A graphitic rod was used as a counter electrode. Electrochemical characterization of ta-C and ta-C+ND electrodes are performed using several solutions, where surface area of both electrodes were A=0.03141 cm^2.

Water window and electric double layer capacitance was measured in 0.1 M perchloric acid (VWR Chemicals). Limits of water window was determined by using threshold current of $200\mu A/cm^2$ [26]. The double layer capacitance C_{dl} of the electrodes was calculated from three different voltammograms where scan rates 10, 50 and 400 mV/s was used. From each voltammogram C_{dl} was examined based on equation (23). Presented values of C_{dl} in table 8 are averages from the three voltammograms with different scan rates.

Electrode kinetics were examined by using outer sphere probe ruthenium which is considered to be insensitive to the electrode surface chemistry. 1 mM $Ru(NH_3)_6^{2+/3+}$ solution was prepared by dissolving 0.0318g of 98% hexaammineruthenium(III) chloride (Sigma-Aldrich) into 100 ml 1mM of potassium chloride (Merck). $Ru(NH_3)_6^{2+/3+}$ measurements were carried out at scan rates 10, 50, 100, 200 and 400 mV/s for

both ta-C and ta-C+ND electrodes. The formal reaction rate k^0 was calculated by using Nicholson method [68]. k^0 is estimated for every scan rate, where the final k^0 presented in table 8 is the average of these values.

The sensitivity and dopamine kinetics at ta-C and ta-C+ND electrodes were studied by measuring DA in different concentrations. First 10mM DA solution was prepared by dissolving 0.18964g of dopamine hydrochloride (Sigma-Aldrich) into 100 ml of PBS with pH 7.4. 10 mM stock solution was further diluted with PBS to obtain series of dopamine concentrations of 1nM to 1mM. Scan rate used was 50 mV/s in all concentrations for both electrodes.

Selectivity was evaluated by using 1mM AA solution containing varying concentrations of DA. First 10mM AA stock solution was prepared by dissolving 0.1779g of L-asborcid acid (Sigma-Aldrich) into 100 ml of PBS. DA and AA stock solution were further diluted with PBS to obtain 1mM AA with dopamine concentrations of 1μM, 10μM, 100μM and 1mM. Additionally plain 1mM AA was also used in CV measurements. Scan rate 50 mV/s was used for all concentrations for both electrodes.

Kinetics of DA and DA+AA was further examined for ta-C+ND electrodes by using different scan rates. Effect of scan rate v on dopamine redox reaction was measured in 100μM DA solution with scan rates 10, 50, 100, 200, 400 and 1000 mV/s. In addition DA+AA kinetics were measured in two different 1 mM AA solutions containing either 100μM or 1mM DA. For 1 mm AA + 100μM DA solution scan rates of 50, 100, 200, 400 and 1000 mV/s were used, whereas measurements in 1mM AA + 1mM DA were carried out with scan rates of 50, 400 and 1000 mV/s.

PBS was purged with N_2 for 30 minutes before preparing DA and AA solutions to prevent premature oxidation of DA. Additionally N_2 line was applied into the electrochemical cell to remove oxygen from the environment. Before DA and DA+AA measurements electrodes background current were stabilized by cycling them in PBS for 20 cycles.

All measurements were performed at room temperature in a Faraday cage. IR compensation was not done for CV results as measured current range was from nanoampere to microampere. With this current range IR-drop is not insignificant. In all voltammograms presented results are first cycles of the measurement if not specified differently.

7 Results

7.1 HRTEM

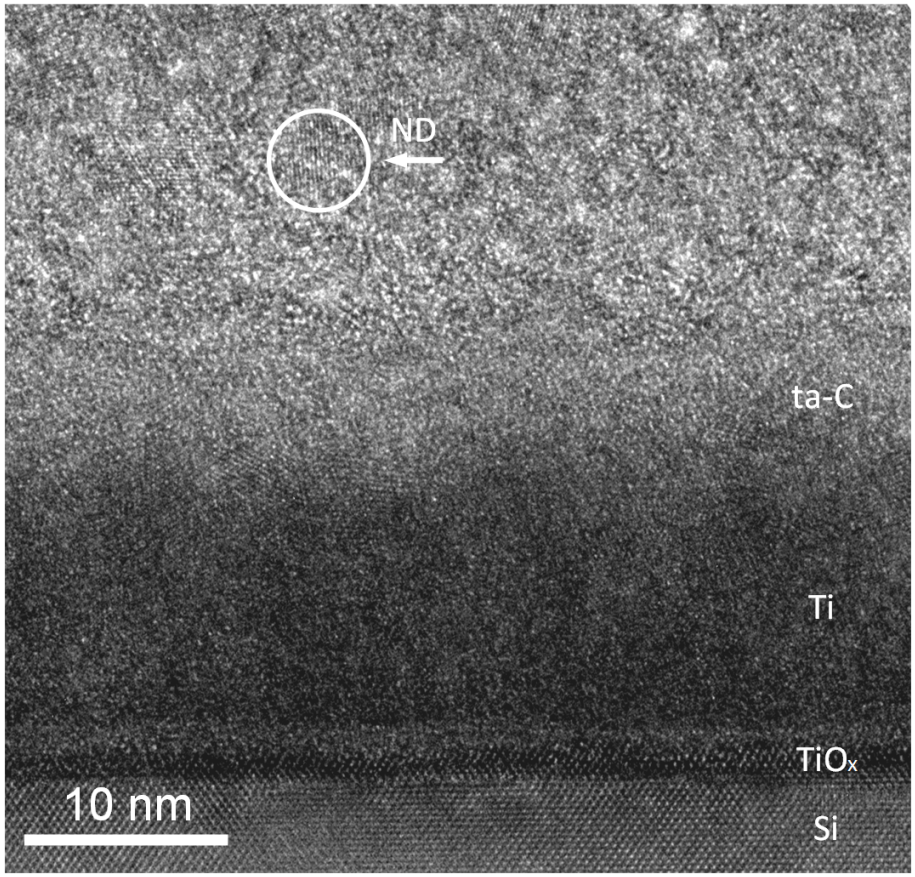

Figure 28: *Cross-sectional HRTEM figure from ta-C+ND electrode.*

Cross-sectional HRTEM micrograph of ta-C+ND electrode is presented in Figure 28. Every deposited layer is seen from the micrograph, where the thickness of Ti and ta-C layers are approximately 20 nm and 7 nm. On top of ta-C, deposited nanodiamonds are seen as crystalline structures. One ND particle is marked with a white circle as an example. Based on micrographs scale, estimated diameter of the ND particle is ∼5 nm. The result is in the same size scale as stated in section 5.2.

7.2 Vacuum annealing of nanodiamonds

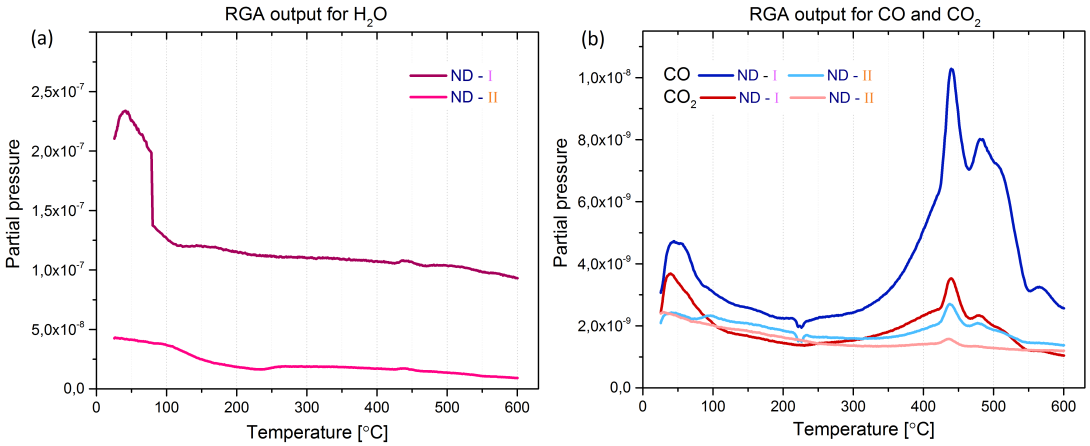

Figure 29: *Partial pressure as function of temperature for two ND samples measured at time periods I and II, where removal of (a) H_2O, (b) CO and CO_2 is shown.*

Vacuum annealing was carried for two ND samples. ND sample that was annealed after the fabrication is referred as I, whereas sample annealed 6 weeks after the fabrication is referred as II. Using RGA, evaporation of water, carbon monoxide and carbon dioxide were observed for sample I below +600°C. Removal of water from the nanodiamonds was seen below +100°C, whereas evaporation of CO and CO_2 appears at temperature range 400-550°C. Removal of CO and CO_2 is most likely due to the decompostion of the oxygen containing surface groups. For further discussion, see section 5.3.1. With sample II observed evaporation of H_2O, CO and CO_2 were significantly lower.

Based on the differences in RGA output of water, it is concluded that over time the amount of water in the ND film is decreased even in ambient air at room temperature.This effect may be due to the use of ethanol as a solvent in ND suspension dilution. Right after ND fabrication, ethanol may absorb water from the ambient air. Over time ethanol and water evaporates from the ND structures and less water is seen with RGA. Furthermore ND surface chemistry is likely altered as less CO and CO_2 evaporates from the longer aged nanodiamonds during vacuum annealing. As used ND suspension is commercially available, it is assumed that surface chemistry of as received nanodiamonds remains constant. After deposition of ethanol diluted suspension on top of silicon, surface chemistry seems less stable. The shape of RGA output for samples I and II are similar, but the partial pressures are different. As the nature of the RGA output remains the same, it is most likely that the amount of oxygen-containing surface groups on ND surface decreases over time. However, performing annealing treatment to nanodiamonds may modify samples surface chemistry to be more alike. This effect is observed with other carbon allotropes such as carbon nanofibers with HNO_3 treatment [121].

7.3 Cyclic voltammetry

7.3.1 Comparison of ta-C and ta-C+ND electrodes

As stated in introduction ta-C has some promising properties for electrochemical detection of DA. However, ta-C itself is not senstive [22] or selective [26] enough for DA detection *in vivo*. In previous studies it is shown that combining ta-C with other carbon allotropes such as carbon nanotubes [26] or carbon nanofibers [11], sensitivity and selectivity towards dopamine can be improved. Here effect of nanodiamonds on the surface of ta-C is shown and compared to plain ta-C electrode.

In Figure 30 voltammograms in $HClO_4$, $Ru(NH_3)_6^{2+/3+}$, DA and DA+AA solutions are presented for ta-C and ta-C+ND electrodes. Electrodes measured in same solutions are shown in the same graph to visualize the differences between ta-C and ta-C+ND. Observed values from the measurements are shown in tables 8 and 9.

Water windows for ta-C and ta-C+ND electrodes were 3.49 V and 3.01 V (Figure 30(a)).±200 μA/cm^2 was used as a limit value. Before the limit values ta-C background current is stable and no Faradaic reactions occur, whereas with ta-C+ND sample oxidation and reduction peaks are observed at around 0.6 and -0.1 V. Additionally with both samples broad reduction peak is seen around -0.75 V. Calculated electric double layer capacitance's were 16.0±3.6 and 25.2±13.2 μF/cm^2 for plain ta-C and ta-C+ND. As seen from the voltammogram, C_{dl} is larger for ND coated ta-C. However calculated margin of error with ta-C+ND C_{dl} is higher than with ta-C. Also plain ta-C C_{dl} is considerably lower compared to other studies results, where estimated values are 105±5 [22] and 62.2±18.6 μF/cm^2 [26].

The potential peak separation ΔE_p in 1mM $Ru(NH_3)_6^{2+/3+}$ for ta-C decreases from 68 mV to 62 mV as the scan rate increases from 10 to 400 mV/s. For ta-C+ND similar behavior was observed as electrodes ΔE_p decreased from 66 mV to 60 mV. Deviations of ΔE_p in both electrodes at different scan rates are small, this it is assumed that the deviation is in the range of accuracy of measurements. As shown in Figure 30(b) ΔE_p of the electrodes is not dependent on scan rate v. Limit value 59 mV of reversible systems was not achieved, but still electrodes show reversible behavior as ΔE_p did not increase with increasing scan rate. Based on Nicholson method the formal reaction rate k^0 for ta-C is 0.165±0.141 cms^{-1} and for ta-C+ND 0.114±0.110 cms^{-1}. High calculated margin of error for both k^0 indicates that using Nicholson method for k^0 approximation is not reliable when ΔE_p is near to reversible system limit $59/n$ mV (see page 21). Only clear difference between ta-C and ta-C+ND electrodes in $Ru(NH_3)_6^{2+/3+}$ is the enhanced redox currents at scan rates of 50, 100, 200 and 400 mV/s, where increase of cathodic current peak $i_{p,c}$ is slightly stronger than in i_{pa}.

Hybrid electrode sensitivity towards dopamine was low as 100 nM DA, whereas plain ta-C did not detect dopamine until 500 nM and above (Figure 30(c)). Increase of Faradaic current was observed with increase of dopamine concentration with both electrodes. At small concentrations of DA, background current of ta-C+ND hybrid

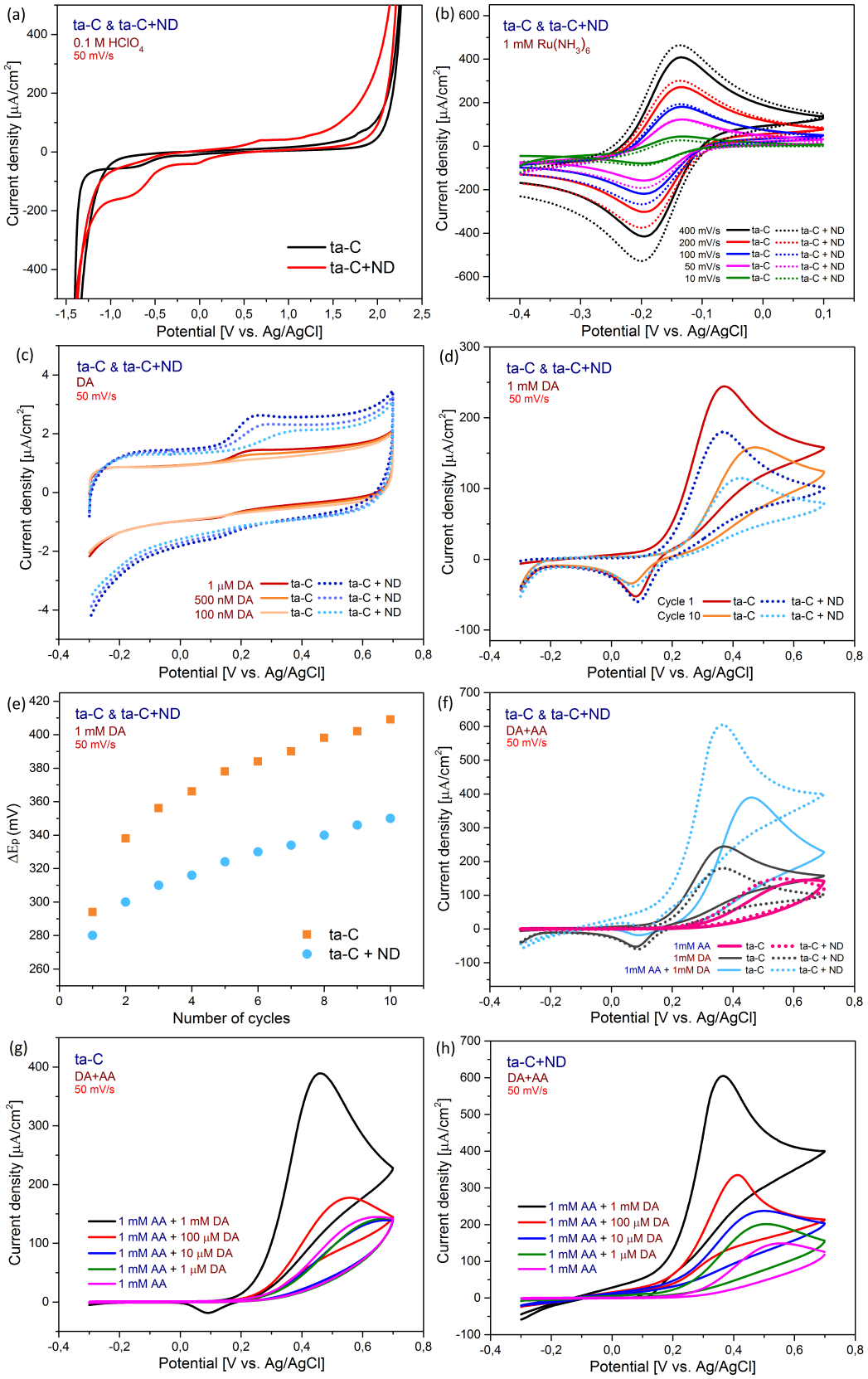

Figure 30: *Comparison of ta-C and ta-C+ND samples, where figures shows (a) water windows, (b) electron transfer kinetics in* $Ru(NH_3)_6^{2+/3+}$*, DA results at (c) low and (d) high concentrations, (e)* ΔE_p *in 1mM DA as function of cycles, (f) DA and DA+AA results for both samples, (g) DA+AA results for ta-C and (h) DA+AA results for ta-C+ND.*

Table 8: *Experimental parameters from $HClO_4$ and $Ru(NH_3)_6^{2+/3+}$ measurements.*

				ΔE_p (mV)				
	Water	C_{dl}	k^0	Scan rate v (mV/s)				
Sample	window (V)	(μF/cm^2)	(cms^{-1})	10	50	100	200	400
ta-C	3.49	16.0±3.6$^{(a)}$	0.165±0.141$^{(b)}$	68	64	64	62	62
ta-C+ND	3.01	25.2±13.2$^{(a)}$	0.114±0.110$^{(b)}$	66	62	62	62	60

(a) Average of C_{dl} values from scan rates 10, 50, 400 mV/s

(b) Average of k^0 values from scan rates 10, 50, 100, 200 and 400 mV/s

Table 9: *DA and DA+AA experiments parameters for ta-C and ta-C+ND samples.*

Sample	DA detection limit (nM)	ΔE_p (mV), 100μM DA	ΔE_p (mV), 1mM DA Cycles 1(10)	E_{ox} (mV), 1mM DA Cycles 1(10)	E_{ox} (mV), 1mM AA	Selective towards AA (yes/no)
ta-C	500	202	294 (409)	373(471)	650	no
ta-C+ND	100	176	280 (350)	367(425)	560	no

electrode is increased compared to ta-C electrode. This result is an agreement with the values of C_{dl}. Electrodes response and passivation at higher DA concentration (1mM DA) shows clear differences (Figure 30(d,e)). Both samples were cycled in DA for 10 cycles. ta-C anodic current peak at cycles 1 and 10 are considerably enhanced compared to ta-C+ND electrode. In addition during cycling dopamine oxidation potential E_{ox} with ta-C electrode increases from 373 to 471 mV. Respectively at the ta-C+ND $E_{ox,DA}$ increases from 367 to 425 mV. When compering just $E_{ox,DA}$ values between electrodes, no significant difference is observed. However when investigating the ΔE_p values as function of cycles (Figure 30(e)), clear deviation is observed between plain ta-C and ta-C+ND. At cycle 1 ΔE_p for ta-C and ta-C+ND are 294 and 280 mV. Respectively at cycle 10 ΔE_p increases to values 409 and 350 mV. Kinetics at the ta-C electrode decelerate more than at the hybrid electrode.

Selectivity between DA and AA is not achieved with neither of the electrodes as only one oxidation peak is observed in solution containing both analytes (Figure 30(f)). However the behavior of the electrodes is different in the DA+AA solution. At the ta-C+ND DA+AA oxidation occurs at same potentials with DA and the response current is considerably higher compared to ta-C electrode. Also at the plain ta-C DA+AA oxidation is observed at more anodic potentials compered to ta-C+ND. In addition, increase of current and shift of oxidation potential to cathodic direction is seen more clearly at the ta-C+ND response when the concentration of dopamine is increased in the AA solution (Figure 30(g,h)).

Based on the observed results nanodiamonds at the ta-C surface improves sensitivity towards dopamine and the resistance against passivation. As dopamine is surface sensitive redox system, oxidation of DA requires an spesific adsorption step on the electrode surface. Therefore strong interaction between dopamine and electrode has important role on the sensitivity. Thus, it seems that the surface properties of ta-C+ND are more attractive for DA oxidation than plain ta-C. This may be due

to the different surface chemistry and/or changed morphology of the surface of ND compared to ta-C. These properties possibly alter the passivation resistance of the electrode surface. It is difficult to evaluate why the passivation of the hybrid electrode is weaker compared to plain ta-C as the phenomena itself is poorly understood.

As stated above, selectivity towards dopamine in presence of AA is not achieved by adding nanodiamonds on the ta-C surface. At ND surface regeneration of DA is considerably stronger than in plain ta-C surface. As catalysing mechanism of AA is still under debate, it cannot be said why this effect is stronger at ND surface on than ta-C. As DA and AA both are surface sensitive redox analytes, surface chemistry of the samples most likely determines the reaction.

Deposition of nanodiamonds most likely increases the surface area and roughness of the ta-C electrode. The increased surface area may be the cause of enhanced redox currents in $Ru(NH_3)_6^{2+/3+}$. As discussed in section 5.4.2.1, Holt et al. [92, 98] have proposed that ND oxygen containing functional groups may regenerate ruthenium during reduction reaction and enhance quantity of $i_{p,c}$. However, with ta-C+ND both anodic and cathodic currents are enhanced compared to ta-C.

Overall addition of ND on top of the ta-C improves electrodes properties towards DA detection. However when measurements were repeated in DA and DA+AA solutions, nanodiamond coated electrodes performance was not repeatable. More detailed behavior of ta-C+ND hybrid electrodes are discussed in chapter 7.4.2.

7.3.2 More detailed study of ta-C+ND electrodes

During this work it was found that nanodiamonds properties at the ta-C surface were not repeatable. It was observed that experiments done in a same day with different ta-C+ND samples had similar behaviour, whereas measurements performed in different days showed considerable deviation between the results. Therefore time dependency of the ta-C+ND samples results are included as one observed parameter. Number of measurements done in different solutions are presented as function of time in Figure 31, where experiments are divided in five time periods. In the figure '0' indicates the fabrication of ta-C+ND samples and the period is presented as one month.

From Figure 31 it can be seen that there were inconsistencies in amount of experiments done for each sample-analyte pair. This is due to that the initial hypothesis was that the ND-coatings are stable and their properties would not change significantly. However when ND behavior was realized, focus was directed into repeating dopamine measurements with untreated ta-C+ND and annealed ta-C+ND-600 samples. Nanodiamonds vacuum annealing was done to investigate the role of oxygen containing surface groups in detection of dopamine. Assumption was that during the annealing decomposition of oxygen containing surface groups would occur. In CV this was expected to be seen as a degradation of electrochemical behavior towards dopamine. For further information, see sections 5.3.1 and 5.4.1.

Here DA results of ta-C+ND and ta-C+ND-600 electrodes are presented. In addition, effect of scanning rate and deviation in DA+AA results are shown for untreated ta-C+ND. As there are lot of results, only some of the selected ones are presented. Every sample is color coded based on the period when the measurement was done.

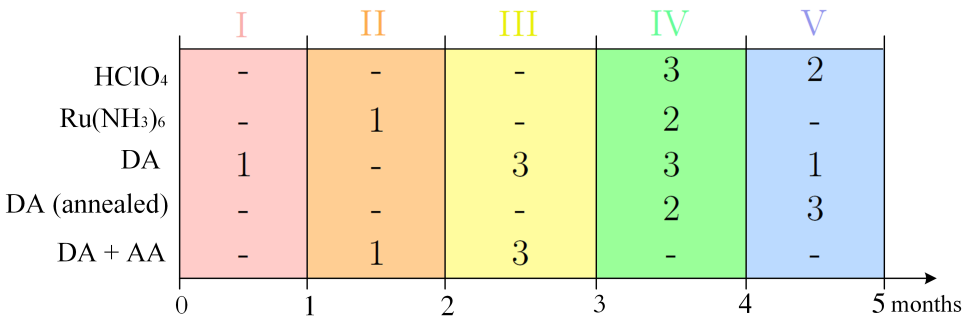

Figure 31: *CV experiments as function of time. Number in the figure indicates the repetition of the measurement during te one time period.*

Table 10: *Observed behaviour of different parameters in DA and DA+AA measurements and their reproducibility.*

	Reproducibility		
Measurements	**Poor**	**Mediocre**	**Good**
DA (with untreated samples)	• Sensitivity • i_{pa} (1mM, 100μM & 10μM) • ΔE_p (10μM) • Extra reduction peak at -0.2 V	• 'Quinone' peak [a] • $E_{o,x}$(1mM & 100μM) • ΔE_p(1mM & 100μM) • Backgroung current • E_{red}[b]	
DA (with annealed samples)	• i_{pa} (1mM, 100μM & 10μM)	• 'Quinone' peak [a] • ΔE_p (1mM) • Sensitivity [c] • Background current	• ΔE_p(100μM & 10μM) • Oxidation pre-peak at 100μM & 10μM • Extra reduction at -0.25V • E_{red}[b]
DA+AA (with untreated samples)	• i_{pa} (in all solutions) • E_{ox} (1mM AA + 100μM • Linear response to addition of DA	• E_{ox} (1mM AA, 10μM DA+1mM AA & 1μM DA+1mM AA) • DA shifts E_{ox} to cathodic direction	• E_{ox} (1mM AA + 1mM DA)

(a) 'Quinone' peak only appears at time period IV
(b) In concentrations where reduction is observed
(c) If no 'quinone' peak is observed

7.3.2.1 Dopamine measurements with ta-C+ND electrodes

Three type of trends in DA detection was observed with ta-C+ND samples in three different time periods III, IV and V. Voltammograms in PBS and different DA concentrations with these samples are shown in Figure 32(a-c). With sample III clear oxidation peak is observed for DA which increases as function of concentration. Detection limit for III is 100 nM DA. Sample measured in period IV shows reversible redox reaction in PBS. As PBS does not contain any reactive analyte, redox reactions could be caused by some reactive group on the ND surface. Oxidation peak has same position as sample III $E_{ox,DA}$ (Figure 32(d)). As seen from Figure 32(b) response of DA is covered behind the characteristic peak of the material IV. Anodic current increases as concentration of DA is increased, but as there are no peaks for DA oxidation. Therefore detection limit is difficult to evaluate. ta-C+ND measured in period V shows that nanodiamonds own redox reaction on the surface has disappeared. For DA more broad oxidation peak is observed in 500 nM and above. Deviation of the ta-C samples in different time periods are shown in Figure 32(d) and table 15.

Passivation of the samples were investigated in 1 mM DA for cycling every sample for 10 cycles (Figure 32(e)). $E_{ox,DA}$ for samples III, IV and V were 280, 306 and 274 mV at cycle 1. At cycle 10 increase of ΔE_p were 70, 84 and 94 mV. Trend in DA oxidation potential and in increasing ΔE_p (Figure 32(f)) is similar between samples. Observed differences in ta-C+ND samples were the magnitudes of their oxidation peak currents. V has highest current values for DA oxidation, whereas III current quantity is the lowest. Also V has the strongest reduction peak for DA. Observed values for DA measurements are listed in table 15.

Variation in observed results is most likely caused by changes in the nanodiamonds surface properties, which can be related to the RGA results (see section 7.3). Why and how this change proceeds is unknown. RGA indicates that samples stored in ambient room temperature for longer time have less water in them. Additionally, amount of carboxyl functionalization may decrease as surface groups are possibly transformed into other oxygen-containing functional groups under ambient air as discussed in section 7.3. Furthermore, the reversible redox peak with sample IV may be caused by a 'quinone' group on ND surface that can participate on redox reactions [122, 123]. However without any surface characterization it cannot be said what causes redox reactions with sample IV.

Current changes between samples III, IV and V is most likely due to the change in the surface area and in amount of nanodiamonds on the ta-C surface. By observing ta-C+ND electrodes with eye, ND layer on top of ta-C does not seem to be uniform. Therefore it can be expected that there are different amounts of nanodiamonds top of ta-C. Also it is possible that with some samples ta-C is not fully covered on ND layer and oxidation of DA may take place on both ta-C and ND surface, which can cause changes in the electrochemical performance of the electrodes. In addition nanodiamonds may agglomerate on top ta-C which can cause changes in current density or in other features such as oxidation potential or sensitivity towards DA.

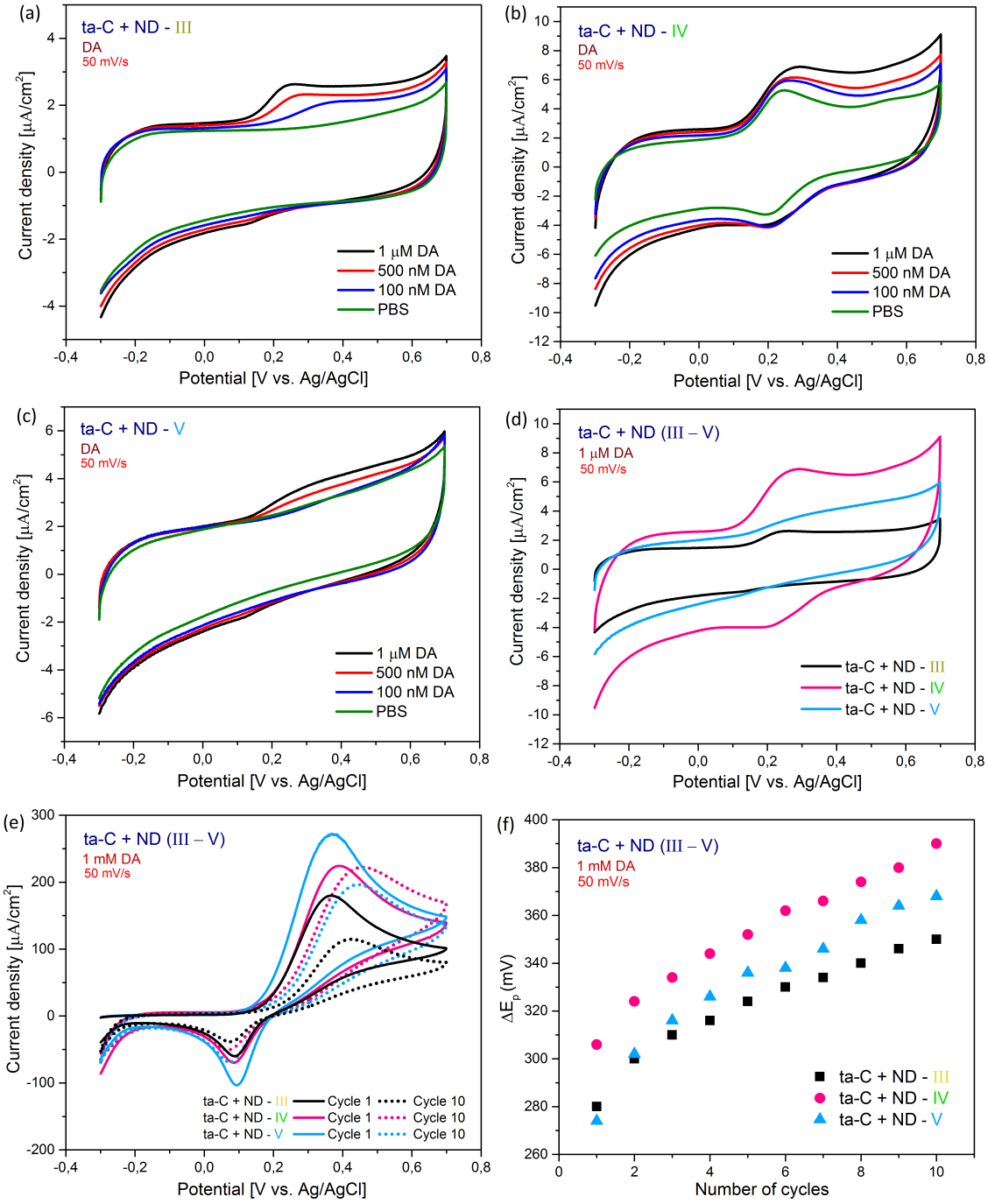

Figure 32: *Dopamine results for three ta-C+ND samples measured at time periods III, IV and V. Behavior in low DA concentrations shown for (a) ta-C+ND -III, (b) ta-C+ND -IV and (c) ta-C+ND -V. Figure (d) show comparison of these three electrodes behaviour at 1µM DA. Passivation is presented (e) as 1st and 10th cycle in 1mM DA and (f) ΔE_p as function of cycles.*

7.3.2.2 Dopamine measurements with annealed ta-C+ND electrodes

Annealed ta-C+ND-600 samples measured in time periods IV and V are presented in Figure 33. In period IV reversible redox reaction is again seen in PBS at ∼0.2 V as with untreated ta-C+ND sample (see Figure 34(b)). When DA concentration is increased, it can be observed that DA shifts oxidation peak to more cathodic values in concentrations of 500nM, 750nM, 1μM and 10μM (Figure 33(a)). Detection limit of DA cannot be evaluated as response of small dopamine concentrations are covered behind 'quinone' peak. In addition at 10μM another oxidation and reduction peak is observed at approximately 0.1 and 0.15 V. Also strong reduction is seen at -0.35 V at concentration 250 nM of DA and above. Similar behavior is also observed with sample measured at V (Figure 33(b)). At 10 μM two oxidation peaks are present at around 0.2 V. Also two reduction peaks are observed at 0.15 V and -0.35 V. However with sample ta-C+ND-600-V 'quinone' peak is not seen. Oxidation of DA is detectect at 50 nM. Shape of the oxidation peak is sharp and the quantity of Faradaic current increases as the concentration increases. Moreover DA kinetics at V are reversible as the reduction reaction is seen already in 250 nM with ΔE_p=62 mV. Figures 33(c) and 33(d) shows that double redox peaks are seen with both samples at concentrations of 10 and 100 μM of DA.

Behaviour of both samples in 1 mM DA are shown in Figure 33(d,f). Dopamine oxidation is observed for IV at 90 mV and for V at 74mV. Increase of ΔE_p during 10 cycles are 78 and 122 mV. Based on the change of ΔE_p, sample V passivates more strongly which is also seen from the larger decrease of current density. At cycle 1 V has clearly higher current density then IV, but after 10 cycles current densities of DA oxidations are similar. In addition at cycle 10 extra oxidation peak is observed with both samples at -0.2 V.

Again 'quinone' peak appears with sample measured at IV and disappears at V. Contrary to hypothesis, annealing of the ta-C+ND samples improves electrodes kinetics and sensitivity towards DA. With RGA carbon monoxide and carbon dioxide are detected during annealing, which indicates decomposition of some oxygen-containing surface groups. Based on the literary data carboxyl, anhydride and lactone groups decompose below 600°C, whereas ketonic and ether groups requires higher temperature [101, 105]. However without more detailed surface characterization it can't be concluded what is the actual surface chemistry of nanodiamonds after annealing. In addition to this, during annealing ND surface may undergo phase transformation after decomposition of surface groups, where the quantity of sp^2 increases (see sections 5.3.1 and 5.3.2). Also if the surface of ta-C is exposed from under ND layer, some changes may occur in ta-C itself.

Peak observed at lower cathodic potential before DA oxidation (Figure 33(c,e)) may be caused by strong adsorption of DA oxidation product DAQ. Furthermore reduction at -0.25 V could be due to the reduction of dopaminechrome into leucodopaminechrome. If these two proposed reaction take place at first cycle in DA, solution should already contain oxidation products before electrochemical oxidation of DA. This may happen as DA can spontaneously oxidize under alkaline solutions [104]. However in Figure

33(d) additional oxidation is seen at cycle 10. This response is most likely oxidation of LDC into DAC. To investigate adsorption peak behavior in more detail, different scan rates can be used. If pre-peak before DA is caused by adsorption, i_{pa} is linearly dependent on v.

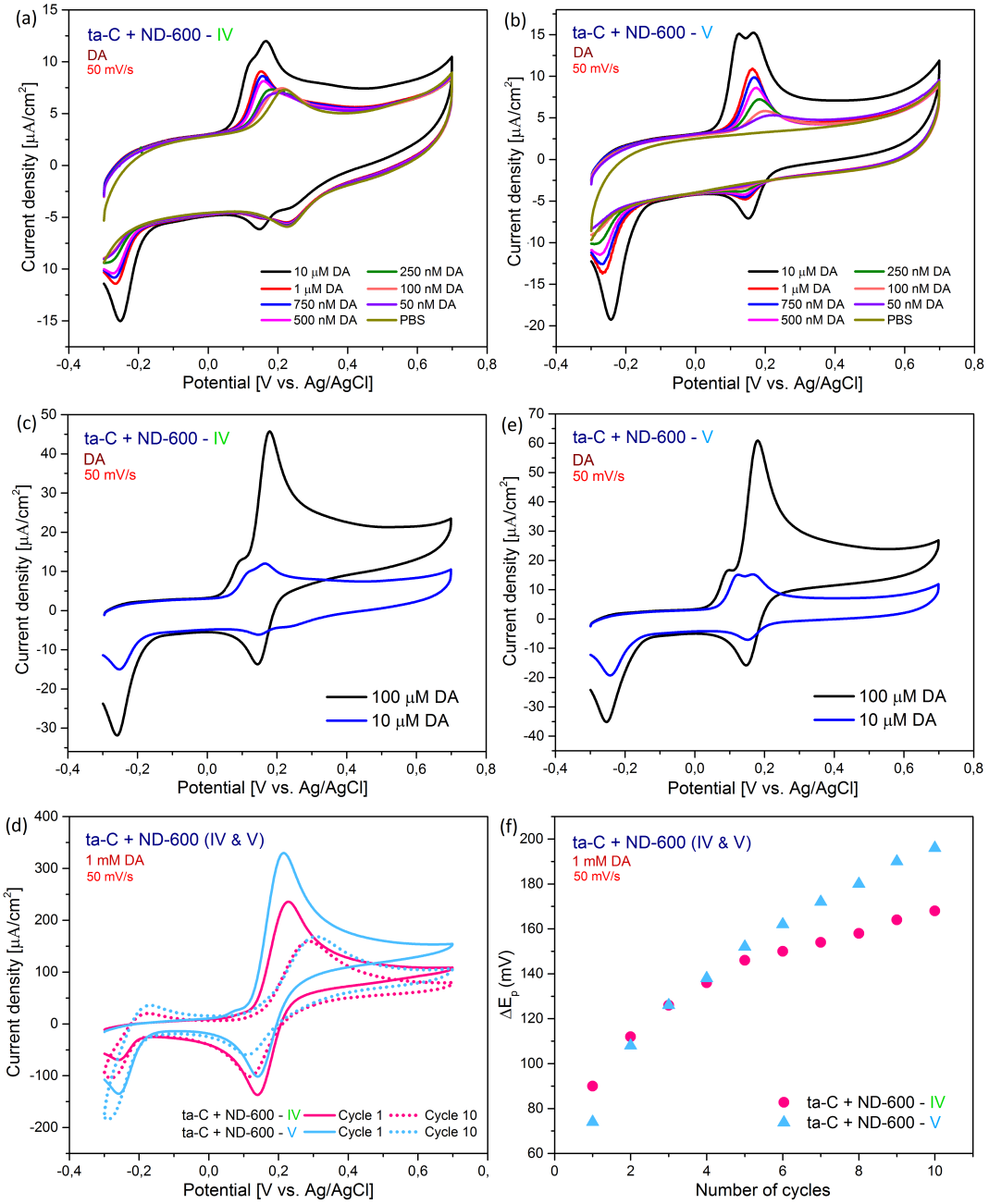

Figure 33: *Dopamine results for annealed samples measured at IV and V. Behavior in low DA concentrations shown for (a) ta-C+ND-600-IV and (b) ta-C+ND-600-V. Observed adsorption peak in concentration of 10 and 100μM presented for (d)ta-C+ND-600-IV and (e) ta-C+ND-600-V. Passivation behavior of both samples is presented in 1mM DA as (d) 1st and 10th cycle and (f) ΔE_p as function of cycles.*

7.3.2.3 Comparison of untreated ta-C+ND and annealed ta-C+ND-600 electrodes

Comparison of untreated ta-C+ND and annealed ta-C+ND is displayed in Figure 34 and in table 15. Comparison between measurements in low concentrations of DA is done for samples that are measured at the same time period. From these results it is observed that sensitivity towards DA is improved. At the same time shifting in DA oxidation to more cathodic potentials is seen. Kinetics are also faster with annealed samples as reduction for DA product is seen already at 1μM with low ΔE_p. In 1mM ΔE_p for annealed samples are 74 and 90 mV, where as for untreated ta-C+ND observed values were 215 and 229 mV. In addition, there are clear difference in the passivation of the samples (Figure 34(d)). Passivation of annealed ta-C+ND-600 is less severe than for untreated ta-C+ND. Another clear difference is that additional adsorption and reduction peaks are not seen with untreated ta-C+ND samples.

As no surface characterization is done with annealed ta-C+ND samples, reliable evaluation of reasons why annealing improves electrodes properties towards DA or why additional redox reactions occur can not be done. To understand the changes between samples, characterization of surface chemistry and content of hybridized carbons are needed. For example these characterizations can be done with XPS, XAS, FTIR and Raman spectroscopy. Also CV should be done in other redox probes than only DA. $Ru(NH_3)_6^{2+/3+}$ experiments would provide information if electron transfer properties of the hybrid electrode is changed during annealing.

Based on present knowledge and speculation, (i) content of sp^2 carbon may increase during annealing, (ii) impurities from the vacuum furnace improves electrochemical properties of the electrode or (iii) decompositon or transformation of carboxyl groups from nanodiamonds could create more attractive surface for DA oxidation. Changes in carboxyl groups are assumed as the as received ND suspension is carboxyl terminated. Also it could be possible that some changes occur in ta-C during annealing.

Table 11: *Experimental values for dopamine measurements with untreated and annealed ta-C+ND electrodes.*

Sample	Detection limit (nM)	ΔE_p (mV), 10μM	ΔE_p (mV), 1 mM DA Cycles 1(10)	E_{ox} (mV), 1mM DA Cycles 1(10)
ta-C+ND - III	100	170	280 (350)	367 (425)
ta-C+ND - IV	(a)	(a)	306 (390)	391 (457)
ta-C+ND - V	500	205	274 (368)	367 (443)
ta-C+ND-600 - IV	(a)	18	90 (168)	229 (287)
ta-C+ND-600 - V	50	14	74 (196)	215 (307)

(a) DA response overlapping with 'quinone' peak

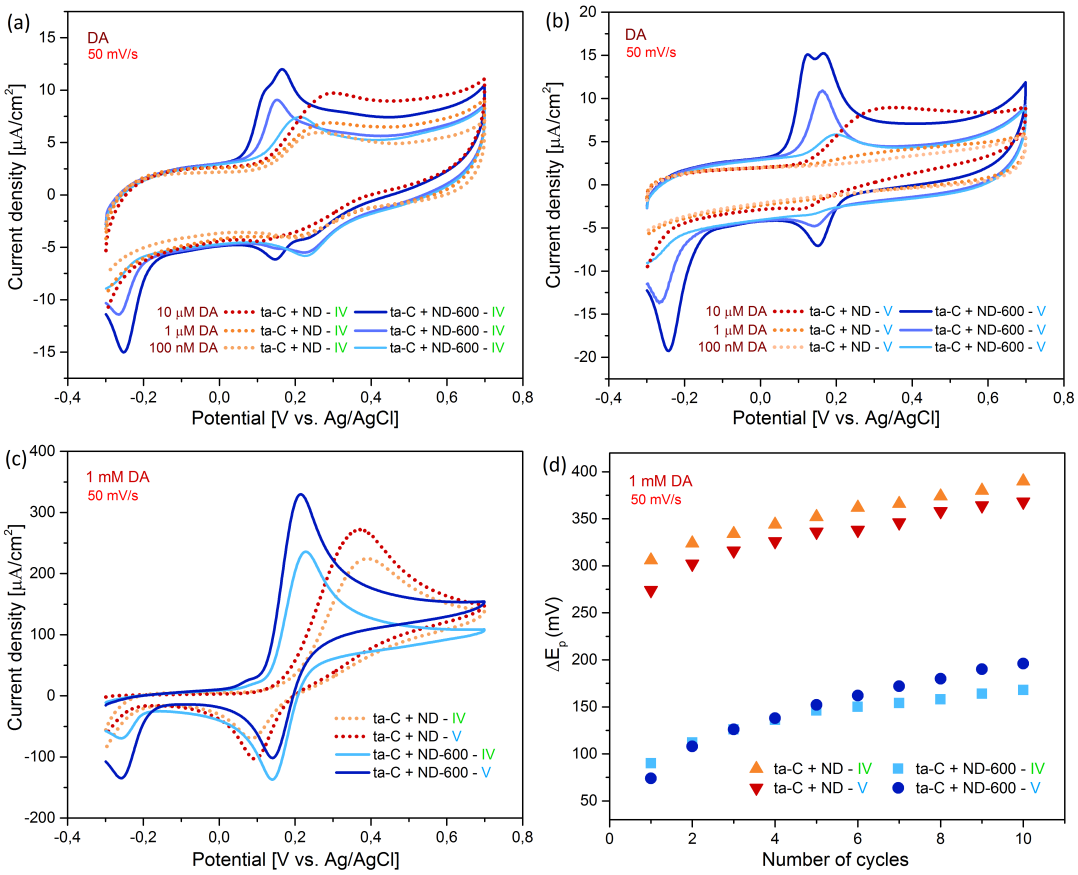

Figure 34: *Comparison of dopamine results between untreated and annealed ta-C+ND electrodes. Behavior at low concentrations of DA are done with samples measured at (a) IV and (b) V. Passivation of the electrodes in 1 mM DA shown as (c) 1st cycles and (d) ΔE_p as function of cycles.*

7.3.2.4 DA+AA results with ta-C+ND samples

Here samples measured in periods II and III are presented (Figure 35). There are some deviation between these two samples, but neither of one is selective towards DA in presence of AA. Differences between II and III, is that II oxidation current has more linear response when DA concentration is increased. Also with II oxidation potentials are more cathodic than with III. In 1mm AA + 1mM DA solution E_{ox} for II and III are 365 and 391 mV, whereas for 1 mM AA 557 and 643 mV. Addition of DA in AA solution shifts oxidation potentials towards cathodic values. Additionally, differences in current densities are again observed. From Figure 35(d) catalyzing mechanism of AA is seen for sample III. i_{pa} for solution 1mM AA + 1mM DA is significantly higher than peak current for plain DA or AA, which supports theory of AA catalyzing mechanism (see section 2.2.2).

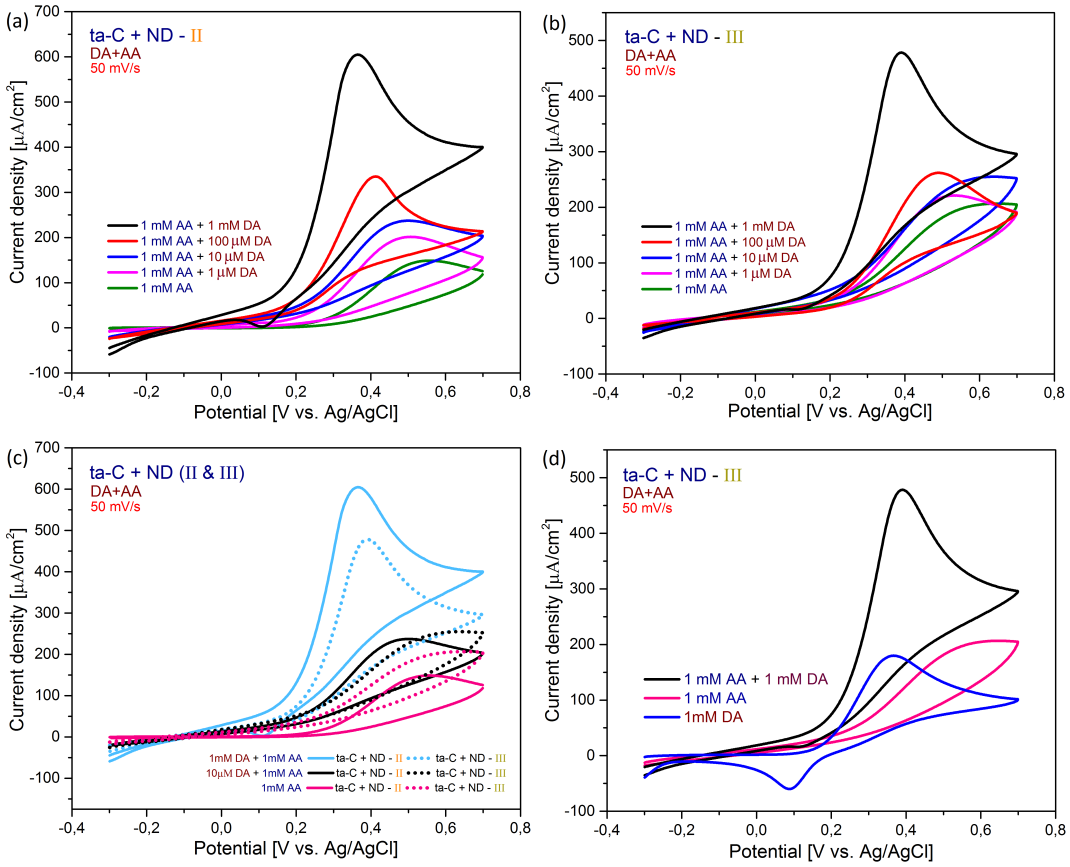

Figure 35: *DA+AA measurements for (a) ta-C+ND-II and (b) ta-C+ND-III, where (c) comparison of the samples is presented and (d) results of DA, AA and DA+AA is shown for ta-C+ND-III.*

7.3.2.5 Effect of scan rate

To investigate reaction kinetics of the ta-C+ND electrodes, different scan rates were used in DA and DA+AA solutions (Figure 36). Experiments were done at time period III. Dopamine kinetics were tested in 100 μM solutions, where scan rates 10, 50, 100, 200, 400 and 1000 mV/s were used (Figure 36(a)). ΔE_p values for used v are listed in table 16. It is observed that in DA solution ΔE_p increases as function of v. This indicates that speed of electron transfer is not sufficiently high. The relation of anodic peak current is shown in Figure 36(b). As i_{pa} is directly proportional to square root of v, DA reaction is diffusion controlled.

In DA+AA measurements aim was to test if DA and AA can be separated by using different scan rates (Figure 36(c,d)). In 1mM AA + 100μM DA used potential window is too narrow, as at higher scan rates clear oxidation peak is not observed. Also i_{pa} does not increase as function of scan rate. Response of anodic current is more random. However in 1mM AA + 1mM DA same potential window was used and clear oxidation peaks are observed at scan rates 50, 400 and 1000 mV/s. Increasing the DA concentration, DA+AA oxidation potential shifts to more cathodic direction.

However, oxidation peaks for DA and AA cannot be separated with higher scan rates. At least with not scan rates used in this work. This indicates that both analytes reactions kinetics are limited and affected by the scan rate.

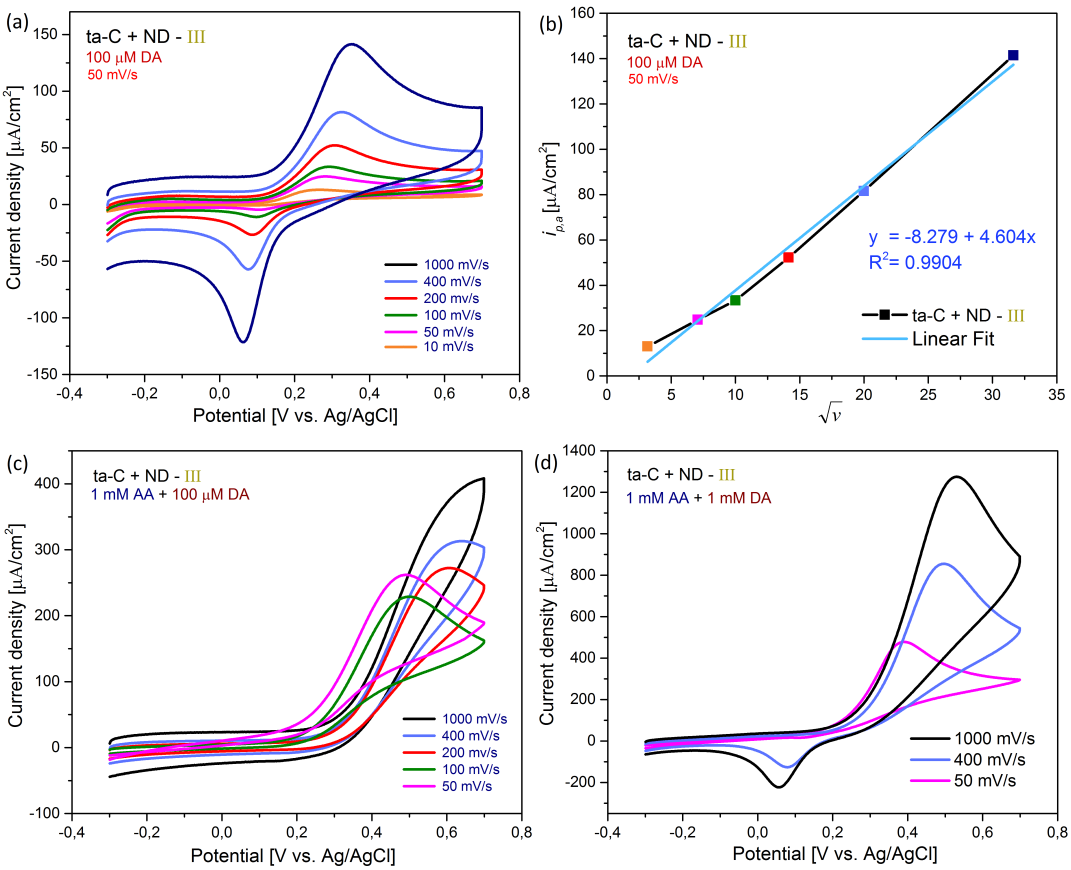

Figure 36: *Effect of scan rate on DA and DA+AA solutions. ta-C+ND-III was measured in (a) 100µ DA solution, where (b) anodic peak current i_{pa} was directly dependent on square root of v. Kinetics of DA+AA was measured in solution of (c) 1mM AA + 100µM DA and (d) 1mM AA + 1mM DA.*

Table 12: *Potential peak separation ΔE_p values at different scan rates v in solutions 100µM DA and 1mM AA + 1mM DA.*

		ΔE_p (mV)					
		Scan rate (mV/s)					
Sample	Solution	10	50	100	200	400	1000
ta-C+ND -III	100 μM DA	(a)	176	196	220	250	288
ta-C+ND -III	1mM DA +1mM AA	-	(a)	-	-	418	474

(a) No reduction observed

8 Discussion

Based on the found literature, it is difficult provide any reliable explanation for electrochemical behavior of the nanodiamonds. In literature there is inadequate information of the nanodiamonds synthesis and characteristics. As discussed in section 5.1, cooling medium used during detonation synthesis affects ND sp^2 shell thickness, whereas the post-synthesis liquid oxidant determines the surface functionalization of the nanodiamond. These specs are rarely given in the literature, which indicates that the properties of the used nanodiamonds are not well known.

Among the inadequate characterization, there are inconsistencies in the electrochemical experiments found from the literature. For example in Holt's publications, several electrode materials are used together with nanodiamonds. These materials are GC [98], BDD [92, 117] and gold [98]. Instead of doing profound characterization for one specific nanodiamond hybrid electrode, measurements are carried out with several electrodes in limited amount of redox probes, such as $Ru(NH_3)_6^{+2/+3}$ and $Fe(CN)_6^{3-/4-}$. Based on these results, Holt's 'molecular-like' theory proposes that enhanced redox currents arises from interactions of the redox probe and the ND surface groups [92]. However, theory is based on the results with outher sphere probes and according to Bard [66] these analytes are not dependent on the electrodes surface chemistry. To investigate the role of ND surface groups, inner sphere redox probes should be used.

Additionally, ND electrochemical activity does not only arise from the oxygen-containing surface functionalization as in this work performance of ta-C+ND electrode improved considerably due to vacuum annealing. Against the initial assumption, decomposition of some of the surface groups did not diminis the electrochemical activity of nanodiamonds. However, without any characterization of surface chemistry and sp^2/sp^3 ratio it is difficult to evaluate what actually causes enhanced behavior towards DA. It is likely that the conductive sp^2 shell around the nanodiamonds has an important role in the the electrochemical behavior. It is possible that during annealing the content of sp^2 increases, which enhanced the sensitivity and kinetics towards DA. However, role of the surface chemistry can't be left out as it affect the adsorption process of the inner sphere probes such as dopamine.

Furthermore, the unstable behavior of nanodiamonds is not brought up in any paper found from the literature. No information is given how many times experiments are repeated in the publications, thus it is difficult to evaluate if the results are reproducible or if only the 'best' ones are chosen for publications.

9 Conclusion

CV results with hybrid ta-C+ND electrode were equally good or improved compared to plain ta-C electrode. Enhanced behavior with ta-C+ND was seen in DA measurements, where (i) the passivation of the electrode was reduced and (ii) sensitivity towards dopamine was improved. However, selectivity towards DA in presence of AA was not achieved with ND coating. Furthermore, major challenge in ta-C+ND electrochemical characterization was that CV measurements were not reproducible over time in DA and AA solution.

Annealing of the ta-C+ND improved electrodes electrochemical properties towards DA. Following enhancements were observed in DA solutions: (i) sensitivity, (ii) reaction kinetics and (iii) reduced passivation. Unstable behavior of ta-C+ND electrodes were also seen with annealed samples. However, annealing improved experiments repeatability as was seen in table 10.

As CV was the only characterization method in this work, it is hard to evaluate what causes the unstable behavior of ta-C+ND or why the properties are improved towards DA during annealing. To investigate these phenomenas more, next steps would be (i) extensive characterization of surface chemistry (XPS, XAS, NMR) and morphology (HRTEM, Raman), (ii) simulations of the system for example with density functional theory and (iii) CV experiments with several redox probes using different scan rates. Especially for investigating possible adsorption peak and electrode passivation in DA solution, using different scan rates provides information of the nature of these phenomenas. Furthermore, to study the changing properties and time dependency of ta-C+ND electrodes, the experiments need to be performed more systematic.

References

[1] O. Shenderova, V. Zhirnov, and D. Brenner, "Carbon nanostructures," *Critical Reviews in Solid State and Material Sciences*, vol. 27, no. 3-4, pp. 227–356, 2002.

[2] A. Mostofizadeh, Y. Li, B. Song, and Y. Huang, "Synthesis, properties, and applications of low-dimensional carbon-related nanomaterials," *Journal of nanomaterials*, vol. 2011, p. 16, 2011.

[3] R. L. McCreery, "Advanced carbon electrode materials for molecular electrochemistry," *Chem. Rev*, vol. 108, no. 7, pp. 2646–2687, 2008.

[4] K. Jackowska and P. Krysinski, "New trends in the electrochemical sensing of dopamine," *Analytical and bioanalytical chemistry*, vol. 405, no. 11, pp. 3753–3771, 2013.

[5] R. M. Wightman, L. J. May, and A. C. Michael, "Detection of dopamine dynamics in the brain," *Analytical Chemistry*, vol. 60, no. 13, pp. 769A–793A, 1988.

[6] D. L. Robinson, B. J. Venton, M. L. Heien, and R. M. Wightman, "Detecting subsecond dopamine release with fast-scan cyclic voltammetry in vivo," *Clinical chemistry*, vol. 49, no. 10, pp. 1763–1773, 2003.

[7] Y. Shao, J. Wang, H. Wu, J. Liu, I. A. Aksay, and Y. Lin, "Graphene based electrochemical sensors and biosensors: a review," *Electroanalysis*, vol. 22, no. 10, pp. 1027–1036, 2010.

[8] V. Danilenko, "On the history of the discovery of nanodiamond synthesis," *Physics of the Solid State*, vol. 46, no. 4, pp. 595–599, 2004.

[9] E. Peltola, N. Wester, K. B. Holt, L.-S. Johansson, J. Koskinen, V. Myllymäki, and T. Laurila, "Nanodiamonds on tetrahedral amorphous carbon significantly enhance dopamine detection and cell viability," *Biosensors and Bioelectronics*, 2016.

[10] V. Y. Dolmatov, "Detonation-synthesis nanodiamonds: synthesis, structure, properties and applications," *Russian Chemical Reviews*, vol. 76, no. 4, p. 339, 2007.

[11] S. Sainio, T. Palomäki, N. Tujunen, V. Protopopova, J. Koehne, K. Kordas, J. Koskinen, M. Meyyappan, and T. Laurila, "Integrated carbon nanostructures for detection of neurotransmitters," *Molecular neurobiology*, vol. 52, no. 2, pp. 859–866, 2015.

[12] C. Missale, S. R. Nash, S. W. Robinson, M. Jaber, and M. G. Caron, "Dopamine receptors: from structure to function," *Physiological reviews*, vol. 78, no. 1, pp. 189–225, 1998.

[13] D. L. Robinson, A. Hermans, A. T. Seipel, and R. M. Wightman, "Monitoring rapid chemical communication in the brain," *Chemical reviews*, vol. 108, no. 7, pp. 2554–2584, 2008.

[14] W. Schultz, "Predictive reward signal of dopamine neurons," *Journal of neurophysiology*, vol. 80, no. 1, pp. 1–27, 1998.

[15] K. L. Davis, R. S. Kahn, G. Ko, and M. Davidson, "Dopamine in schizophrenia: a review and reconceptualization," *Am J psychiatry*, vol. 148, no. 11, pp. 1474–1486, 1991.

[16] J. Biederman, "Attention-deficit/hyperactivity disorder: a selective overview," *Biological psychiatry*, vol. 57, no. 11, pp. 1215–1220, 2005.

[17] G. F. Koob and N. D. Volkow, "Neurocircuitry of addiction," *Neuropsychopharmacology*, vol. 35, no. 1, pp. 217–238, 2010.

[18] B. J. Venton and R. M. Wightman, "Psychoanalytical electrochemistry: dopamine and behavior," *Analytical Chemistry*, vol. 75, no. 19, pp. 414–A, 2003.

[19] G. S. Wilson and R. Gifford, "Biosensors for real-time in vivo measurements," *Biosensors and Bioelectronics*, vol. 20, no. 12, pp. 2388–2403, 2005.

[20] T. Laurila, A. Rautiainen, S. Sintonen, H. Jiang, E. Kaivosoja, and J. Koskinen, "Diamond-like carbon (dlc) thin film bioelectrodes: Effect of thermal post-treatments and the use of ti adhesion layer," *Materials Science and Engineering: C*, vol. 34, pp. 446–454, 2014.

[21] T. Laurila, "Hybrid carbon nanomaterials for electrochemical detection of biomolecules," *Physica Scripta*, vol. 90, no. 9, p. 094006, 2015.

[22] E. Kaivosoja, S. Sainio, J. Lyytinen, T. Palomäki, T. Laurila, S. I. Kim, J. G. Han, and J. Koskinen, "Carbon thin films as electrode material in neural sensing," *Surface and Coatings Technology*, vol. 259, pp. 33–38, 2014.

[23] J. Robertson, "Diamond-like amorphous carbon," *Materials Science and Engineering: R: Reports*, vol. 37, no. 4, pp. 129–281, 2002.

[24] R. G. Compton, J. S. Foord, and F. Marken, "Electroanalysis at diamond-like and doped-diamond electrodes," *Electroanalysis*, vol. 15, no. 17, pp. 1349–1363, 2003.

[25] E. Kaivosoja, P. Suvanto, G. Barreto, S. Aura, A. Soininen, S. Franssila, and Y. T. Konttinen, "Cell adhesion and osteogenic differentiation on three-dimensional pillar surfaces," *Journal of Biomedical Materials Research Part A*, vol. 101, no. 3, pp. 842–852, 2013.

[26] S. Sainio, T. Palomäki, S. Rhode, M. Kauppila, O. Pitkänen, T. Selkälä, G. Toth, M. Moram, K. Kordas, J. Koskinen, *et al.*, "Carbon nanotube (cnt) forest grown on diamond-like carbon (dlc) thin films significantly improves electrochemical sensitivity and selectivity towards dopamine," *Sensors and Actuators B: Chemical*, vol. 211, pp. 177–186, 2015.

[27] S. Chandra and D. K. Wong, "Electrochemical detection of neurotransmitters at structurally small electrodes," 2009.

[28] T. Palomäki, "Electrochemical measurement of dopamine with diamond-like carbon/pt composite electrodes," Master's thesis, Aalto University, 2013.

[29] N. Wester, "Tetrahedral amorphous carbon–graphene hybrid electrode for detection of dopamine," Master's thesis, Aalto University, 2015.

[30] J. Wang, "Electrochemical glucose biosensors," *Chemical reviews*, vol. 108, no. 2, pp. 814–825, 2008.

[31] N.-M. Tujunen, "Glutamaatin amperometrinen mittaaminen," Master's thesis, Aalto University, 2013.

[32] J. Wagner, P. Vitali, M. G. Palfreyman, M. Zraika, and S. Huot, "Simultaneous determination of 3, 4-dihydroxyphenylalanine, 5-hydroxytryptophan, dopamine, 4-hydroxy-3-methoxyphenylalanine, norepinephrine, 3, 4-dihydroxyphenylacetic acid, homovanillic acid, serotonin, and 5-hydroxyindoleacetic acid in rat cerebrospinal fluid and brain by high-performance liquid chromatography with electrochemical detection," *Journal of neurochemistry*, vol. 38, no. 5, pp. 1241–1254, 1982.

[33] B. Fornstedt, E. Rosengren, and A. Carlsson, "Occurrence and distribution of 5-s-cysteinyl derivatives of dopamine, dopa and dopac in the brains of eight mammalian species," *Neuropharmacology*, vol. 25, no. 4, pp. 451–454, 1986.

[34] Y.-M. Wang, F. Xu, R. R. Gainetdinov, and M. G. Caron, "Genetic approaches to studying norepinephrine function: knockout of the mouse norepinephrine transporter gene," *Biological psychiatry*, vol. 46, no. 9, pp. 1124–1130, 1999.

[35] I. Mefford, A. Oke, R. Keller, R. Adams, and G. Jonsson, "Epinephrine distribution in human brain," *Neuroscience letters*, vol. 9, no. 2, pp. 227–231, 1978.

[36] P. Wester, J. Hardy, J. Marcusson, P. Nyberg, and B. Winblad, "Serotonin concentrations in normal aging human brains: relation to serotonin receptors," *Neurobiology of aging*, vol. 5, no. 3, pp. 199–203, 1984.

[37] P. Riederer, E. Sofic, W.-D. Rausch, B. Schmidt, G. P. Reynolds, K. Jellinger, and M. B. Youdim, "Transition metals, ferritin, glutathione, and ascorbic acid in parkinsonian brains," *Journal of neurochemistry*, vol. 52, no. 2, pp. 515–520, 1989.

[38] K. Iriyama, T. Iwamoto, M. Yoshiura, and T. Aoki, "Postmortem changes in uric acid and ascorbic acid in human cerebral cortex tissues excised after cardiac death," *Biochemical medicine and metabolic biology*, vol. 36, no. 2, pp. 186–193, 1986.

[39] M. A. Dayton, A. G. Ewing, and R. M. Wightman, "Response of microvoltammetric electrodes to homogeneous catalytic and slow heterogeneous charge-transfer reactions," *Analytical Chemistry*, vol. 52, no. 14, pp. 2392–2396, 1980.

[40] M. Gelbert and D. Curran, "Alternating current voltammetry of dopamine and ascorbic acid at carbon paste and stearic acid modified carbon paste electrodes," *Analytical chemistry*, vol. 58, no. 6, pp. 1028–1032, 1986.

[41] W. Harreither, R. Trouillon, P. Poulin, W. Neri, A. G. Ewing, and G. Safina, "Carbon nanotube fiber microelectrodes show a higher resistance to dopamine fouling," *Analytical chemistry*, vol. 85, no. 15, pp. 7447–7453, 2013.

[42] A. N. Patel, S.-y. Tan, T. S. Miller, J. V. Macpherson, and P. R. Unwin, "Comparison and reappraisal of carbon electrodes for the voltammetric detection of dopamine," *Analytical chemistry*, vol. 85, no. 24, pp. 11755–11764, 2013.

[43] T. Kato, S. Fierro, T. Watanabe, K. Yoshimi, and Y. Einaga, "Dopamine detection on boron-doped diamond electrodes using fast cyclic voltammetry," *Chemistry Letters*, vol. 41, no. 3, pp. 224–226, 2012.

[44] U. E. Majewska, K. Chmurski, K. Biesiada, A. R. Olszyna, and R. Bilewicz, "Dopamine oxidation at per (6-deoxy-6-thio)-α-cyclodextrin monolayer modified gold electrodes," *Electroanalysis*, vol. 18, no. 15, pp. 1463–1470, 2006.

[45] S. H. DuVall and R. L. McCreery, "Control of catechol and hydroquinone electron-transfer kinetics on native and modified glassy carbon electrodes," *Analytical Chemistry*, vol. 71, no. 20, pp. 4594–4602, 1999.

[46] A. Domenech, H. Garcia, M. Domenech-Carbo, and M. Galletero, "2, 4, 6-triphenylpyrylium ion encapsulated into zeolite y as a selective electrode for the electrochemical determination of dopamine in the presence of ascorbic acid," *Analytical chemistry*, vol. 74, no. 3, pp. 562–569, 2002.

[47] S. Corona-Avendaño, G. Alarcón-Angeles, M. T. Ramírez-Silva, G. Rosquete-Pina, M. Romero-Romo, and M. Palomar-Pardavé, "On the electrochemistry of dopamine in aqueous solution. part i: The role of [sds] on the voltammetric behavior of dopamine on a carbon paste electrode," *Journal of Electroanalytical Chemistry*, vol. 609, no. 1, pp. 17–26, 2007.

[48] X.-L. Wen, Y.-H. Jia, and Z.-L. Liu, "Micellar effects on the electrochemistry of dopamine and its selective detection in the presence of ascorbic acid," *Talanta*, vol. 50, no. 5, pp. 1027–1033, 1999.

[49] D. C. Tse, R. L. McCreery, and R. N. Adams, "Potential oxidative pathways of brain catecholamines," *Journal of medicinal chemistry*, vol. 19, no. 1, pp. 37–40, 1976.

[50] Y. Li, M. Liu, C. Xiang, Q. Xie, and S. Yao, "Electrochemical quartz crystal microbalance study on growth and property of the polymer deposit at gold electrodes during oxidation of dopamine in aqueous solutions," *Thin Solid Films*, vol. 497, no. 1, pp. 270–278, 2006.

[51] F. Bernsmann, V. Ball, F. Addiego, A. Ponche, M. Michel, J. J. d. A. Gracio, V. Toniazzo, and D. Ruch, "Dopamine- melanin film deposition depends on the used oxidant and buffer solution," *Langmuir*, vol. 27, no. 6, pp. 2819–2825, 2011.

[52] Y. Liu, K. Ai, and L. Lu, "Polydopamine and its derivative materials: synthesis and promising applications in energy, environmental, and biomedical fields," *Chemical reviews*, vol. 114, no. 9, pp. 5057–5115, 2014.

[53] D. R. Dreyer, D. J. Miller, B. D. Freeman, D. R. Paul, and C. W. Bielawski, "Elucidating the structure of poly (dopamine)," *Langmuir*, vol. 28, no. 15, pp. 6428–6435, 2012.

[54] S. Hong, Y. S. Na, S. Choi, I. T. Song, W. Y. Kim, and H. Lee, "Non-covalent self-assembly and covalent polymerization co-contribute to polydopamine formation," *Advanced Functional Materials*, vol. 22, no. 22, pp. 4711–4717, 2012.

[55] N. F. Della Vecchia, R. Avolio, M. Alfè, M. E. Errico, A. Napolitano, and M. d'Ischia, "Building-block diversity in polydopamine underpins a multifunctional eumelanin-type platform tunable through a quinone control point," *Advanced Functional Materials*, vol. 23, no. 10, pp. 1331–1340, 2013.

[56] I. N. Mefford, A. F. Oke, and R. N. Adams, "Regional distribution of ascorbate in human brain," *Brain research*, vol. 212, no. 1, pp. 223–226, 1981.

[57] G. Nagy, M. E. Rice, and R. N. Adams, "A new type of enzyme electrode: the ascorbic acid eliminator electrode," *Life Sciences*, vol. 31, no. 23, pp. 2611–2616, 1982.

[58] T. Kondo, Y. Niwano, A. Tamura, J. Imai, K. Honda, Y. Einaga, D. A. Tryk, A. Fujishima, and T. Kawai, "Enhanced electrochemical response in oxidative differential pulse voltammetry of dopamine in the presence of ascorbic acid at carboxyl-terminated boron-doped diamond electrodes," *Electrochimica Acta*, vol. 54, no. 8, pp. 2312–2319, 2009.

[59] S.-Y. Yi, H.-Y. Chang, H.-h. Cho, Y. C. Park, S. H. Lee, and Z.-U. Bae, "Resolution of dopamine and ascorbic acid using nickel (ii) complex polymer-modified electrodes," *Journal of Electroanalytical Chemistry*, vol. 602, no. 2, pp. 217–225, 2007.

[60] N. Wisniewski and M. Reichert, "Methods for reducing biosensor membrane biofouling," *Colloids and Surfaces B: Biointerfaces*, vol. 18, no. 3, pp. 197–219, 2000.

[61] J. S. Wilson, *Sensor technology handbook*. Elsevier, 2004.

[62] A. M. Schrand, S. A. C. Hens, and O. A. Shenderova, "Nanodiamond particles: properties and perspectives for bioapplications," *Critical reviews in solid state and materials sciences*, vol. 34, no. 1-2, pp. 18–74, 2009.

[63] D. Takagi, Y. Kobayashi, and Y. Homma, "Carbon nanotube growth from diamond," *Journal of the American Chemical Society*, vol. 131, no. 20, pp. 6922–6923, 2009.

[64] J. Aromaa, *Sähkökemialliset mittausmenetelmät*. Otamedia oy, 2002.

[65] L. Murtomäki, T. Kallio, R. Lahtinen, and K. Kontturi, *Sähkökemia*. Aalto University, 2010.

[66] A. J. Bard, L. R. Faulkner, J. Leddy, and C. G. Zoski, *Electrochemical methods: fundamentals and applications*, vol. 2. Wiley New York, 1980.

[67] R. G. Compton and C. E. Banks, *Understanding voltammetry*. World Scientific, 2007.

[68] R. S. Nicholson, "Theory and application of cyclic voltammetry for measurement of electrode reaction kinetics.," *Analytical Chemistry*, vol. 37, no. 11, pp. 1351–1355, 1965.

[69] N. G. Shang, P. Papakonstantinou, M. McMullan, M. Chu, A. Stamboulis, A. Potenza, S. S. Dhesi, and H. Marchetto, "Catalyst-free efficient growth, orientation and biosensing properties of multilayer graphene nanoflake films with sharp edge planes," *Advanced functional materials*, vol. 18, no. 21, pp. 3506–3514, 2008.

[70] Z.-H. Sheng, X.-Q. Zheng, J.-Y. Xu, W.-J. Bao, F.-B. Wang, and X.-H. Xia, "Electrochemical sensor based on nitrogen doped graphene: simultaneous determination of ascorbic acid, dopamine and uric acid," *Biosensors and Bioelectronics*, vol. 34, no. 1, pp. 125–131, 2012.

[71] L. Yang, D. Liu, J. Huang, and T. You, "Simultaneous determination of dopamine, ascorbic acid and uric acid at electrochemically reduced graphene oxide modified electrode," *Sensors and Actuators B: Chemical*, vol. 193, pp. 166–172, 2014.

[72] Z. Wang, J. Liu, Q. Liang, Y. Wang, and G. Luo, "Carbon nanotube-modified electrodes for the simultaneous determination of dopamine and ascorbic acid," *Analyst*, vol. 127, no. 5, pp. 653–658, 2002.

[73] W. C. Poh, K. P. Loh, W. D. Zhang, S. Triparthy, J.-S. Ye, and F.-S. Sheu, "Biosensing properties of diamond and carbon nanotubes," *Langmuir*, vol. 20, no. 13, pp. 5484–5492, 2004.

[74] M. Wei, L.-G. Sun, Z.-Y. Xie, J.-F. Zhii, A. Fujishima, Y. Einaga, D.-G. Fu, X.-M. Wang, and Z.-Z. Gu, "Selective determination of dopamine on a boron-doped diamond electrode modified with gold nanoparticle/polyelectrolyte-coated polystyrene colloids," *Advanced Functional Materials*, vol. 18, no. 9, pp. 1414–1421, 2008.

[75] R. T. Kachoosangi and R. G. Compton, "A simple electroanalytical methodology for the simultaneous determination of dopamine, serotonin and ascorbic acid using an unmodified edge plane pyrolytic graphite electrode," *Analytical and bioanalytical chemistry*, vol. 387, no. 8, pp. 2793–2800, 2007.

[76] M. D. Rubianes and G. A. Rivas, "Carbon nanotubes paste electrode," *Electrochemistry Communications*, vol. 5, no. 8, pp. 689–694, 2003.

[77] N. Wester, S. Sainio, T. Palomäki, D. Nordlund, V. K. Singh, L.-S. Johansson, T. Laurila, and J. Koskinen, "Partially reduced graphene oxide (prgo) modified tetrahedral amorphous carbon (ta-c) thin film electrodes as a platform for nanomolar detection of dopamine (submitted)," *Royal Society of Chemistry*, 2016.

[78] D. M. Shenderova, Olga A. Gruen, *Ultrananocrystalline Diamond - Synthesis, Properties, and Applications.* St. Petersburg, Russia: William Andrew Publishing, 2006.

[79] V. Y. Dolmatov, "Detonation synthesis ultradispersed diamonds: properties and applications," *Russian Chemical Reviews*, vol. 70, no. 7, pp. 607–626, 2001.

[80] V. Yu. Dolmatov, "Up-to-date commercial production technology for detonation nanodiamonds and their main applications. Report 1," 2006.

[81] V. Mazanov, "Macrokinetics of the retention of condensed carbon and detonation diamond in a hermetic explosion chamber," *Physics of the solid state*, vol. 46, no. 4, pp. 629–635, 2004.

[82] A. Aleksenskii, M. Baidakova, A. Y. Vul, and V. Siklitskii, "The structure of diamond nanoclusters," *Physics of the solid state*, vol. 41, no. 4, pp. 668–671, 1999.

[83] V. N. Mochalin, O. Shenderova, D. Ho, and Y. Gogotsi, "The properties and applications of nanodiamonds," *Nature nanotechnology*, vol. 7, no. 1, pp. 11–23, 2012.

[84] A. Krueger, "The structure and reactivity of nanoscale diamond," *Journal of Materials Chemistry*, vol. 18, no. 13, pp. 1485–1492, 2008.

[85] A. Krueger, M. Ozawa, G. Jarre, Y. Liang, J. Stegk, and L. Lu, "Deagglomeration and functionalisation of detonation diamond," *Physica status solidi (a)*, vol. 204, no. 9, pp. 2881–2887, 2007.

[86] S. Osswald, G. Yushin, V. Mochalin, S. O. Kucheyev, and Y. Gogotsi, "Control of sp2/sp3 carbon ratio and surface chemistry of nanodiamond powders by selective oxidation in air," *Journal of the American Chemical Society*, vol. 128, no. 35, pp. 11635–11642, 2006.

[87] J.-Y. Raty and G. Galli, "Ultradispersity of diamond at the nanoscale," *Nature materials*, vol. 2, no. 12, pp. 792–795, 2003.

[88] J.-B. Donnet, C. Lemoigne, K. W. Tong, C.-M. Peng, M. Samirant, and A. Eckhardt, "Detonation and shock synthesis of nanodiamonds," *Bulletin de la Société Chimique de France*, vol. 10, no. 134, pp. 875–890, 1997.

[89] J.-Y. Raty, G. Galli, C. Bostedt, T. W. van Buuren, and L. J. Terminello, "Quantum confinement and fullerenelike surface reconstructions in nanodiamonds," *Physical review letters*, vol. 90, no. 3, p. 037401, 2003.

[90] A. Barnard, S. Russo, and I. Snook, "Coexistence of bucky diamond with nanodiamond and fullerene carbon phases," *Physical Review B*, vol. 68, no. 7, p. 073406, 2003.

[91] A. Panich, A. Shames, H.-M. Vieth, E. Ōsawa, M. Takahashi, and A. Y. Vul, "Nuclear magnetic resonance study of ultrananocrystalline diamonds," *The European Physical Journal B-Condensed Matter and Complex Systems*, vol. 52, no. 3, pp. 397–402, 2006.

[92] K. B. Holt, "Undoped diamond nanoparticles: origins of surface redox chemistry," *Physical chemistry chemical physics*, vol. 12, no. 9, pp. 2048–2058, 2010.

[93] X. Fang, J. Mao, E. Levin, and K. Schmidt-Rohr, "Nonaromatic core- shell structure of nanodiamond from solid-state nmr spectroscopy," *Journal of the American Chemical Society*, vol. 131, no. 4, pp. 1426–1435, 2009.

[94] I. Kulakova, "Surface chemistry of nanodiamonds," *Physics of the solid state*, vol. 46, no. 4, pp. 636–643, 2004.

[95] O. Shenderova, A. Koscheev, N. Zaripov, I. Petrov, Y. Skryabin, P. Detkov, S. Turner, and G. Van Tendeloo, "Surface chemistry and properties of ozone-purified detonation nanodiamonds," *The Journal of Physical Chemistry C*, vol. 115, no. 20, pp. 9827–9837, 2011.

[96] T. Jiang and K. Xu, "Ftir study of ultradispersed diamond powder synthesized by explosive detonation," *Carbon*, vol. 33, no. 12, pp. 1663–1671, 1995.

[97] V. Kuznetsov, M. Aleksandrov, I. Zagoruiko, A. Chuvilin, E. Moroz, V. Kolomiichuk, V. Likholobov, P. Brylyakov, and G. Sakovitch, "Study of ultradispersed diamond powders obtained using explosion energy," *Carbon*, vol. 29, no. 4, pp. 665–668, 1991.

[98] K. B. Holt, C. Ziegler, D. J. Caruana, J. Zang, E. J. Millán-Barrios, J. Hu, and J. S. Foord, "Redox properties of undoped 5 nm diamond nanoparticles," *Physical Chemistry Chemical Physics*, vol. 10, no. 2, pp. 303–310, 2008.

[99] D. Mitev, R. Dimitrova, M. Spassova, C. Minchev, and S. Stavrev, "Surface peculiarities of detonation nanodiamonds in dependence of fabrication and purification methods," *Diamond and related materials*, vol. 16, no. 4, pp. 776–780, 2007.

[100] O. Shenderova, I. Petrov, J. Walsh, V. Grichko, V. Grishko, T. Tyler, and G. Cunningham, "Modification of detonation nanodiamonds by heat treatment in air," *Diamond and related materials*, vol. 15, no. 11, pp. 1799–1803, 2006.

[101] Y. V. Butenko, V. Kuznetsov, E. Paukshtis, A. Stadnichenko, I. Mazov, S. Moseenkov, A. Boronin, and S. Kosheev, "The thermal stability of nanodiamond surface groups and onset of nanodiamond graphitization," *Fullerenes, Nanotubes, and Carbon Nonstructures*, vol. 14, no. 2-3, pp. 557–564, 2006.

[102] V. Loktev, V. Makal'skii, I. Stoyanova, A. Kalinkin, V. Likholobov, and V. Mit'kin, "Surface modification of ultradispersed diamonds," *Carbon*, vol. 29, no. 7, pp. 817–819, 1991.

[103] R. Berman and J. Thewlis, "The graphite–diamond equilibrium," 1955.

[104] J. Viecelli, S. Bastea, J. Glosli, and F. Ree, "Phase transformations of nanometer size carbon particles in shocked hydrocarbons and explosives," *The Journal of Chemical Physics*, vol. 115, no. 6, pp. 2730–2736, 2001.

[105] J. Zang, Y. Wang, L. Bian, J. Zhang, F. Meng, Y. Zhao, S. Ren, and X. Qu, "Surface modification and electrochemical behaviour of undoped nanodiamonds," *Electrochimica Acta*, vol. 72, pp. 68–73, 2012.

[106] X. Xu, Z. Yu, Y. Zhu, and B. Wang, "Influence of surface modification adopting thermal treatments on dispersion of detonation nanodiamond," *Journal of Solid State Chemistry*, vol. 178, no. 3, pp. 688–693, 2005.

[107] F. Cataldo and A. P. Koscheev, "A study on the action of ozone and on the thermal stability of nanodiamond," *Fullerenes, Nanotubes and Carbon Nanostructures*, vol. 11, no. 3, pp. 201–218, 2003.

[108] A. M. Panich, A. I. Shames, N. A. Sergeev, M. Olszewski, J. K. McDonough, V. Mochalin, and Y. Gogotsi, "Nanodiamond graphitization: a magnetic resonance study," *Journal of Physics: Condensed Matter*, vol. 25, no. 24, p. 245303, 2013.

[109] S. Tomita, T. Sakurai, H. Ohta, M. Fujii, and S. Hayashi, "Structure and electronic properties of carbon onions," *The Journal of Chemical Physics*, vol. 114, no. 17, pp. 7477–7482, 2001.

[110] Q. Zou, M. Wang, Y. Li, B. Lv, and Y. Zhao, "Hrtem and raman characterisation of the onion-like carbon synthesised by annealing detonation nanodiamond at lower temperature and vacuum," *Journal of Experimental Nanoscience*, vol. 5, no. 6, pp. 473–487, 2010.

[111] J. Cebik, J. K. McDonough, F. Peerally, R. Medrano, I. Neitzel, Y. Gogotsi, and S. Osswald, "Raman spectroscopy study of the nanodiamond-to-carbon onion transformation," *Nanotechnology*, vol. 24, no. 20, p. 205703, 2013.

[112] T. Petit, J.-C. Arnault, H. A. Girard, M. Sennour, and P. Bergonzo, "Early stages of surface graphitization on nanodiamond probed by x-ray photoelectron spectroscopy," *Physical Review B*, vol. 84, no. 23, p. 233407, 2011.

[113] J. Chen, S. Deng, J. Chen, Z. Yu, and N. Xu, "Graphitization of nanodiamond powder annealed in argon ambient," *Applied physics letters*, vol. 74, no. 24, p. 3651, 1999.

[114] V. Kuznetsov, Y. V. Butenko, V. Zaikovskii, and A. Chuvilin, "Carbon redistribution processes in nanocarbons," *Carbon*, vol. 42, no. 5, pp. 1057–1061, 2004.

[115] J. Qian, C. Pantea, G. Voronin, and T. Zerda, "Partial graphitization of diamond crystals under high-pressure and high-temperature conditions," *Journal of Applied Physics*, vol. 90, no. 3, pp. 1632–1637, 2001.

[116] L. Chen, J. Zang, Y. Wang, and L. Bian, "Electrochemical oxidation of nitrite on nanodiamond powder electrode," *Electrochimica Acta*, vol. 53, no. 8, pp. 3442–3445, 2008.

[117] K. B. Holt, D. J. Caruana, and E. J. Millán-Barrios, "Electrochemistry of undoped diamond nanoparticles: accessing surface redox states," *Journal of the American Chemical Society*, vol. 131, no. 32, pp. 11272–11273, 2009.

[118] T. S. Varley, M. Hirani, G. Harrison, and K. B. Holt, "Nanodiamond surface redox chemistry: influence of physicochemical properties on catalytic processes," *Faraday discussions*, vol. 172, pp. 349–364, 2014.

[119] J. Zang, Y. Wang, S. Zhao, L. Bian, and J. Lu, "Electrochemical properties of nanodiamond powder electrodes," *Diamond and related materials*, vol. 16, no. 1, pp. 16–20, 2007.

[120] I. Novoselova, E. Fedoryshena, V. Panov, A. Bochechka, and L. Romanko, "Electrochemical properties of compacts of nano-and microdisperse diamond powders in aqueous electrolytes," *Physics of the Solid State*, vol. 46, no. 4, pp. 748–750, 2004.

[121] S. Sainio, D. Nordlund, R. Gandhiraman, H. Jiang, J. Koehne, J. Koskinen, M. Meyyappan, and T. Laurila, "What does nitric acid really do to carbon nanofibers?," *The Journal of Physical Chemistry C*, vol. 120, no. 39, pp. 22655–22662, 2016.

[122] B. D. Epstein, E. Dalle-Molle, and J. S. Mattson, "Electrochemical investigations of surface functional groups on isotropic pyrolytic carbon," *Carbon*, vol. 9, no. 5, pp. 609–615, 1971.

[123] K. Kinoshita and J. Bett, "Potentiodynamic analysis of surface oxides on carbon blacks," *Carbon*, vol. 11, no. 4, pp. 403–411, 1973.

A CV results for all measured samples

Table 13: *Water window experiments in $HClO_4$.*

Sample	'Quinone' peaks (yes/no)	Water window (V) Scan rate (mV/s) 10	50	400
ta-C	no	-	3.49	1.03
ta-C+ND - III-I	yes	3.47	3.47	2.54
ta-C+ND - III-II	yes	3.46	3.43	2.20
ta-C+ND - III-III	yes	3.45	3.42	2.21
ta-C+ND - V-I	no	-	3.01	-

(a) Water window limits 200 μA/cm^2

Table 14: *ΔE_p and k^0 values in $Ru(NH_3)_6^{2+/3+}$ with different scan rates.*

	ΔE_p (mV) Scan rate (mV/s)					k^o (cms^{-1}) [a] Scan rate (mV/s)				
Sample	10	50	100	200	400	10	50	100	200	400
ta-C	66	62	62	62	60	0.011	0.094	0.134	0.189	0.397
ta-C+ND - II	64	62	62	58	60	0.0197	0.0945	0.1336	0.3653	0.3973
ta-C+ND - IV-I	68	64	64	62	62	0.0056	0.0441	0.624	0.189	0.2672
ta-C+ND - IV-II	70	68	66	62	60	0.0065	0.0176	0.0347	0.1890	0.3973

(a) k^0 values were calculated with Nicholson method

Table 15: *Experimental values for dopamine measurements with untreated and annealed ta-C+ND electrodes.*

Sample	Detection limit (nM)	ΔE_p (mV), 10μM	ΔE_p (mV), 100μM	ΔE_p (mV), 1 mM DA Cycles 1(10)	E_{ox} (mV), 1mM DA Cycles 1(10)	'Quinone' peak (yes/no)
ta-C+ND - I	250	124	142	270 (-)	361 (-)	no
ta-C+ND - III	100000	212	216	280 (388)	369 (455)	no
ta-C+ND - III-II	100000	192	180	256(332)	349 (409)	no
ta-C+ND - III-III	100	170	176	280 (350)	367 (425)	no
ta-C+ND - IV-I	(a)	(a)	162	258 (360)	347 (433)	yes
ta-C+ND - IV-II	(a)	(a)	172	370 (526)	431 (561)	yes
ta-C+ND - IV-III	(a)	(a)	190	306 (390)	391 (457)	yes
ta-C+ND - V	500	205	-	274 (368)	367 (443)	no
ta-C+ND-600 - IV-I	(a)	18	34	90 (168)	229 (287)	yes
ta-C+ND-600 - IV-II[b]	(a)	18	34	84 (172)	223 (289)	yes
ta-C+ND-600 - V-I	100	18	36	106 (224)	239 (323)	no
ta-C+ND-600 - V-II[b]	50	40	56	126 (270)	249 (357)	no
ta-C+ND-600 - V-III	50	14	34	74 (196)	215 (307)	no

(a) DA response overlapping with 'quinone' peak

(b) After annealing samples was stored in ambient air for 1h

Table 16: ΔE_p *at different scan rates in solutions 100µM DA and 1mM AA + 1mM DA.*

		ΔE_p (mV)					
		Scan rate (mV/s)					
Sample	Solution	10	50	100	200	400	1000
ta-C+ND -III-I	100 μM DA	(a)	176	196	220	250	288
ta-C+ND -III-II	100 μM DA	(a)	216	236	260	296	338
ta-C+ND -III-III	100 μM DA	(a)	180	196	222	250	298
ta-C+ND -III-I[(b)]	1mM DA +1mM AA	-	286	-	-	424	476
ta-C+ND -III-II[(b)]	1mM DA +1mM AA	-	(a)	-	-	426	526
ta-C+ND -III-III[(b)]	1mM DA +1mM AA	-	(a)	-	-	418	474

(a) No reduction observed

(b) Samples were not selective